In Vitro – In Vivo Extrapolation Predicts Drug – Drug Interactions Arising from Inhibition of Codeine Glucuronidation by Inhibitors in Humans

Pritsana Raungrut

A Thesis Submitted in Fulfillment of the Requirements for the Degree of

Doctor of Philosophy in Biomedical Sciences

Prince of Songkla University

2010

Thesis Title	In Vitro – In Vivo Extrapolation Predicts Drug – Drug Interactions Arising from Inhibition of Codeine Glucuronidation by Inhibitors in Humans
Author	Miss Pritsana Raungrut
Major Program	Biomedical Sciences

Major Advisor:	**Examining Committee:**
.....	.....Chairperson
(Assoc. Prof. Dr. Benjamas Janchawee)	(Assoc. Prof. Dr. Wichittra Tassaneeyakul)
	.....
Co-advisors:	(Assoc. Prof. Dr. Benjamas Janchawee)
.....	.....
(Prof. John O Miners)	(Asst. Prof. Dr. Verawan Uchaipichat)
.....	.....
(Asst. Prof. Dr. Verawan Uchaipichat)	(Dr. Wandee Udomuksorn)

The Graduate School, Prince of Songkla University, has approved this thesis as fulfillment of the requirements for the Doctor of Philosophy Degree in Biomedical Sciences

.....

(Prof. Dr. Amornrat Phongdara)

Dean of Graduate School

ชื่อวิทยานิพนธ์	การประมาณค่าแนวโน้ม นอกกาย-ในกายเพื่อทำนายผลการเกิดการอันตรกิริยาของยาที่เกิดจากการยับยั้งปฏิกิริยากลูคิวโรนิเดชันของยาโคเดอีนโดยตัวยับยั้งในคน
ผู้เขียน	นางสาวปฤษณา เรืองรัตน์
สาขาวิชา	ชีวเวชศาสตร์
ปีการศึกษา	2553

บทคัดย่อ

เนื่องจากยาโคเดอีนถูกกำจัดออกจากร่างกายโดยใช้ปฏิกิริยากลูคิวโรนิเดชันเป็นหลัก ด้วยเหตุนี้ปัจจัยที่เปลี่ยนแปลงการสร้างสารแปรรูปกลูคิวโรไนด์ของยาโคเดอีนอาจส่งผลต่อทั้งสัดส่วนของขนาดยาที่ถูกเปลี่ยนไปเป็นสารแปรรูปมอร์ฟีนซึ่งมีฤทธิ์ทางเภสัชวิทยา หรือระดับความเข้มข้นของยาโคเดอีนในกระแสเลือด ดังนั้นวิธีการประมาณค่าแนวโน้มนอกกาย-ในกายจึงถูกนำมาใช้เพื่อประเมินการเกิดอันตรกิริยาของยาที่เกิดขึ้นจากการยับยั้งปฏิกิริยากลูคิวโรนิเดชันของยาโคเดอีนในคน การศึกษาเบื้องต้นชี้ให้เห็นถึงจลนศาสตร์ของการสร้างสารแปรรูปกลูคิวโรไนด์ของยาโคเดอีน (C6G) โดยใช้ไมโครโซมตับของคนและแสดงให้เห็นว่าค่าพารามิเตอร์ K_m ลดลง 88% (0.29 เปรียบเทียบกับ 2.32 mM) ในสภาวะที่มีอัลบูมิน (2%) จากการศึกษาโดยใช้ recombinant UGT เอนไซม์ 13 ชนิด ต่อปฏิกิริยากลูคิวโรนิเดชันของยาโคเดอีน พบว่ามีเพียงเอนไซม์ UGT2B4 และ UGT2B7 ที่มีผลต่อปฏิกิริยานี้ โดยค่าพารามิเตอร์ S_{50} (0.32 และ 0.27 mM) ที่ได้ในสภาวะที่มีอัลบูมินมีค่าใกล้เคียงกับค่าเฉลี่ย K_m ที่ได้จากไมโครโซมตับของคน นอกจากนี้ตัวยับยั้งที่เคยมีรายงานผลการยับยั้งของเอนไซม์ UGT2B7 ทั้งนอกกายหรือในกายได้ถูกนำมาศึกษาเพื่อดูผลของการยับยั้งต่อการสร้างสารแปรรูป C6G โดยใช้ไมโครโซมตับของคน ผลในการยับยั้งแสดงให้เห็นว่าการเกิดอันตรกิริยาของยาอาจเกิดขึ้นกับตัวยับยั้งฟลูโคนาโซล, คีตามีน, และคีโตโคนาโซล ค่าพารามิเตอร์ K_i ที่ได้สำหรับตัวยับยั้งฟลูโคนาโซล (202 μM), คีตามีน (3.51 μM), และ คีโตโคนาโซล (0.66 μM) ทำนายผลการเพิ่มขึ้นของค่า AUC ratio ของยาโคเดอีนในกาย เป็น 1.60, 1.10, และ 2.97 เท่าตามลำดับ ด้วยเหตุนี้การเกิดอันตรกิริยาของยาโคเดอีนกับตัวยับยั้งฟลูโคนาโซลและคีโตโคนาโซลแต่ไม่ใช่คีตามีนมีแนวโน้มอาจเกิดขึ้นได้ซึ่งส่งผลต่อฤทธิ์ระงับปวดทั้งประสิทธิภาพหรือระยะเวลาในการออกฤทธิ์และการเกิดพิษของยาโคเดอีน นอกจากนั้นในการศึกษานี้แสดงให้เห็นถึงปฏิสัมพันธ์ทางจลนศาสตร์ที่ซับซ้อนระหว่างยาโคเดอีนและตัวยับยั้งวาโปรอิคเอซิด ทั้งในสภาวะที่มีและไม่มีอัลบูมิล การเติมวาโปรอิคเอซิดส่งผลต่อการเปลี่ยนแปลง

จลนศาสตร์ของการสร้างสารแปรรูป C6G จาก Michaelis-Menten หรือ Substrate inhibition ไปเป็น Sigmoidal โดยการเพิ่มขึ้นของค่าพารามิเตอร์ K_m (หรือ S_{50}) โดยประมาณ 4.8-7.7 เท่า ข้อมูลนี้อาจสันนิษฐานได้ว่าวาโปรอิคเอซิดจับกับ effector site ของเอนไซม์ซึ่งมีผลต่อจลนศาสตร์ของปฏิกิริยากลูคิวโรนิเดชันของยาโคเดอีนที่ซับซ้อนขึ้น

Thesis Title	In Vitro – In Vivo Extrapolation Predicts Drug – Drug Interactions Arising from Inhibition of Codeine Glucuronidation by Inhibitors in Humans
Author	Miss Pritsana Raungrut
Major Program	Biomedical Sciences
Academic Year	2010

ABSTRACT

Since COD (codeine) is eliminated primarily via glucuronidation, factors that alter COD glucuronide formation potentially affect either the proportion of the dose converted to the pharmacologically active metabolite morphine or COD concentration in plasma. Thus, in vitro – in vivo extrapolation (IV-IVE) approaches were utilized to identify potential drug-drug interactions (DDIs) arising from inhibition of COD glucuronidation in humans. Initial studies characterized the kinetics of COD 6-glucuronide (C6G) formation by human liver microsome (HLM), and demonstrated an 88% reduction in K_m (0.29 vs. 2.32 mM) for incubations performed in the presence of 2% bovine serum albumin (BSA). Of 13 recombinant UGT enzymes screened for COD glucuronidation activity, only UGT2B4 and UGT2B7 exhibited activity. The respective S_{50} values (0.32 and 0.27 mM) generated in the presence of BSA were comparable to the mean K_m observed in HLM. Known inhibitors of UGT2B7 activity in vitro or in vivo were investigated for inhibition of C6G formation by HLM. Inhibition screening identified potential DDIs with fluconazole, ketamine, and ketoconazole. K_i values generated for fluconazole (202 μM), ketamine (3.51 μM), and ketoconazole (0.66 μM) predicted 1.60, 1.10, and 2.97-fold increases, respectively in the AUC ratio for COD in vivo. DDIs of COD with fluconazole and ketoconazole, but not ketamine potentially affect the COD analgesia, either intensity or duration and COD toxicity. In addition, this work showed a complex kinetic interaction between COD and valproic acid in both the absence and presence of BSA. Addition of valproic acid changed the kinetics of C6G formation from the Michaelis-Menten or Substrate inhibition to Sigmoidal kinetics with increasing of K_m (or S_{50}) values by approximately 4.8- to 7.7-fold. This data is further assumed

that valproic acid binds to a distinct effector site of enzyme, which results in the complex COD glucuronidation kinetics.

ACKNOWLEDGEMENTS

I would like to express my deepest appreciation to Prof. John O Miners, my supervisor in Australia, for helpful suggestion, valuable guidance, financial support and constructive comments throughout my experimental work in Department of Clinical Pharmacology, Flinders University School of Medicine, Australia and, in particular, his assistance in the writing of my thesis.

I am grateful to Assoc. Prof. Dr. Benjamas Janchawee, my supervisor in Thailand, and Asst. Dr. Verawan Uchaipichat, my co-advisor, for their valuable contribution, comment, and assistance in the writing of my thesis. I would like to offer my special gratitude to the examining committee, Assoc. Prof. Dr. Wichittra Tassaneeyakul and Dr. Wandee Udomuksorn, in devotion of their valuable time for the thesis examination. Also, I would like to thank Assoc. Prof. Dr. Nongporn Towatana and Dr. Suvina Ratanachaiyavong for their valuable recommendations and in devotion of their time for the proposal examination.

I sincerely thank David Elliot for his guidance and helping for the HPLC assay, and Kushari Bowalgaha for preparing human liver microsomes and recombinant UGT enzymes. I would also like to thank Heather Aubert for her assistance. I wish particularly to thank all students and staff of the Department of Clinical Pharmacology, Flinders University School of Medicine, Australia for their support and friendship.

In addition, I wish to thank my parents, elder sisters, grandsons, friends, and Mr.Attharat Pattanawongsa for their encouragement and willpower throughout my period of study.

Finally, I would like to express my thanks to the Prince of Songkla University which gave me the grant for the partial financial support to this thesis.

Pritsana Raungrut

CONTENTS

CONTENTS (CONTINUED)

LIST OF TABLES

LIST OF TABLES (CONTINUED)

LIST OF FIGURES

LIST OF FIGURES (CONTINUED)

LIST OF FIGURES (CONTINUED)

LIST OF ABBREVIATIONS AND SYMBOLS

Abbreviation	Definition
[E]	Enzyme concentration
$[E]_t$	Total enzyme concentration
[I]	Inhibitor concentration
[S]	Substrate concentration
f_m	Fraction of the dose metabolized by the enzyme and pathway of interest
f_u	Fraction unbound concentration in blood
$f_{u,inc}$	Fraction unbound of drug in incubation
$f_{u,p}$	Fraction unbound concentration in plasma
$^{\circ}C$	Degree celsius
υ	Metabolic rate or velocity
α	Interaction factor associated with changes in binding affinity in the case of homotropic cooperativity
β	Interaction factor associated with changes in the rate of product formation in the case of homotropic cooperativity
γ	Interaction factor associated with changes in the rate of product formation in the case of heterotropic cooperativity
δ	Interaction factor associated with changes in binding affinity in the case of heterotropic cooperativity
1-NP	1-naphthol
4-MU	4-methylumbelliferone
A	Activator
AUC	Area under the plasma concentration–time curve
AZT	Zidovudine
bp	Base pair
Brij 58	Polyoxyethylene monocetyl ether
BSA	Bovine serum albumin
C	Carboxy

LIST OF ABBREVIATIONS AND SYMBOLS (CONTINUED)

Abbreviation	Definition
C6G	COD-6-glucuronide
C_a	Drug concentration in blood entering the liver
ca.	Circa (Latin): synonym for "in approximately"
CAZy	Continuously updated carbohydrateactive enzyme database
C_b	Drug concentrations in blood
C_b^*	Concentation of compound in dialysis chambers containing in buffer
cDNAs	Complementary DNAs
CL	Clearance
CL_H	Hepatic clearance
CL_{int}	In vitro intrinsic clearance
$CL_{int,un}$	In vivo intrinsic clearance corrected for the fraction unbound in plasma
$CL_{int.liver}$	Whole-liver intrinsic clearance
CL_{max}	Maximum clearance
CL_{Other}	Clearance by all other routes
CL_R	Renal clearance
CL_S	Systemic clearance
CNS	Central nervous system
CO_2	Carbondioxide
COD	Codeine
COOH	Carboxyl
C_p	Drug concentrations in plasma
C_p^*	Concentation of compound in dialysis chambers containing in protein
Cu^{2+}	Cupric(II) ion
C_v	Drug concentration in blood leaving the liver
CYP	Cytochrome P450 protein
Da	Dalton
DDIs	Drug-drug interactions

LIST OF ABBREVIATIONS AND SYMBOLS (CONTINUED)

Abbreviation	Definition
DNA	Deoxyribonucleic acid
E	Enzyme
E. coli	*Escherichia coli*
e.g.	exampli gratia (Latin): synonym for "for example"
EC	Enzyme commission
E_H	Hepatic extraction ratio
EI	Enzyme-inhibitor
EMs	Extensive metabolisms
ER	Endoplasmic reticulum
ES	Enzyme-substrate
ESI	Enzyme-substrate-inhibitor
et al.	et alii (Latin): synonym for "and others"
etc.	Et cetera (Latin): synnonym for "and the others"
F_a	Fraction of oral dose absorbed from the GI tract into the portal vein
FLZ	Fluconazole
FMO	Flavin monooxygenase
g	Gram
GABA	γ-aminobutyric acid
GI	Gastrointestinal
GST	Glutathione-*S*-transferase
GtfA	Glucosyltransferase A
GTs	Glycosyltransferases
$HClO_4$	Perchloric acid
HEK293	Human embryonic kidney293 cell line
Hill	Hill equation
HIM	Human intestinal microsome
HKM	Human kidney microsome

LIST OF ABBREVIATIONS AND SYMBOLS (CONTINUED)

Abbreviation	Definition
HL	Human liver
HLM	Human liver microsome
HomPGGL	Milligram of homogenate protein per gram of liver
HPGL	Hepatocytes per gram of liver or hepatocellularity
HPLC	High performance liquid chromatography
hr	Hour
HSA	Human serum albumin
I	Inhibitor
i.e.	id est (Latin):synonym for "that is"
IC_{50}	Concentration of inhibitor that produces 50% inhibition
I_{inlet}	Maximum hepatic inlet concentration
$I_{inlet,max}$	Hepatic maximum unbound inlet concentration
$I_{inlet,u}$	Unbound inhibitor hepatic inlet concentration
IM	Intramuscular
I_{max}	Maximum inhibitor concentration in the hepatic artery and portal vein
IV	Intravenous
IV-IVE	In vitro – in vivo extrapolation
K_a	Activator constant
k_a	First-order absorption rate constant
kb	Kilo base pair
kDa	Kilodalton
kg	Kilogram
K_i'	Dissociation constant of inhibitor to the ES complex
K_i	Inhibitor constant or Dissociation constant of inhibitor to the enzyme
K_m	Michaelis-Menten constant
KOH	Potassium hydroxide
K_p	Rate of product formation

LIST OF ABBREVIATIONS AND SYMBOLS (CONTINUED)

Abbreviation	Definition
K_s	Substrate dissociation constant
K_{si}	Constant describing the substrate inhibition interaction
KTM	Ketamine
KTZ	Ketoconazole
L	Litre
LTG	Lamotrigine
LW	Average weight of a human liver
M	Molar
Mb	Mega base pair
MES	Modifier-enzyme-substrate
μg	Microgram
mg	Miligram
Mg^{2+}	Magnesium(II) ion
$MgCl_2$	Magnesium chloride
min	Minute
μL	Microliter
mL	Milliliter
MM	Michaelis-Menten
μM	Micromolar
mm	Millimeter
mM	Millimolar
Mn^{2+}	Manganese(II) ion
MPPGL	Milligram of microsomal protein per gram of liver
mRNA	Messenger RNA
MRP	Maltose binding protein
MT	Methyltransferase
MW.	Molecular weight

LIST OF ABBREVIATIONS AND SYMBOLS (CONTINUED)

Abbreviation	Definition
N	Amino
n	Hill coefficient
NAT	*N*-acetyltransferase
NH_2	Amino
nm	Nanometer
NMR	Nuclear magnetic resonance
NSAIDs	Nonsteroidal anti-inflammatory drugs
OH	Hydroxyl
P	Product
PAPS	3-phosphoadenosine-5-phosphosulfate
pH	Potential of hydrogen ion
pmol	Picomole
PMs	Poor metabolisms
PO	Per oral
PR	Per rectal
Q_H	Sum of hepatic portal and hepatic arterial blood flow or hepatic blood flow
QSAR	Quantitative structure-activity relationships
R_B	Blood to plasma concentration ratio
RBCs	Red blood cells
RNA	Ribonucleic acid
rpm	Revolutions per minute
S	Substrate
S_{50}	Substrate concentration resulting in 50% of V_{max}
SAM	*S*-adenosyl-*L*-methionin
SC	Subcutaneous
SD.	Standard deviation
SE	Substrate-enzyme

LIST OF ABBREVIATIONS AND SYMBOLS (CONTINUED)

Abbreviation	Definition
SE.	Standard error
SES	Substrate-enzyme-substrate
SH	Thiol
SI	Substrate inhibition
ST	Sulfotransferase
$t_{1/2,ab}$	Absorption half life in plasma
TEA	Triethylamine
TFP	Trifluoperazine
T_{max}	Time to maximum drug concentration
U	Unit
UDP	Uridine diphosphate
UDPGA	Uridine diphosphate glucuronic acid
UGT	UDP-glucuronosyltransferase
UGT2B7CT	C-terminal domain of UGT2B7
UMs	Ultrarapid metabolisms
UV	Ultra violet
v/v	Volume per volume
viz.	Videlicet (Latin): synonyms for "namely" or "as follows"
V_{max}	Maximum velocity
VPA	Valproic acid
VvGT1	Vitis vinifera anthocyanidin 3-*O*-glucosyltransferase
w/v	Weight per volume
*x*g	Relative gravity force
Zn^{2+}	Zinc(II) ion

LIST OF AMINO ACID ABBREVIATIONS

Abbreviation		Amino acid name
Ala	A	Alanine
Arg	R	Arginine
Asn	N	Asparagine
Asp	D	Aspartic acid (Aspartate)
Cys	C	Cysteine
Gln	Q	Glutamine
Glu	E	Glutamic acid (Glutamate)
Gly	G	Glycine
His	H	Histidine
Ile	I	Isoleucine
Leu	L	Leucine
Lys	K	Lysine
Met	M	Methionine
Phe	F	Phenylalanine
Pro	P	Proline
Ser	S	Serine
Thr	T	Threonine
Trp	W	Tryptophan
Tyr	Y	Tyrosine
Val	V	Valine
Asx	B	Aspartic acid or Asparagine
Glx	Z	Glutamine or Glutamic acid

CHAPTER 1

INTRODUCTIONS

1.1 Background and rationale

The opioid codeine (COD) is one of the most widely used drugs worldwide. COD is employed extensively in the treatment of mild to moderate pain, either alone or in combination with other analgesics. Furthermore, COD is used as an antitussive and for the treatment of diarrhea. It is generally accepted that COD analgesia arises from cytochrome P450 (CYP) 2D6 catalyzed *O*-demethylation to form morphine (Somogyi *et al*., 2007). Approximately 4 to 10% of a COD dose is converted to morphine in CYP2D6 extensive and ultrarapid metabolizers (Chen *et al*., 1991; Yue *et al*., 1991; Kirchheiner *et al*., 2007). Other elimination pathways include glucuronidation, *N*-demethylation and renal clearance of unchanged drug. Of these, glucuronidation, to form COD-6-glucuronide (C6G), is the dominant metabolic pathway, accounting for 80-85% of the COD dose recovered in urine (Yue *et al*., 1991).

Accumulating evidence indicates that the relative formation of morphine plays a pivotal role in COD response. In particular, variability in COD *O*-demethylation due to genetic polymorphism of CYP2D6 is known to influence both analgesia and the occurrence of morphine-related adverse effects. In relation to adverse effects, individuals who are ultrarapid metabolisers (UMs) of CYP2D6 have on average 50% higher plasma concentrations of morphine than extensive metabolisers (EMs), which results in a higher incidence of central nervous system (CNS) depression (Gasche *et al*., 2004; Kirchheiner *et al*., 2007; Samogyi *et al*., 2007). Additionally, a relationship between maternal COD use and neonatal toxicity has been reported. Breastfed infants of mothers who are CYP2D6 UMs are at increased risk of potentially life-threatening CNS depression (Madadi *et al*., 2009). Although there is no evidence to confirm a shift to minor pathways, especially conversion to morphine due to inhibition of COD glucuronidation, the amount of COD available for other pathways may be increased. Since

glucuronidation is the dominant route of COD metabolism, changes in C6G formation will potentially affect the proportion of the dose metabolized via the *O*-demethylation pathway and hence the intensity and duration of pharmacological response. However, factors that influence COD glucuronidation in humans are poorly understood. Furthermore, serious adverse effects may arise from COD toxicity. In this regard, six fatalities have been reported from poisonings with COD. These deaths showed that a high COD concentration in plasma (> 0.4 mg/L of free COD concentration and > 2 mg/L of total COD concentration) may be sufficient to cause death in the absence of any other contributing factors (Gerostamoulos *et al*., 1996).

It has been reported that COD 6-glucuronidation is catalyzed by UDP-glucuronosyltransferase (UGT)2B7, with a possible contribution of UGT2B4 (Coffman *et al*., 1998; Court *et al*., 2003). UGT2B7 is arguably the most important drug metabolizing UGT enzyme in humans (Miners *et al*., 2010). Apart from COD, UGT2B7 also glucuronidates other opioids (e.g. morphine, naloxone), many non-steroidal anti-inflammatory agents (viz. ketoprofen, ibuprofen, diclofenac, and naxoprofen), valproic acid (VPA), and zidovudine (AZT). Among these, morphine and AZT are commonly used drugs that could potentially serve as UGT2B7 probes. A relatively common coding region polymorphism, UGT2B7*2 (His268Tyr), appears not to affect the glucuronidation of opioids, including COD (Bhasker *et al*., 2000; Court *et al*., 2003).

Compelling evidence linking other UGT2B7 variants and opioid disposition and response is similarly lacking (Thorn *et al*., 2009). In contrast, data from both in vitro and in vivo studies indicate that inhibition of the metabolism of UGT2B7 substrates may result in significant drug-drug interactions (DDIs), with reduced clearance via glucuronidation. For example, DDIs in vivo have been reported between fluconazole (FLZ) and AZT. Administration of FLZ in a therapeutic dose (400 mg/day) decreased the apparent clearance of AZT by 47% corresponding to a 1.92-fold increase in the mean area under the plasma concentration–time curve (AUC) of AZT in patients infected with human immunodeficiency virus (Sahai *et al*., 1994). Consistent with in vitro studies, FLZ, ketamine (KTM), ketoconazole (KTZ), and VPA have been shown to inhibit in vitro probe substrates for UGT2B7. An inhibitor constant (K_i) for FLZ inhibition of AZT glucuronidation by human liver microsomes (HLM) was 1133 μM and reduced to 145 μM in the absence and presence of bovine serum albumin (BSA), respectively (Uchaipichat *et al*., 2006a), whereas the respective concentrations which caused 50% inhibition (IC_{50}) reported by Trapnell *et*

al. (1998) were 163 μM (FLZ) and 693 μM (VPA). Similar to AZT glucuronidation, the K_i value of KTM inhibition on morphine-6-glucuronide formation in the presence and absence of 2% BSA were 35 μM and 5 μM, respectively (Miners JO; unpublished data), whereas the reported K_i value of KTZ inhibition on morphine-3-glucuronide formation was 118 μM in the absence of BSA (Takeda *et al*., 2006).

Recent studies in this laboratory have demonstrated that the magnitude of an in vivo inhibitory DDI with a UGT2B7 substrate as the object drug may be predicted accurately from a K_i value generated in vitro when incubations of HLM are conducted in the presence of BSA. Long-chain unsaturated fatty acids released from the microsomal membrane during the course of an incubation act as potent competitive inhibitors of UGT2B7 and UGT1A9 resulting in over-estimation of the Michaelis-Menten constant (K_m) and K_i values of substrates and inhibitors of these enzymes (Rowland *et al*., 2007 and 2008a). BSA sequesters the inhibitory unsaturated long-chain fatty acids and, as a consequence, K_i (and K_m) values are reduced by approximately an order of magnitude compared to data generated in the absence of albumin (Miners *et al*., 2006 and 2010). Importantly, in vitro K_i values obtained in the presence of 2% BSA accurately predicted the magnitude of the FLZ – AZT and VPA – lamotrigine (LTG) interactions in vivo (Rowland *et al*., 2006; Uchaipichat *et al*., 2006a).

The primary aim of the present study was to employ in vitro – in vivo extrapolation (IV-IVE) to identify potential DDIs resulting in inhibition of COD glucuronidation. In vitro inhibition data were generated using HLM, with and without BSA, as the enzyme source. Drugs investigated included those previously identified from in vitro and in vivo inhibition studies with UGT2B7 substrates (viz. FLZ, KTM, KTZ, and VPA). The work additionally sought to confirm the involvement of both UGT2B7 and UGT2B4 in C6G formation and characterize the effect of BSA (2%) on the kinetics of COD glucuronidation in vitro, and to assess the relative inhibition of these enzymes by inhibitors of human liver microsomal COD glucuronidation.

1.2 Review of the Literature

1.2.1 Overview of drug metabolism

Generally, a drug that is administered by any route other than intravenous (IV) route must be absorbed from the site of administration into the bloodstream. Following distribution into various body fluids and tissues, including those sites where the drug exerts its pharmacological effect(s), it is eliminated from the body, by metabolism and excretion (Holford and Sheiner, 1981; Holford, 2004). Metabolism is an important process that determines the metabolic clearance of an administered drug. For a drug that undergoes metabolism, several factors, such as certain disease states, genetics, and DDIs, may influence the extent of metabolism and lead to toxic or subtherapeutic plasma drug concentrations (Holford, 2004). Ideally, metabolic reactions generate more polar, inactive metabolites that are readily excreted from the body in urine or bile. However, in some cases, metabolites with potent biological activity or toxic properties are generated (Buxton, 2006).

The metabolic conversion of drugs is enzymatic in nature. The enzyme systems involved in the metabolism of drugs are mainly localized in the liver. Other organs with significant metabolic capacity include the gastrointestinal (GI) tract, kidneys, and lungs. Within a given cell, most drug metabolizing activity is found in the endoplasmic reticulum (ER) and the cytosol, although drug metabolism also can occur in the mitocondria, nuclear envelope, and plasma membrane. Upon homogenization and differential centrifugation of tissues, the ER breaks up and fragments of the membrane form microvesicles, referred to as microsomes. Drug-metabolizing enzymes can be classified into two major groups, functionalisation and conjugation (Gonzalez and Tukey, 2006).

1.2.1.1 Functionalisation

Functionalisation enzymes are responsible for the either the introduction of a polar functional group or the unmasking of a polar functionality. The three main types of

functionalisation reactions are oxidation, reduction and hydrolysis. Oxidation reactions are catalyzed by enzymes, such as CYP, flavin monooxygenase (FMO) and amine, xanthine, alcohol and aldehyde oxidases (Zhang *et al.*, 2006). Of these, the CYP enzymes are considered the main functionalisation enzyme. It is estimated that CYP superfamily enzymes are involved in the metabolism, accounting for ~75% of marketed drugs (Guengerich, 2008). CYP catalyzes many reactions which mostly involve oxidation such as *N*-, *O*-, and *S*-dealkylation, *N*-oxidation, and *C*- and *N*-hydroxylation etc. (Gonzalez and Tukey, 2006). The other possible functionalisation reactions are epoxidation, oxidative deamination, nitroreduction, azoreduction, reductive dehalogenation and hydrolysis reactions. Thus, functionalisation reactions a functional group (e.g. -OH, -COOH, $-NH_2$ or -SH) is typically introduced or 'unmasked'. These reactions are not uncommonly followed by a conjugation reaction (Zhang *et al.*, 2006).

1.2.1.2 Conjugation reactions

Conjugation enzymes lead to the formation of a covalent bond between a suitable functional group present in the parent compound or functionalisation metabolite with endogenously derived glucuronic acid, sulfate, glutathione, amino acid, or acetyl group. These generally polar conjugates are normally inactive and are excreted in the urine and feces. The major conjugation enzymes are UGT, glutathione *S*-transferase (GST), sulfotransferase (ST), *N*-acetyltransferase (NAT), and methyltransferase (MT) (Gonzalez and Tukey, 2006). Table 1.1 summarizes the characteristics of conjugation reactions.

Table 1.1. Characterization of conjugation reactions[a] (Modified from Liston *et al.*, 2001).

Conjugation enzyme	Co-Factor	Locations	Reaction	Common substrates
UGT	UDPGA	Liver, kidney, intestine, lung, skin, prostate, brain	Glucuronidation	Acetaminophen Bilirubin Ethinylestradiol Morphine Lorazepam Oxazepam Valproic acid Lamotrigine Olanzapine
ST	PAPS	Liver, kidney, intestine	Sulfate conjugation	Acetaminophen Albuterol Terbutaline Methyldopa
GST	Glutathione	Liver, kidney	Glutathione conjugation	Azathioprine 6-Mercaptopurine Nitroglycerin Organophosphates
NAT	Acetyl coenzyme A	Liver, lung, spleen, gastric mucosa, RBCs, lymphocytes	N-acetylation	Dapsone Hydralazine Isoniazid Phenelzine Procainamide
MT	SAM	Liver, kidney, lung, CNS	Methylation	Dobutamine Dopamine Levodopa Norepinephrime Serotonin

[a]UGT, UDP-glucuronosyltransferase; UDPGA, Uridine diphosphate glucuronic acid; ST, Sulfotransferase: PAPS, 3-phosphoadenosine-5-phosphosulfate; GST, Glutathione-*S*-transferase; NAT, *N*-acetyltransferase; RBCs, red blood cells; MT, Methyltransferase; SAM, *S*-adenosyl-*L*-methionin; CNS, Central nervous system.

The most important conjugation reaction is glucuronidation, which is catalyzed by UGTs. This enzyme is responsible for the majority of all drugs metabolized by conjugation pathways.

1.2.2 Glycosyltransferases (GTs)

Based on amino acid sequence and predicted structure, human UGT enzymes belong to the GT superfamily. GTs are a large family of enzymes that are involved in the biosynthesis of oligosaccharides, polysaccharides, and glycoconjugates. They catalyze the transfer of a sugar moiety from an activated donor sugar onto a protein, lipid, deoxyribonucleic acid (DNA) or small molecule (Breton *et al.*, 2006). The classification of GTs is based on the identities of their amino acid sequences. GTs have been classified into 91 gene families, available from the continuously updated carbohydrateactive enzyme database (CAZy) at http://afmb.cnrs-mrs.fr/CAZY (Campbell *et al.*, 1998; Coutinho *et al.*, 2003). Currently, structural information is available for only a limited number of GT families, revealing two distinct structural folds, GT-A and GT-B (Breton *et al.*, 2006). GT folds have been observed to consist primarily of $\alpha/\beta/\alpha$ sandwiches, similar or very close to the Rossmann-like fold, a classical structural motif (six-stranded parallel β-sheet with 321456 topology) found in many nucleotide binding proteins (Lesk, 1995). The GT-A fold consists of a single $\alpha/\beta/\alpha$ sandwich (a seven stranded β-sheet with 3214657 topology in which strand 6 is antiparallel to the rest) that resembles a Rossman-like fold (Fig.1.1A). The central β-sheet is flanked by a smaller one, and the association of both creates the active site. Almost all the GT-A family members have a common DxD motif, which is involved in coordinating a divalent cation, usually Mn^{2+}, in the catalytic centre. This metal ion is required for the binding of the nucleotide sugar (Wiggins and Munro, 1998; Breton and Imberty, 1999; Breton *et al.*, 2006).

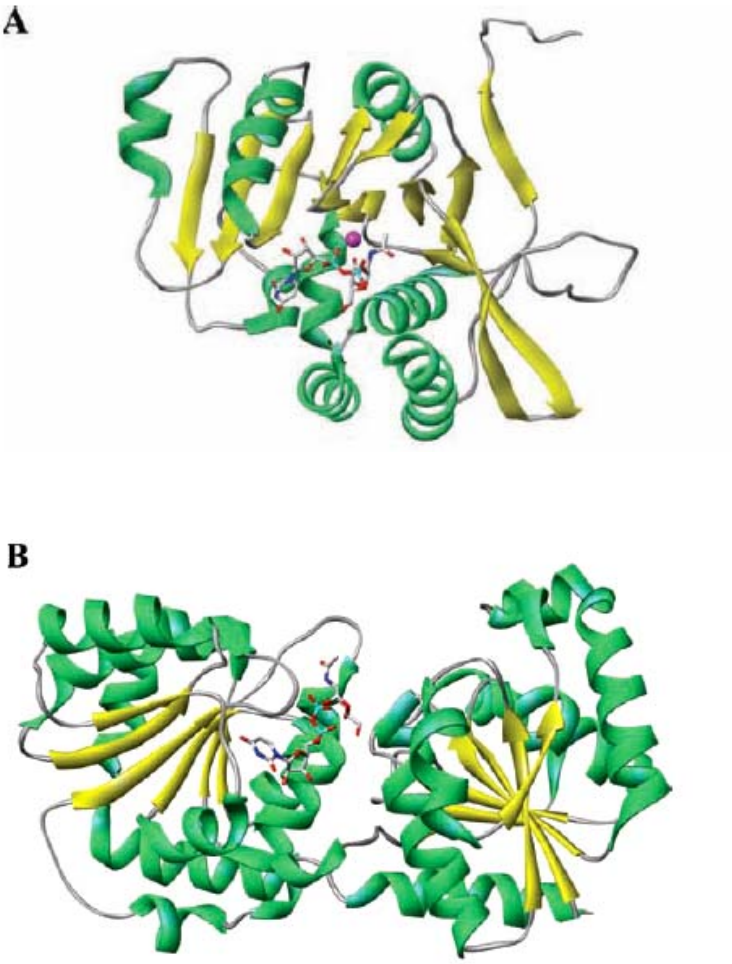

Figure 1.1 Ribbon diagram of GTs (Taken from Breton *et al*., 2006):

A) GT-A fold; mouse α-1,4-*N*-acetylhexosaminyltransferase complexed with UDP-GalNAc.

B) GT-B fold; *E. coli* MurG complexed with UDP-GlcNAc.

The GT-B fold (Fig.1.1B) consists of two separate Rossmann domains with a connecting linker region and a catalytic site located between the domains. Carboxy (C)-terminal domain corresponds to the nucleotide-binding domain, while amino (N)-terminal domain binds the acceptor. Variations are more pronounced in the N-terminal domains, in the loops and helices which point towards the active site (Breton *et al.*, 2006).

1.2.3 UDP-glucuronosyltransferases (UGTs)

1.2.3.1 The glucuronidation reaction

Glucuronidation is a synthetic reaction catalyzed the UGT enzymes (EC 2.4.1.17) (Miners and Mackenzie, 1991; Radominska-Pandya *et al.*, 1999; Tukey and Strassburg, 2000). This reaction involves the covalent linkage (or "conjugation") of a suitable functional group present on a substrate with glucuronic acid (Fig.1.2). In mammals, glucuronic acid is the main sugar that is used to prevent the accumulation of waste products of metabolism and lipophilic chemicals from the environment to toxic levels in the body. In the glucuronidation reaction, glucuronic acid from the donor uridine diphosphate glucuronic acid (UDPGA) is covalently linked to a functional group, most commonly -OH, -COOH, $-NH_2$ or -SH group on the target molecule (aglycone), leading to the formation of *O*-, *N*-, or *S*-glucuronides, respectively (Radominska-Pandya *et al.*, 1999; King *et al.*, 2000; Gonzalez and Tukey, 2006).

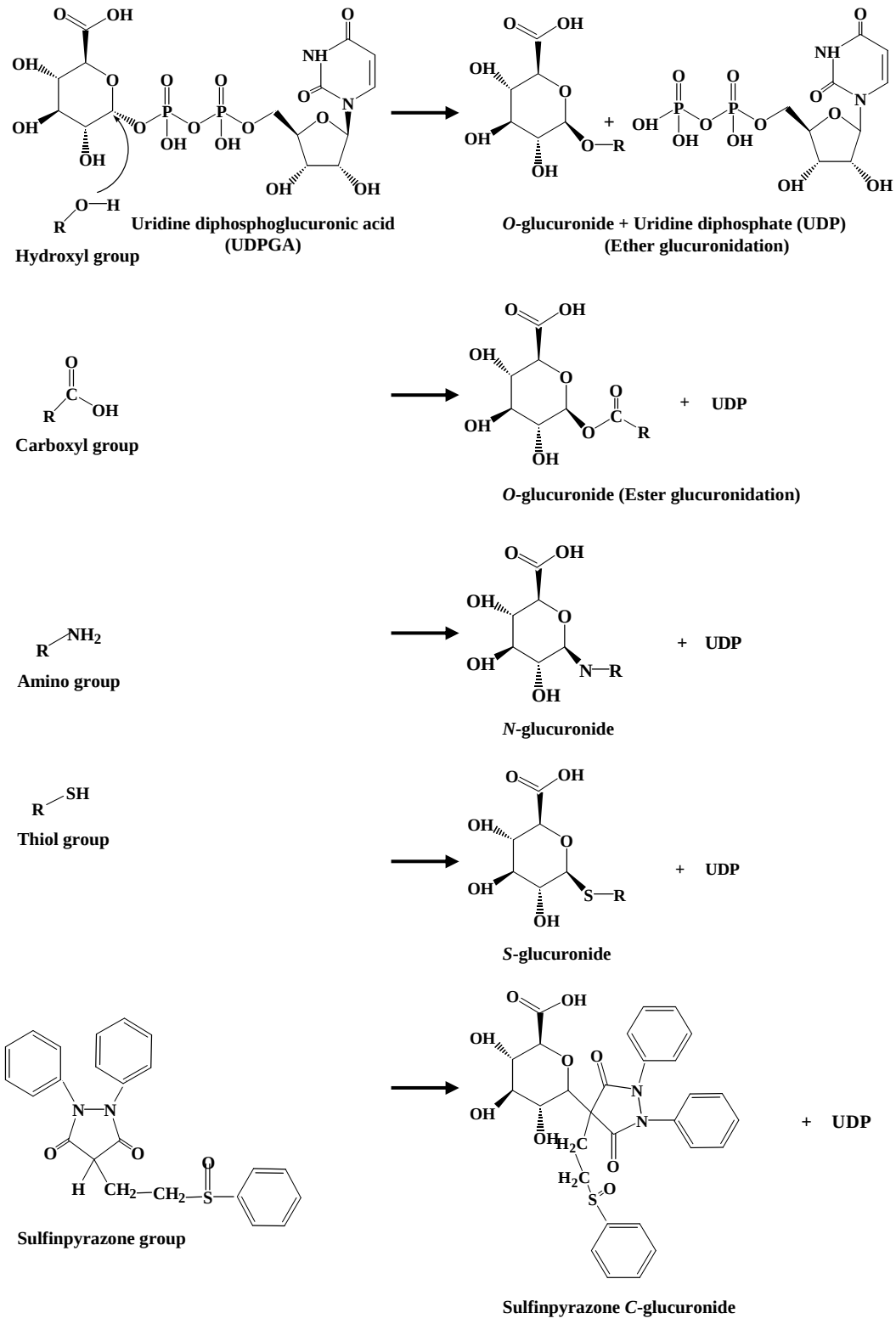

Figure 1.2 Scheme for the conjugation of substrates with glucuronic acid.

(Modified from Gonzalez and Tukey, 2006).

Glucuronidation additionally serves as an elimination pathway in humans for numerous dietary chemicals, environmental pollutants, and endogenous compounds (e.g., bilirubin, bile acids, and hydroxysteroids). Moreover, glucuronidation facilitates excretion of these compounds and the products of functionalisation metabolism in urine and bile as their hydrophilic conjugates, and generally results in detoxification, although a limited number of glucuronides possess biological activity (Ritter, 2000).

1.2.3.2 UGT heterogeneity

A nomenclature system for the UGT superfamily based on divergent evolution of the genes is in place. Several novel UGT genes have been identified in the human, mouse and rat genomes and in other mammalian species. The mammalian UGT gene superfamily is classified on the basis of sequence homology. It currently has 117 members that can be divided into four families, UGT1, UGT2, UGT3 and UGT8 (Fig.1.3) (Burchell *et al.*, 1991; Mackenzie *et al.*, 1997; Mackenzie *et al.*, 2005). The UGT1 and UGT2 families are most efficient at using UDPGA as the glycosyl donor. However, other uridine diphosphate (UDP) sugars, including UDP glucose and UDP xylose, may be used as the sugar donor by these enzymes (Senafi *et al.*, 1994; Mackenzie *et al.*, 2003).

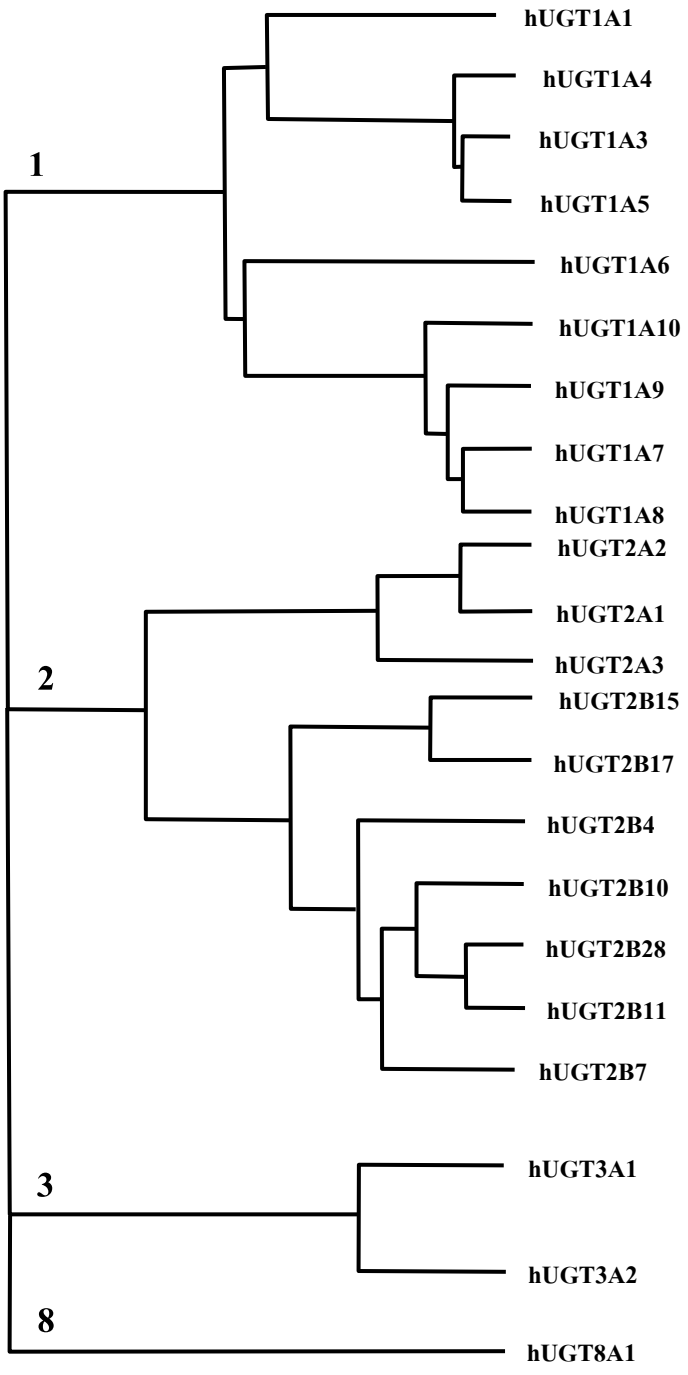

Figure 1.3 A Phylogram of the human UGT families.

(Modified from Mackenzie *et al*., 2005).

The human UGT1 family constitutes a complex gene on chromosome 2q37 (Fig.1.4A). It comprises 13 individual promoters/first exons that encode the unique N-terminal domains of the UGT1A proteins and a shared set of exons 2–5 that encode the C-terminal domain, which is identical in all UGT1A family members (Owens and Ritter, 1992; Mackenzie *et al.*, 2005). Each first exon directs the synthesis of RNA transcript which is then spliced to the shared exons 2–5. The human UGT1 gene extends over approximately 200 kb. Nine members (UGT1A1, 1A3, 1A4, 1A5, 1A6, 1A7, 1A8, 1A9, and 1A10) can be generated from the UGT1. However, four members (UGT1A2P, 1A11P, 1A12P and 1A13P) contain mutations and are designated as pseudogenes (Tukey and Strassburg, 2000; Mackenzie *et al.*, 2005).

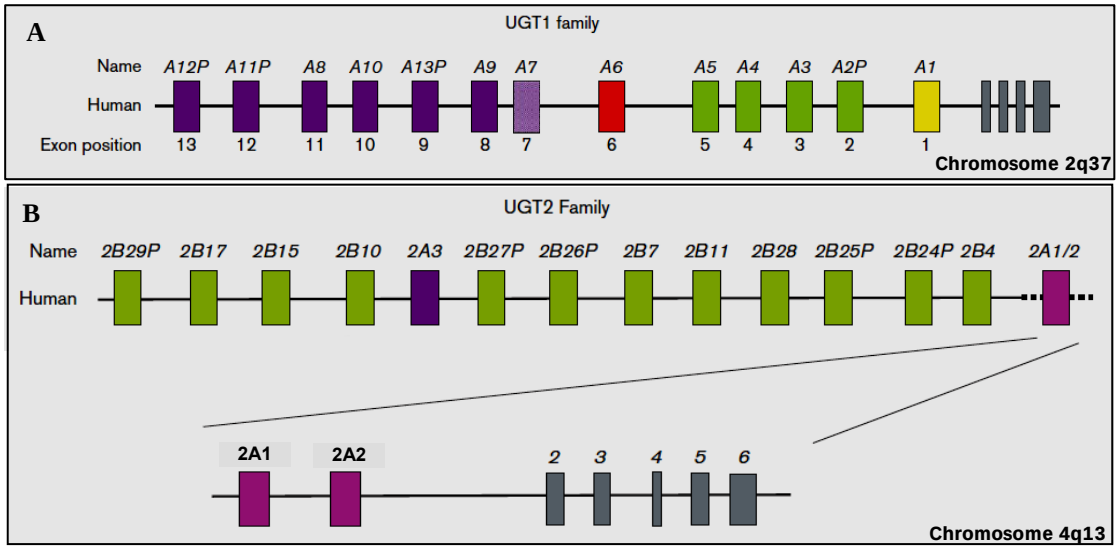

Figure 1.4 Oganization of the human UGTs (Modified from Mackenzie *et al*., 2005):

A) UGT1 family; Each exon 1 is represented by a coloured rectangle, labeled A1, A2, A3, etc. and its position relative to exons 2–5 is indicated. Exons 2–5, which are joined to each first exon in the mature transcript, are shown in grey.

B) UGT2 family; Each gene in the human consisting of six exons, is represented by a coloured rectangle, except for that which is labeled '2A1/2', which represents seven exons. The human UGT2A1 and UGT2A2 genes contain unique first exons (2A1 and 2A2) and a shared set of five downstream exons (exons 2–6 in grey). Pseudogene names end in the label P.

The human UGT2 family consists of the UGT2A and UGT2B subfamilies; human UGT2 genes extend over approximately 1.45 Mb. The UGT2A subfamily contains three members (UGT2A1, 2A2, and 2A3), whereas the UGT2B includes seven members (UGT2B4, 2B7, 2B10, 2B11, 2B15, 2B17, and 2B18) and five pseudogenes (UGT2B24P, 2B25P, 2B26P, 2B27P, and 2B29P) (Mackenzie *et al.*, 2005). In contrast to the UGT1 family, the UGT2 family is encoded by separate genes clustered on chromosome 4q13 (Fig.1.4B). Each UGT2 gene comprises six exons that are not shared between the UGT2 family members, excepting UGT2A1 and 2A2 which are encoded by seven exons (Tukey and Strassburg, 2000; Mackenzie *et al.*, 2005). By contrast, the UGT2A3 gene is composed of six exons that are not shared with UGT2A1 and 2A2 (Mackenzie *et al.*, 2005).

The recently identified human UGT3 family comprises only two members, UGT3A1 and 3A2. They apparently consist of seven exons and are located on chromosome 5p13.2 (Mackenzie *et al.*, 2005). The human UGT8 family consists of a single gene (UGT8A1) that encodes UDP-galactose ceramide galactosyltransferase. The gene consists of five protein-coding exons on human chromosome 4q26 (Mackenzie *et al.*, 2005).

1.2.3.3 UGT membrane localization

The UGTs are membrane-bound glycoproteins consisting of approximately 530 amino acids in length localized in the ER and nuclear compartment of cells (Radominska-Pandya *et al.*, 1999) (Fig.1.5). The majority of the protein is in the ER lumen and is composed of two functional domains, the N-terminal and C-terminal domains. The first 25 or so residues of the N-terminal domain form a signal sequence that directs the enzyme to the ER and is later cleaved. Thus the length of the mature protein is between 500 and 510 residues (Kurkela *et al.*, 2003). The enzymes are 50-60 kDa in size and most of their mass is located in the ER lumen with the carboxyl-terminal 19–26 amino acids protruding into the cytoplasm with a single-pass 17-residue long transmembrane helix near the C-terminal domain (Meech and Mackenzie, 1998; Radominska-Pandya *et al.*, 1999). The presence of the transmembrane domain is a critical requirement for UGT activity, whereas the cytoplasmic domain seems to be a non-essential modulator of activity (Meech *et al.*, 1996). The N-terminal domain is primarily responsible for

binding aglycones, whereas the C-terminal domain binds the common co-substrate, UDPGA (Mackenzie, 1990).

Mammalian UGTs may function as dimers or higher oligomers (Meech and Mackenzie, 1997; Finel and Kurkela, 2008). Evidence for a functional dimerization between UGTs is provided by studies on mutated forms of UGT2B1. Catalytically active homodimers of the rat enzyme UGT2B1 that appear to interact through their amino terminal regions have been detected (Meech and Mackenzie, 1997). Homodimers of rat UGT1A6 (Ikushiro *et al.*, 1997), human UGT1A1 (Ghosh *et al.*, 2001), and human UGT1A9 (Kurkela *et al.*, 2003), and heterodimers of UGT2B1 and UGT1A6 (Ikushiro *et al.*, 1997) have also been detected by chemical cross-linking and co-immunopurification. It has been postulated that the stability of the interaction or the rates of dimerization may be governed by the specific UGT monomers involved and/or by interaction with substrate (Radominska-Pandya *et al.*, 1999).

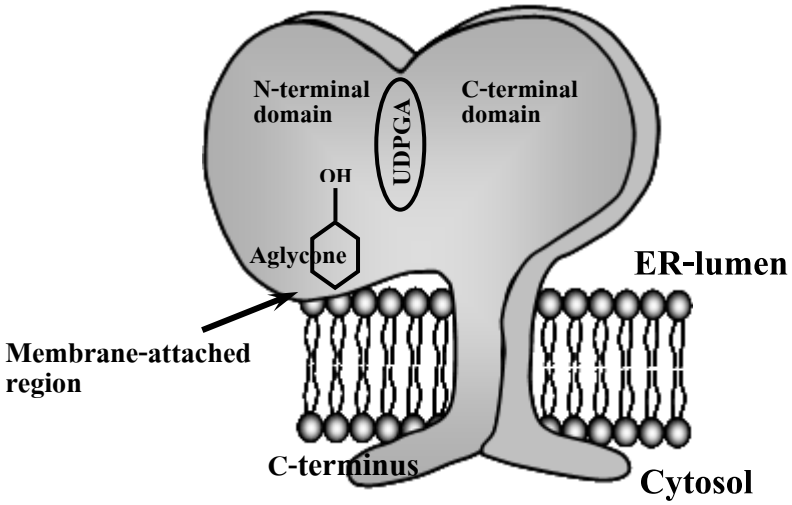

Figure 1.5 Schematic representation of human UGT topology.

(Modified from Radominska-Pandya *et al*., 1999 and Finel and Kurkela, 2008).

1.2.3.4 UGT isoenzyme selective substrates

UGTs have highly similar C-terminal domains and highly variable N-terminal domains, thereby imparting to each enzyme a distinct, but often overlapping set of substrate specificities (Meech and Mackenzie, 1998; Miners *et al.*, 2004 and 2006). Many studies have been carried out using chimeric constructs of different UGT cDNAs followed by expression of the hybrid protein. These data indicate that the N-terminal domain may be important in substrate selectivity of the different UGTs (Mackenzie, 1990; Mackenzie *et al.*, 2005). Mackenzie (1990) showed that exchanging the N-terminal half between two rat UGT2B forms, UGT2B2 and UGT2B3, resulted in switching of their respective substrate selectivities. In addition, site-directed mutagenesis studies have provided important insights into UGT structure-function relationships, particularly the importance of an N-terminal domain histidine. Mutation of the conserved N-terminal domain histidine to a proline in UGT 1A1, 1A6 and 1A9 (viz. UGT1A1(His39Pro), UGT1A6(His38Pro) and UGT1A9(His37Pro)) resulted in proteins that lacked the ability to metabolize 4-methylumbelliferone (4-MU), 1-naphthol (1-NP) and naproxen, while all glucuronidated LTG. Conversely, the UGT2B7(His35Pro) mutation resulted in a protein that lacked activity towards all substrates. Substitution of leucine-40 for histidine in UGT2B10 provided an enzyme that glucuronidated 4-MU and 1-NP (Kerdpin *et al.*, 2009). The UGT1A3(His40Pro) mutation conferred LTG and trifluoperazine (TFP) glucuronidation, whereas the UGT1A4(Thr36Ile) conferred 1-NP and 4-MU glucuronidation (Kubota *et al.*, 2007). In contrast to the N-terminal domain, substrate selectivity is not associated with the C-terminal domain (Mackenzie, 1990; Ritter *et al.*, 1992; Meech *et al.*, 1996). For examples, exchanging the C-terminal 232 residues of the rat proteins UGT2B2 and UGT2B3 did not the affect substrate selectivity of either enzyme (Mackenzie, 1990), while substituting the C-terminal 231 amino acids of the rabbit enzymes UGT2B16 and UGT2B13 did not alter UGT2B16 substrate selectivity (Li *et al.*, 1997).

Furthermore, considerable effort has been directed toward predicting the substrate and inhibitor selectivities of human UGTs. Molecular modeling techniques including pharmacophore, 2D, and 3D quantitative structure-activity relationships (QSAR) have been developed (Sorich *et al.*, 2002; Smith *et al.*, 2003a and 2003b; Sorich *et al.*, 2008).

Pharmacophores represent a configuration of structural features associated with biological activity (in this case metabolism by an individual UGT form), and represent one of the most intuitive 3D-descriptors (Miners *et al.*, 2004; Smith *et al.*, 2004). Common features pharmacophores for UGT1A1, UGT1A4, and UGT1A9 include an essential glucuronidation feature and two hydrophobic domains, with the possible contribution of a hydrogen bond acceptor in the case of UGT1A9 (Sorich *et al.*, 2002; Smith *et al.*, 2003a and 2003b; Miners *et al.*, 2004; Smith *et al.*, 2004). This observation implies the ability of most UGTs to confer glucuronidation activity towards small hydrophobic compounds such as simple phenols (Smith *et al.*, 2004), although increasing structural complexity results in greater enzyme selectivity due to steric, polar and hydrophobic interactions (Miners *et al*., 2010).

To date, only limited numbers of enzyme-selective UGT substrates and inhibitors have been identified (Table 1.2) (Miners *et al.*, 2006 and 2010). Just two selective inhibitors have been characterized; hecogenin and FLZ, which inhibit UGT1A4 and UGT2B7, respectively (Uchaipichat *et al.*, 2006a and 2006b). Although apparently form selective substrates have been used as inhibitors in some studies, further confirmation of inhibition selectivity is advisable given previous experience with other enzyme systems (e.g. potent inhibition of CYP2D6 by the CYP3A4 substrate quinidine) (Miners *et al.*, 2006). Indeed, there is an evidence that bilirubin, a specific UGT1A1 substrate, may inhibit UGT1A4 (Ghosal *et al.*, 2004).

Table 1.2 Selective substrates of the major hepatically expressed human drug-metabolizing UGT enzymes (Taken from Miners *et al*., 2010).

Enzyme	Substrates	References
UGT1A1	Bilirubin; β-estradiol [a]; Etoposide	(Bosma *et al.*, 1994; Watanabe *et al.*, 2003; Lepine *et al.*, 2004; Itaaho *et al.*, 2008)
UGT1A3	Hexafluoro-1α, 25-dihydroxyvitamin D_3; R-lorazepam	(Court, 2005; Kasai *et al.*, 2005)
UGT1A4	1'-Hydroxymidazolam; Trifluoperazine	(Di Marco *et al.*, 2005; Uchaipichat *et al.*, 2006a; Zhu *et al.*, 2008)
UGT1A6	Deferiprone; Serotonin	(Krishnaswamy *et al.*, 2003; Benoit-Biancamano *et al.*, 2009)
UGT1A9	Mycophenolic acid; Phenylbutazone; Propofol; Sulfinpyrazone	(Bernard and Guillemette, 2004; Soars *et al.*, 2004; Court, 2005; Picard *et al.*, 2005; Kerdpin *et al.*, 2006; Nishiyama *et al.*, 2006)
UGT2B7	Denopamine; Epirubicin; 6α-Hydroxyprogesterone; 21-Hydroxyprogesterone; Morphine (3- and 6-glucuronidation); Zidovudine	(Barbier *et al.*, 2000; Innocenti *et al.*, 2001; Court *et al.*, 2003; Stone *et al.*, 2003; Court, 2005; Kaji and Kume, 2005; Bowalgaha *et al.*, 2007; Ohno *et al.*, 2008)
UGT2B15	S-oxazepam; S-lorazepam [b]	(Court *et al.*, 2002; Court, 2005)

[a] Probably partially selective, with a contribution from UGT1A3.

[b] Supporting experimental data not provided.

1.2.4 UDP-glucuronosyltransferase 2B7 (UGT2B7)

As noted above, UGT genes have been classified into UGT1A and UGT2B subfamilies. Among the UGT2B subfamily, UGT2B7 is the most important member since it conjugates a large variety of compounds (Coffman *et al.*, 1998; Radominska-Pandya *et al.*, 2001; Miners *et al.*, 2010). It is predominantly expressed in the liver, but tissue distribution analysis has also demonstrated expression in the GI tract, kidney, pancreas and brain (Radominska-Pandya *et al.*, 2001). Typical substrates of UGT2B7 are endogenous substances such as hydroxy metabolites of steroid hormones and bile acids (Jin *et al.*, 1993) and xenobiotics including drugs like morphine, COD, and other opioid derivatives (Coffman *et al.*, 1998; Court *et al.*, 2003), and carboxylic acid containing compounds that include nonsteroidal anti-inflammatory drugs (NSAIDs; ketoprofen, ibuprofen, diclofenac, and naprofen), the lipid reducer gemfibrozil or the antiepileptic VPA (Sakaguchi *et al.*, 2004), and a wide range of hydroxylated benzo(a)pyrene and 2-acetylaminofluorene derivatives (Jin *et al.*, 1993).

1.2.4.1 Structure of the UGT2B7 gene

Human UGTs belong to the GT1 family and are predicted to adopt a GT-B fold (Campbell *et al.*, 1997; Coutinho *et al.*, 2003; Breton *et al.*, 2006). There has been a significant effort to characterize the crystal structures of UGT enzymes in recent years. N-and C-terminal domain for UGT2B7 were identified using an *E. coli* expression strategy. The C-terminal domain of UGT2B7 (UGT2B7CT, residues 285-451) was well behaved and crystallized readily. The 1.8 Å resolution x-ray crystal structure of the UGT2B7CT was elucidated. The asymmetric unit contains two 2B7CT molecules that pack together to form an asymmetric dimer (Fig.1.6A). The 2B7CT structure is a globular domain with a Rossman-type fold (Fig.1.6B). At the core of the protein is a single parallel β-sheet consisting of six individual strands surrounded by seven α-helices (Miley *et al.*, 2007).

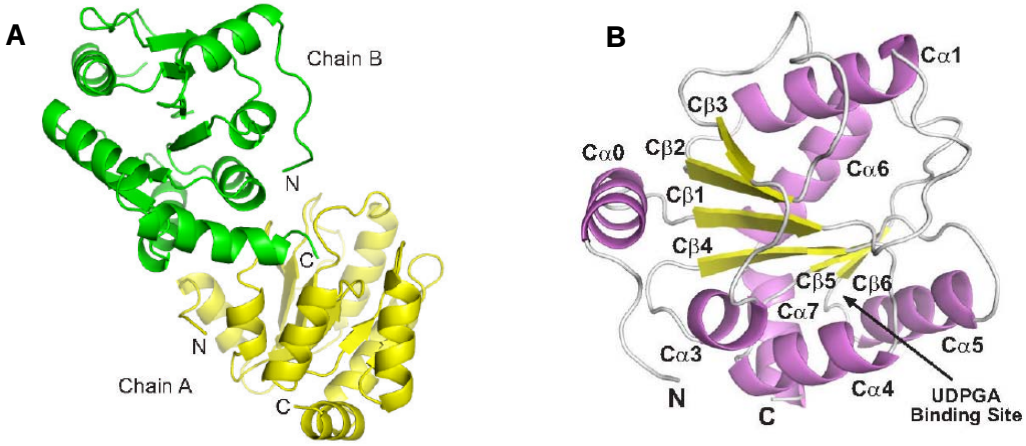

Figure 1.6 Overall structure of the UGT2B7CT (Taken from Miley *et al*., 2007):

A) Asymmetric dimer present in the crystallographic asymmetric unit.

B) Ribbon cartoon of UGT2B7CT with labeled secondary structure elements.

The UGT2B7 gene is composed of six exons spanning approximately 16 kb. The lengths of exons 1 to 6 are 721, 149, 132, 88, 220 and 531 bp, respectively, with introns ranging from 0.7 to 4.2 kb (Fig.1.7) (Carrier *et al.*, 2000). One major difference observed between UGT2B7 and the other UGT2B genes is the size of the introns, which are smaller than the corresponding portions of the other genes (Carrier *et al.*, 2000).

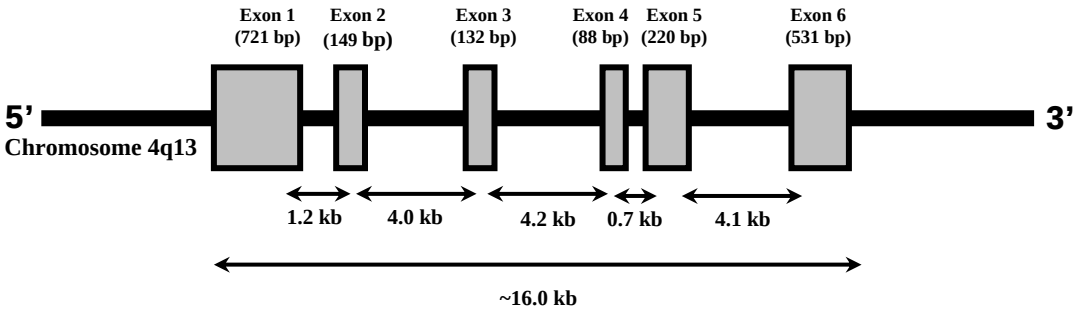

Figure 1.7 Structure of the human UGT2B7 gene**.**

(Modified from Carrier *et al*., 2000).

1.2.4.2 UDPGA binding site

A hallmark feature of GT-B fold-containing enzymes is the di-phosphate nucleotide sugar binding site formed by the C-terminal domain. Structurally characterized GT-B superfamily enzyme nucleotide-sugar binding sites utilize a common structural scaffold. However, the natures of the specific interactions with the donor ligands vary, even amongst enzymes in the same GT family (Miley *et al.*, 2007). The first suggestion that the UDPGA binding site is in the C-terminal domain was based on studies with chimeric UGTs (Mackenzie, 1990). Later, results from inhibitors directed at specific amino acids, photoaffinity labeling, and analysis of amino acid alignments confirmed that the UDPGA binding site is between residues 350 and 400; however, UDPGA interacts not only with the C-terminal but also with the N-terminal domains of UGT (Radominska-Pandya *et al.*, 1999). Comparison of UGT2B7CT with other GT1 family enzyme structures from bacteria and plants (GtfA and VvGT1) suggests that human UGT2B7 binds UDPGA with an analogous site (Fig.1.8). The UDPGA binding site in UGT seems to be remarkably similar to the UDP-glucose binding site in other GT1 enzymes (Mulichak *et al.*, 2001; Li *et al.*, 2007; Miley *et al.*, 2007). Although the majority of secondary structure elements are similar, all structures significantly differ in both length and secondary structure for the amino acids connecting Cβ2 and Cβ3. In VvGT1, both a 3/10 helix and α-helix Cα2 are present in this region, while in both 2B7CT and GtfA a shorter loop structure is observed (Miley *et al.*, 2007).

Furthermore, the UDPGA binding site has been studied by chemical modification (Ouzzine *et al.*, 2000) and site-directed mutagenesis (Miley *et al.*, 2007) to elucidate the specific residues making contacts with UDPGA. The site-directed mutagenesis implicates several residues interacting with the: 1) uracil base, 2) phosphate, or 3) glucuronic acid of the predicted UDPGA binding region.

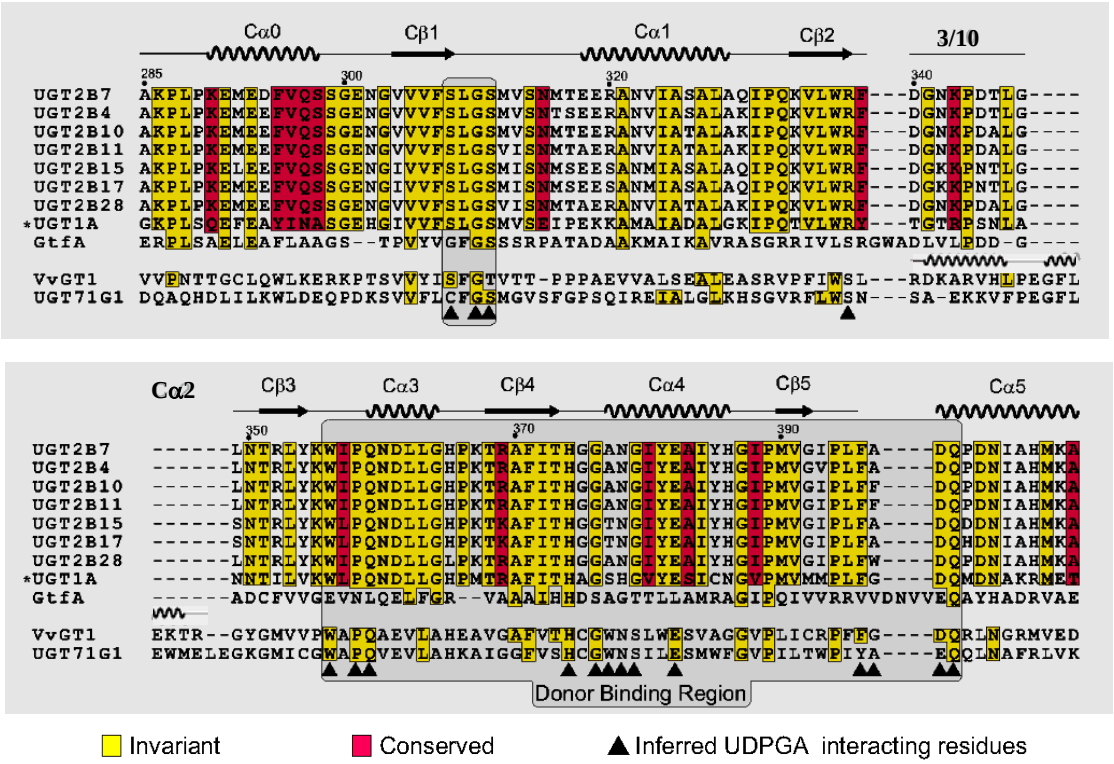

Figure 1.8 Partial sequence alignments of GT1 family enzymes.

(Modified from Miley *et al*., 2007).

Mutations at residues predicted to interact with the di-phosphate and glucuronic acid moiety have suggested significant effects on UGT2B7 function. Mutation at His374 virtually eliminates activity. It has been revealed that His374 assists in neutralizing the negative charge on the β-phosphate where the di-phosphate moiety is predicted to bind (Li *et al.*, 2007; Miley *et al.*, 2007). Mutation at several residues interacting with the di-phosphate moiety suggests that Asn378 is predicted to hydrogen bond to α-phosphate; Gly379 is involved with a pocket formed underneath the α-phosphate; and Thr373 is predicted to interact with the α-phosphate via a water- or ion-mediated contact (Miley *et al.*, 2007). Several residues are predicted to hydrogen bond to the glucuronic acid moiety. Asp398 and Gln399 are predicted to interact with O3'/O4' and O2'/O3' atoms of glucuronic acid, respectively. Mutation of Asp398 is suggested that a negative charge, not just hydrogen bonding potential, is important at this position. In addition, mutation at Asn378 is predicted to involve with donor sugar selectivity (Miley *et al.*, 2007).

1.2.4.3 Aglycone binding site

As mentioned above, the C-terminal domain binds UDPGA, whereas the N-terminal domain, which is formed from first 260 amino acids of the mature protein, binds the aglycone (Mackenzie, 1990). An N-terminal membrane-region located between residues 140-240 may be needed to help highly lipophilic substances to reach the active site of the enzyme (Radominska-Pandya *et al.*, 2005). Maltose binding protein (MRP) fusion constructs with the N-terminal domain of UGT2B7 were analyzed by nuclear magnetic resonance (NMR) spectroscopy and used to identify the opioid binding site of UGT2B7 (Coffman *et al.*, 2001 and 2003). The results demonstrated that the binding site of morphine in UGT2B7 is within amino acids 84 to 118 of the N-terminal domain (Coffman *et al.*, 2003). Furthermore, a recent paper provides evidence for multiple substrate binding and effector sites of UGT2B7 (Uchaipichat *et al.*, 2008). Multisite modeling of kinetic and inhibition data is consistent with the existence of two "catalytic" sites for AZT, 4-MU, and 1-NP within the UGT2B7 substrate binding domain. The complex interaction observed between UGT2B7 substrates, which includes activation and inhibition (due either to competitive displacement or changes in the substrate dissociation constant (K_s) or the maximum velocity (V_{max}) via an effector site), indicates that careful experimental design and kinetic interpretation are necessary for DDIs studies involving this enzyme (Uchaipichat *et al.*, 2008).

1.2.4.4 Catalytic mechanism of UGT2B7

A homology model of UGT2B7 showed that UGT2B7 has residues analogous to VvGT1 at key catalytic positions (Miley *et al*., 2007). Human UGT2B7 use a serine hydrolase-like catalytic mechanism where His35 and Asp151 function as a catalytic diad. His35 is involved in deprotonation of the phenolic group of the acceptor ligand, facilitating nucleophilic attack at the C1 atom of glucuronic acid (Fig.1.9).

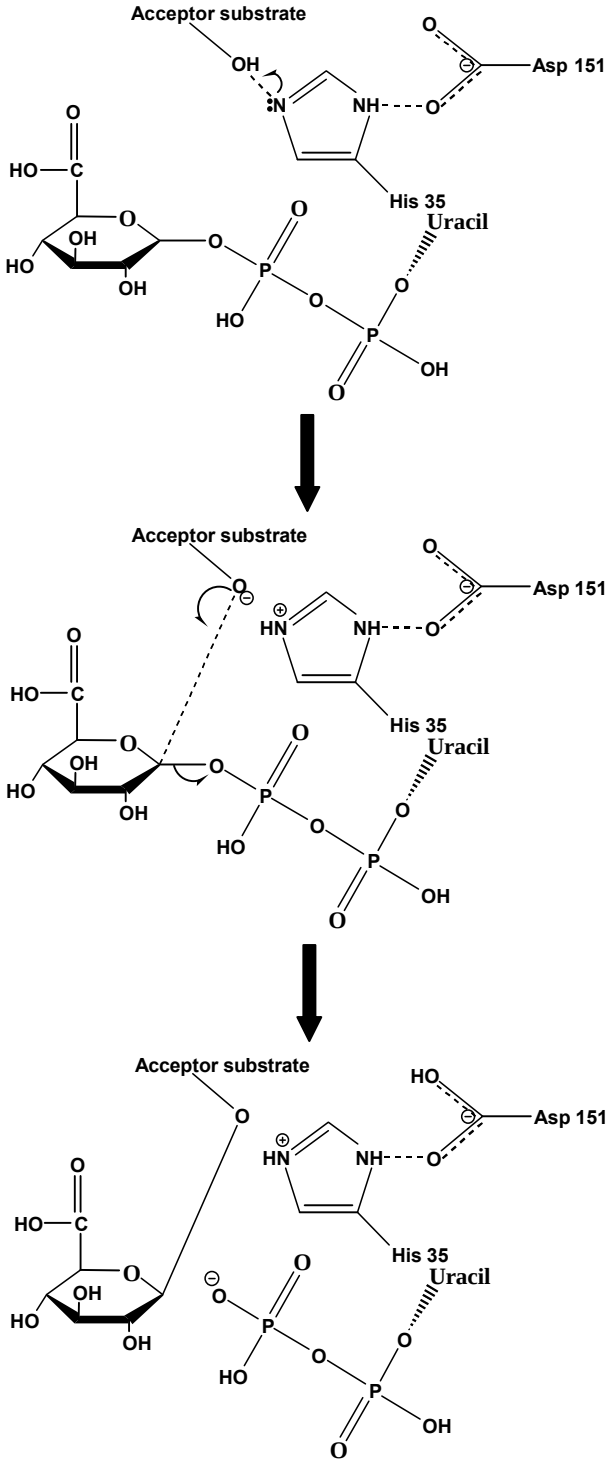

Figure 1.9 Proposed catalytic reaction mechanism for human UGT2B7.

(Modified from Miley *et al*., 2007).

Protonated His35 is stabilized by a neighboring aspartic acid at position 151. The His35 residue predicted in the active site of UGT2B7 is invariant in both human and plant enzymes, while the stabilizing aspartic acid is invariant in humans and the vast majority of plant enzymes (Miley *et al.*, 2007).

1.2.5 Analysis of enzyme kinetics

Enzyme kinetics is the study of the chemical reactions that are catalyzed by enzymes. In enzyme kinetics, the reaction rate is measured and the effects of varying assay conditions on the reaction investigated. Enzyme kinetic studies may also reveal insights into the catalytic mechanism of enzyme, its role in metabolism, how its activity is controlled, and how a drug or other compound might inhibit the enzyme. It usually starts with the investigation of the behavior of the enzyme substrate and its conversion into product. The next steps are the examination of the role of cofactors, inhibitors or activators (Bisswanger, 2008).

1.2.5.1 Graphical determination of the K_m and V_{max} parameters

Because the enzyme velocity versus substrate concentration curve (Fig.1.10A) is a hyperbolic (non-linear plot), it is extremely difficult to determine V_{max} and K_m. Several disadvantages mentioned previously for non-linear plots can be eliminated by applying linearization methods (Marangoni, 2003). The kinetic constants can be derived easily from axis intercepts or from the slopes of the straight lines. In addition, an important advantage of linearization methods is the analysis of enzyme kinetic methods when two or more ligands are varied, as in enzyme inhibitions or multiple substrate reactions. The respective mechanisms can be identified from the resulting straight line pattern. There are many simple linear transformations of the Michaelis-Menten equation such as Lineweaver-Burk plot, Hanes-Woolf plot, Eadie-Hofstee plot etc. (Fig.1.10) (Segel, 1993; Marangoni, 2003).

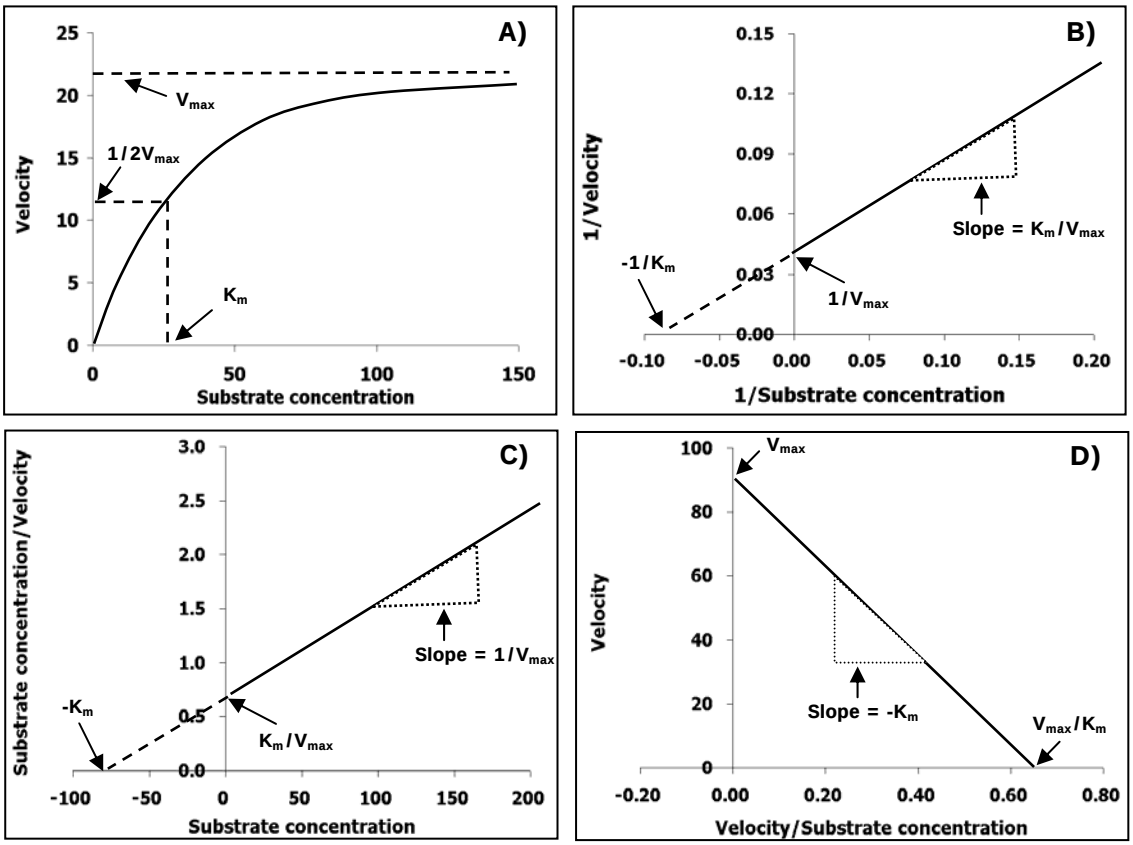

Figure 1.10 Representative different plots of the Michaelis-Menten kinetic (Modified from Segel, 1993 and Bisswanger, 2008):

A) Direct plot (enzyme velocity versus substrate concentration).

B) Lineweaver-Burk plot.

C) Hanes-Woolf plot.

D) Eadie-Hofstee plot.

1.2.5.2 Typical enzyme kinetics and Michaelis-Menten approach

The general rate equation for reaction based on a single site substrate-enzyme interaction was proposed by Henri in 1903. Henri's equation accounted for the observation that the initial rate of a reaction was directly proportional to the concentration of enzyme preparation, but increased in a nonlinear manner with increasing substrate concentration up to a limiting maximum rate. Ten year later Michaelis and Menten confirmed Henri's equation and presented a slightly modified version of the rate equation. The derivation of this approach was based on the following assumptions (Segel, 1993):

a) The enzyme (E) is a catalyst.

b) The E and substrate (S) react rapidly to form an enzyme-substrate (ES) complex.

c) Only a single S and a single ES complex are involved and the ES complex breaks down directly to form free E and product (P).

d) E, S, and the ES complex are at equilibrium; that is, the rate at which ES dissociation to E + S is much faster than the rate at which ES breaks down to form E + P.

e) The substrate concentration [S] is very much larger than the enzyme concentration [E] so that the formation of an ES complex does not alter the [S].

f) The overall rate of the reaction is limited by the breakdown of the ES complex to form free E and P.

g) The velocity (υ) is measured during the very early stages of the reaction so that the reverse reaction is insignificant.

These assumptions are called the quasi-equilibrium or rapid equilibrium assumption. The overall reaction may be described as:

$$\mathbf{E + S} \underset{k_{-1}}{\overset{k_1}{\rightleftharpoons}} \mathbf{ES} \xrightarrow{k_P} \mathbf{E + S + P}$$

where, E, S, ES and P represent enzyme, substrate, enzyme-substrate complex and product, respectively. This reaction is described by the Michaelis-Menten equation:

$$\upsilon = \frac{V_{max} \times [S]}{K_m + [S]} \qquad \text{equation 1.1}$$

where, υ is the metabolic rate or velocity, [S] is the substrate concentration, V_{max} is the maximum velocity, and K_m (k_{-1}/k_1) is the Michaelis-Menten constant (concentration giving $0.5V_{max}$) (Segel, 1993).

1.2.5.3 'Atypical' enzyme kinetics

Assumptions of the Michaelis-Menten equation implicit are the substrate-enzyme interaction occurs at only one site per enzyme and that each site operates independently from others. However, many drug metabolism reactions catalyzed by CYP and UGT exhibit non hyperbolic or 'atypical' kinetic behavior (Houston and Kenworthy, 2000; Uchaipichat *et al.*, 2004 and 2006b). In cooperative kinetics, binding of one substrate molecule induces structural and/or electronic changes that result in altered substrate binding affinities in the remaining vacant sites. The substrate binding affinities can theoretically be either increased (positive cooperativity) or decreased (negative cooperativity). Binding of substrate and nonsubstrate ligands which can act as activators or inhibitors at a site other than the active site can affect on enzyme activity. These responses can be homotropic or heterotropic. Homotropic responses refer to the allosteric modulation of enzyme activity strictly by substrate molecules and heterotropic responses refer to the allosteric modulation of enzyme activity by nonsubstrate molecules or combinations of substrate and nonsubstrate molecules (Marangoni, 2003).

There are three approaches, 'naïve', empirical, and mechanistic, which are generally applied to the analysis of atypical kinetics in vitro. The first approach utilizes the Michaelis–Menten equation regardless of the kinetic behavior observed, ignoring any evidence of sigmoidicity or convexity in the rate-substrate concentration profile. Use of empirical models represents a useful tool for the preliminary analysis of data. However, this approach provides no

mechanistic information of the interactions between homotropic or heterotropic ligands. Mechanistic approaches use multisite kinetic models that allow the simultaneous fit of multiple sets of data to a single equation (Houston and Kenworthy, 2000; Houston and Galetin, 2005).

A-1) Empirical modeling approaches for homotropic cooperative

Homotropic effects represent alterations in either binding affinity or rate of product formation after the binding of a second molecule of the same substrate to the enzyme active site. Enzyme activity may be either increased in a substrate concentration-dependent manner (sigmoidal kinetic profiles defined as autoactivation) or decreased (convex kinetic profiles defined as substrate inhibition and apparent biphatic kinetics) (Ueng *et al.*, 1997; Shou *et al.*, 1999; Lin *et al.*, 2001; Galetin *et al.*, 2002).

a) Autoactivation or sigmoidal kinetics

Autoactivation (positive homotropic cooperativity) results in increased binding affinity for a second substrate molecule. The rate versus substrate concentration plot is sigmoidal while the Eadie-Hofstee plot shows a boomerang shape (Fig.1.11B). The sigmoidal rate plot can be described by the Hill equation (equation 1.2) (Houston and Kenworthy, 2000):

$$\upsilon = \frac{V_{max} \times [S]^n}{S_{50}^n + [S]^n} \qquad \text{equation 1.2}$$

where substrate concentration resulting in 50% of V_{max} (S_{50}) is analogous to the K_m parameter, and n is the Hill coefficient reflecting the degree of sigmoidicity. In terms of clearance, the sigmoidal rate plot translates to a gradual increase in the clearance as substrate concentration is increased to reach a maximum followed by a decrease in the clearance due to saturation, as seen for the Michaelis-Menten case (Houston and Kenworthy, 2000). Equation 1.3 describes the relationship between the various parameters in the Hill equation and the maximum clearance (CL_{max}):

$$CL_{max} = \frac{V_{max}}{S_{50}} \times \frac{(n-1)}{n(n-1)^{1/n}} \qquad \text{equation 1.3}$$

Recently, sigmoidal or autoactivation kinetics have been observed in vitro for both CYP and UGT catalyzed reactions. For examples, the CYP3A4-catalyzed oxidation of testosterone (Ueng *et al.*, 1997) and carbamazepine (Korzekwa *et al.*, 1998), and CYP2C9-mediated dapsone hydroxylation (Korzekwa *et al.*, 1998) exhibit sigmoidal kinetics. Similarly, the formation of estradiol-3-glucuronide by UGT1A1 (Fisher *et al.*, 2000), 4-methylumbelliferone-β-D-glucuronide by UGT2B7 (Uchaipichat *et al.*, 2004), 1-naphthol-β-D-glucuronide by UGT1A9 (Uchaipichat *et al.*, 2004) show autoactivation kinetics. The kinetic of VPA glucuronide formation is also characteristic of autoactivation kinetics, both in vivo in adult sheep and in vitro in sheep liver microsomes (Wong *et al.*, 2007).

b) Substrate inhibition

A substrate that causes a decrease in the rate of product formation as its concentration increases will lead to a reaction that displays substrate inhibition kinetics (Lin *et al.*, 2001). With substrate inhibition, the Eadie-Hofstee plot is convex (Fig.1.11C). This reaction can be considered to be analogous to an uncompetitive type of inhibition mechanism. The initial clearance of substrate inhibition follows Michaelis-Menten kinetics; however, this parameter decreases more rapidly in the saturation portion of the curve due to the impact of the inhibition effect (Houston and Kenworthy, 2000). Substrate inhibition is described by the following equation 1.4:

$$\upsilon = \frac{V_{max}}{(1 + (K_m/[S]) + ([S]/K_{si}))} \quad \text{equation 1.4}$$

where K_{si} is the constant describing the substrate inhibition interaction. Of the CYP-mediated reactions, substrate inhibition is commonly observed; for examples CYP2D6-catalyzed *O*-demethylation of dextromethorphan, CYP3A4-catalyzed 6β-hydroxylation of testosterone, and CYP2C9-catalyzed methyl-hydroxylation of celecoxib (Lin *et al.*, 2001). This kinetic behavior is also observed for substrates metabolized by UGT enzymes; for examples the formation of 4-methylumbelliferone-β-D-glucuronide by UGT1A9 (Tsoutsikos *et al.*, 2004) and TFP glucuronidation by UGT1A4 (Uchaipichat *et al.*, 2006a).

c) Apparent biphasic kinetics

Negative cooperativity can alternatively lead to an apparent biphasic velocity versus substrate concentration curve that is frequently observed in two enzyme reactions. Here a high-affinity, low-capacity enzyme and a low-affinity, high-capacity enzyme contribute to a particular metabolic reaction (Houston and Kenworthy, 2000). The Eadie-Hofstee plot shows that the two components are clearly separated by a difference in their affinities for each enzyme (Fig.1.11D). This kinetics can be described by equation 1.5:

$$\upsilon = \frac{V_{max1} \times [S]}{K_{m1} + [S]} + \frac{V_{max2} \times [S]}{K_{m2} + [S]} \qquad \text{equation 1.5}$$

There are many examples of biphasic kinetics for CYP enzymes. Naphthalene metabolism by CYP3A4 and naproxen metabolism by CYP2C9 demonstrated apparent biphasic kinetics suggestive of a low K_m, low V_{max} and K_m, high V_{max} components. Similar to CYP enzymes, morphine 3-glucuronide and morphine 6-glucuronide formation by UGT2B7 exhibited the apparent biphasic kinetic (Stone *et al.*, 2003).

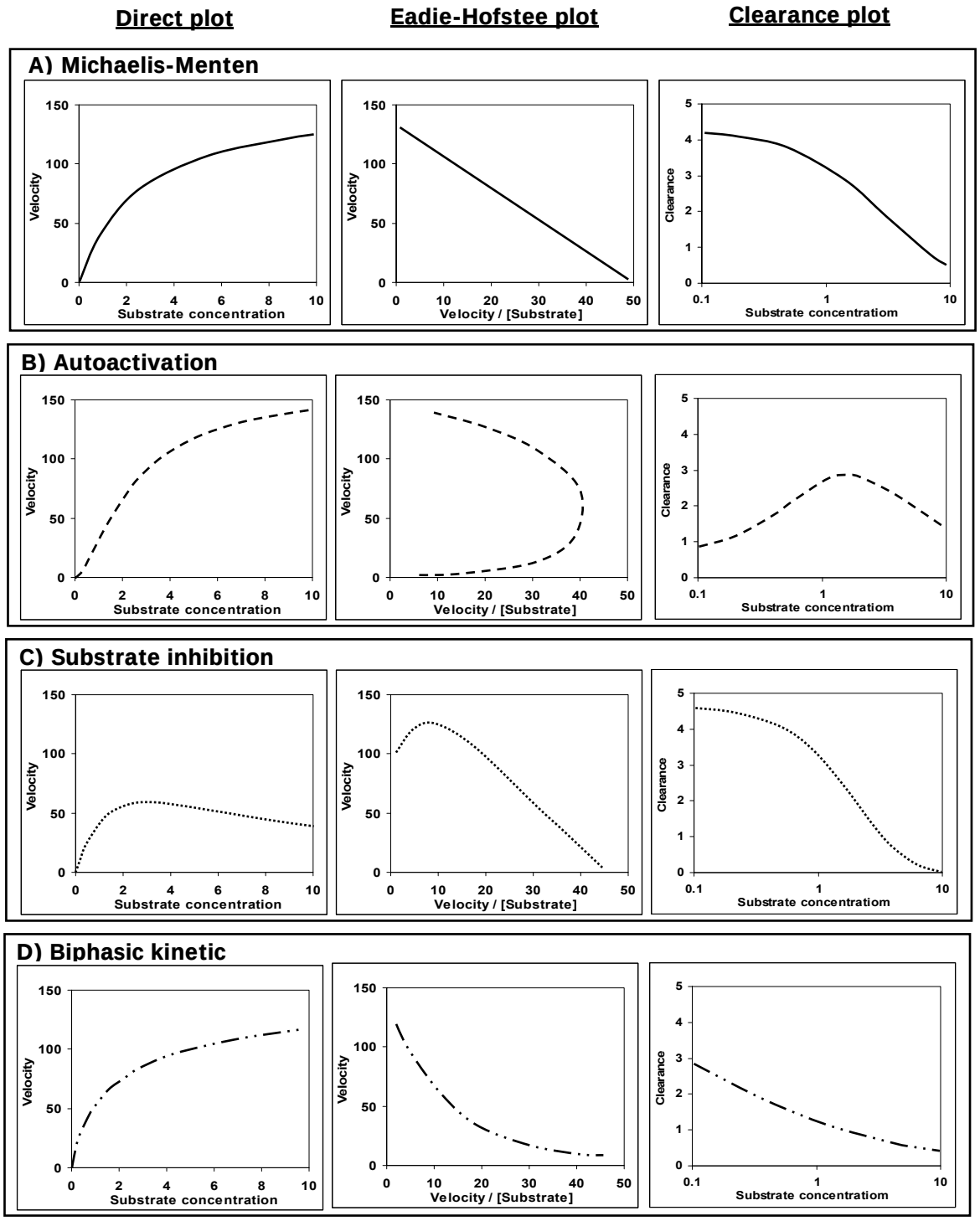

Figure 1.11 Representative kinetic profiles for Direct plot, Eadie-Hofstee plot, and clearance plot (Modified from Houston & Kenworthy, 2000).

A-2) Mechanistic approach for homotropic cooperativity

Atypical kinetics in vitro can be analyzed by a mechanistic approach, the use of multisite kinetic models. This approach is based on the same rapid equilibrium/steady-state principles as the single-site Michaelis–Menten equation (Segel, 1993; Houston and Galetin, 2005). The simplest model accommodating atypical kinetic properties when two molecules of the same substrate bind to the active site is presented in the Fig.1.12. Two binding sites, substrate-enzyme (SE) and ES complex, are identical and no orientation differences in binding of S to E occurs (Segel, 1993; Houston and Kenworthy, 2000; Galetin *et al.*, 2002).

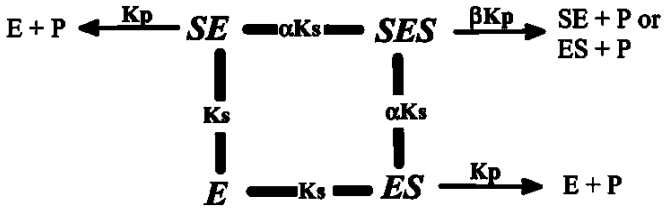

Figure 1.12 A kinetic model for an enzyme with two-substrate binding sites, where the second substrate (S) molecule binds cooperatively (Taken from Geletin *et al*., 2002).

This scheme is represented by following equation:

$$\frac{\upsilon}{V_{max}} = \frac{\frac{[S]}{K_s} + \frac{\beta[S]^2}{\alpha K_s^2}}{1 + \frac{2[S]}{K_s} + \frac{[S]^2}{\alpha K_s^2}} \qquad \text{equation 1.6}$$

In this scheme K_s represents the substrate dissociation constant and K_p is the effective catalytic rate constant. For enzymes with two binding sites, V_{max} is equivalent to $2K_p/[E]_t$, where $[E]_t$ is the total enzyme concentration. The K_s and K_p values change by the interaction factors α and β, respectively (Houston and Kenworthy, 2000). Autoactivation (positive cooperativity) may be a result of either increased binding affinity for a second substrate molecule (K_s changes by the factor $\alpha < 1$), or changes in the K_p by the factor β in the two-substrate-bound complex ($\beta > 1$). In contrast, a negative cooperative effect is observed when the value of α is > 1, resulting in an apparent biphasic kinetics, or when the value of β is < 1, resulting in substrate

inhibition. However, combination of both positive and negative cooperativity may occur when both α and β change simultaneously. Furthermore, it should be mentioned that Michealis-Menten kinetics follow from this equation when α and β are equal to 1 (no interaction between the two substrate binding sites) (Houston and Kenworthy, 2000; Galetin *et al.*, 2002, 2003; Atkins, 2005; Houston and Galetin, 2005).

A-3) Heterotropic cooperativity

In contrast to homotropic cooperativity, heterotropic effects involving two different substrates may result either in activation or inhibition of the rate of product formation (Ueng *et al.*, 1997). In this case, the drug acting as substrate may yield classic hyperbolic behavior, but the second drug acting as modifier (activator or inhibitor) induces non-hyperbolic behavior (Korzekwa *et al.*, 1998; Kenworthy *et al.*, 2001; Galetin *et al.*, 2002). Multisite kinetic equilibria models for both two-site and three-site models adopted from Segel (1993) are based on steady-state and rapid equilibrium approach allowing the simultaneous fit of multiple sets of data to a single equation (Segel, 1993; Galetin *et al.*, 2002).

a) Two-Site Model

A generic two-site model has been used to describe various effects on CYP3A4 such as an activation of substrate metabolism and different types of inhibition, including mixed, partial, and competitive inhibition for substrates with hyperbolic or substrate inhibition kinetic properties (Kenworthy *et al.*, 2001; Galetin *et al.*, 2002, 2003; Houston and Galetin, 2005). Heterotropic cooperativity (either negative or positive effect) can be described by the generic two-site model (Fig.1.13A and equation 1.7). In the generic two-site model, the corresponding interaction factors associated with changes in binding affinity (K_s or K_i) are α-homotropic cooperativity, and δ-heterotropic cooperativity. The interaction factors associated with rate of product formation (K_p) are β (from SES, substrate-enzyme-substrate, complex) and γ (from MES, modifier-enzyme-substrate, complex), where M is modifiers, either activators (A) or inhibitors (I). This model can be applied to both activation (A, K_a) and inhibition (I, K_i) (Houston and Galetin, 2005).

a-1) Heterotropic inhibition or activation of a substrate with hyperbolic kinetics

Equation 1.7 is applied to substrates showing hyperbolic type (Michaelis-Menten) kinetics in the absence of modifiers. No interaction is observed between the substrate molecules (autoactivation); therefore, the kinetic model is simplified eliminating the interaction factor α. In addition, this model can be used to describe the partial inhibition when the formation of a complex containing two different substrate molecules is more or less favorable, depending on the δ value implying the changes in the binding affinities of the substrate and the modifier in the presence of each other. The interaction factor γ affecting alterations in product formation in the presence of a modifier molecule is defined by $\gamma < 1$ for inhibition and $\gamma > 1$ for activation (Table 1.3) (Galetin *et al.*, 2002).

a-2) Heterotropic inhibition of a substrate with substrate inhibition kinetics

A generic two-site model, with only one catalytically active site, has been applied to compounds showing substrate inhibition kinetic. It is assumed that the substrate inhibition site can not be occupied until the active site is filled (sequential binding of substrate molecules). The presence of a modifier molecule in the second binding site causes a decrease in product formation from SES complex, defined by the factor β (< 1) (equation 1.8). When γ is comparable to β (Table 1.3), the effect of a modifier is analogous to the binding of a second substrate molecule, and the substrate inhibition phenomenon remains.

b) Three-Site Model

A three-site model is more complex and describes kinetic behavior where both substrate and effector bind to two sites, and one site is unique to either molecule (Kenworthy *et al.*, 2001). This model shows the existence of a distinct effector binding site, with the possibility of conformational changes upon the binding of the effector molecule (Ueng *et al.*, 1997).

b-1) Heterotropic inhibition of a substrate showing sigmoidal kinetics

The model presented in Fig.1.13B describes the inhibition of substrates showing sigmoidal kinetics. In the absence of the inhibitor, the substrate binds cooperatively with an interaction factor α (< 1); however, the interaction between two substrate binding sites resulting in an increase in the affinity of the vacant substrate sites is prevented in the presence of the inhibitor. An alteration in the K_i value by the interaction factor δ (< 1) is caused by the increased affinity of SE or ES and SES complexes (equation 1.9) (Kenworthy *et al.*, 2001; Galetin *et al.*, 2002, 2003).

b-2) Heterotropic activation of a substrate showing sigmoidal kinetics

A three-site model for heterotropic activation is shown in Fig.1.13C and equation 1.10 describes the activation of a substrate showing sigmoidicity. The two substrate binding sites describe the cooperativity observed when the substrate is incubated alone and an activator molecule mimics the cooperative effects of the second substrate molecule and stimulates the metabolism of the substrate at a distinct activator site (Kenworthy *et al.*, 2001).

b-3) Partial inhibition of a substrate showing sigmoidal kinetics

Similar to previous three-site model, cooperativity in substrate binding is maintained in the presence of an inhibitor. Binding of an inhibitor molecule to the separate effector site causes an alteration in K_i by the factor δ (Fig.1.13D and equation 1.11). Where the interaction factor δ is > 1, the affinity of the second inhibitor molecule is decreased in the presence of the first inhibitor molecule which is consistent with a negative cooperative effect, and this effect contributes to the partial inhibition with the increasing inhibitor concentration. The concentration and contribution of I(SEI), I(SE), and I(SES) complexes to the $[E]_t$ at higher inhibitor concentration is increased, but these enzyme species are not productive (Galetin *et al.*, 2002).

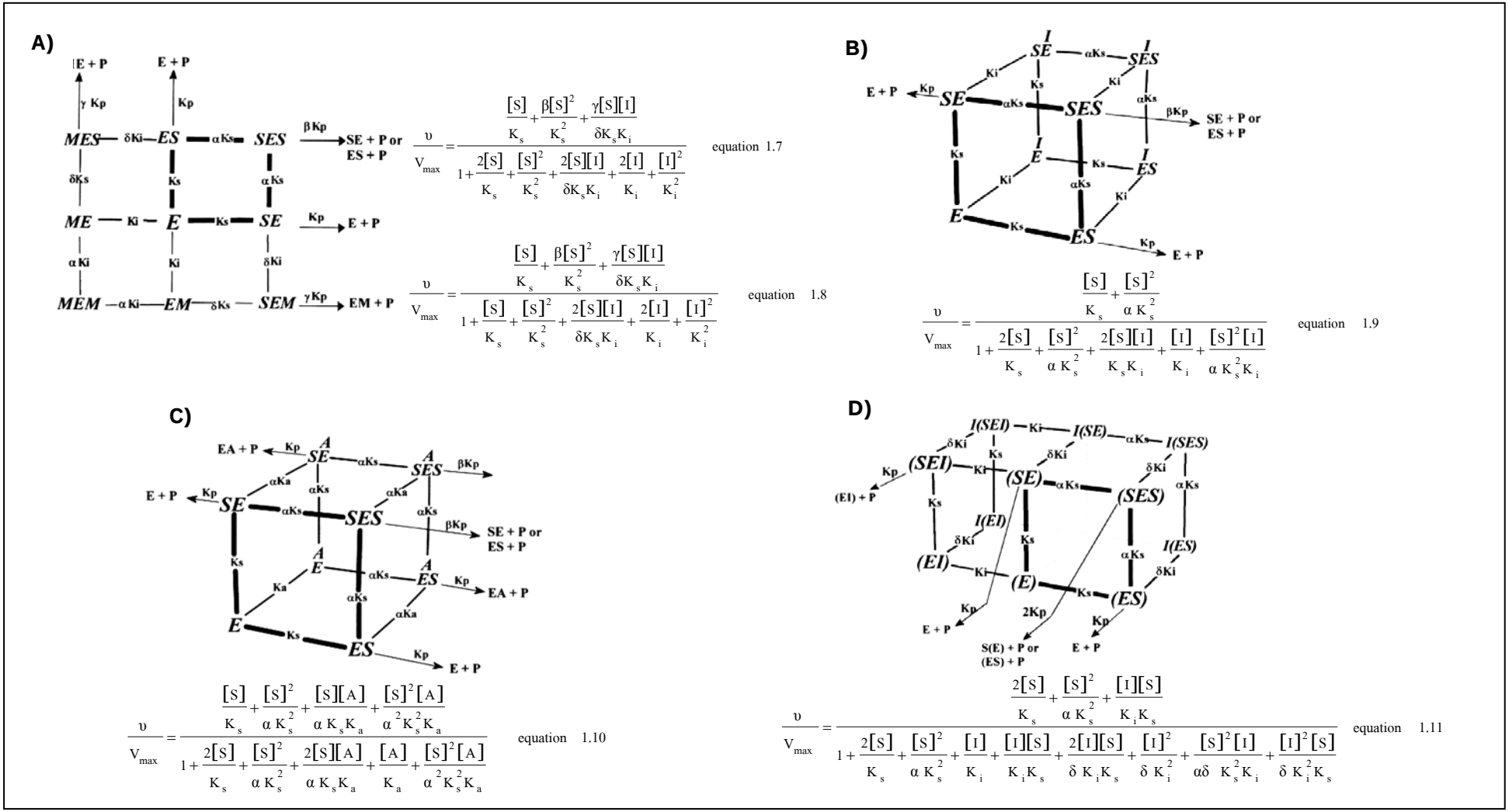

$$\frac{\upsilon}{V_{max}} = \frac{\frac{[S]}{K_s} + \frac{\beta[S]^2}{K_s^2} + \frac{\gamma[S][I]}{\delta K_s K_i}}{1 + \frac{2[S]}{K_s} + \frac{[S]^2}{K_s^2} + \frac{2[S][I]}{\delta K_s K_i} + \frac{2[I]}{K_i} + \frac{[I]^2}{K_i^2}} \quad \text{equation 1.7}$$

$$\frac{\upsilon}{V_{max}} = \frac{\frac{[S]}{K_s} + \frac{\beta[S]^2}{K_s^2} + \frac{\gamma[S][I]}{\delta K_s K_i}}{1 + \frac{[S]}{K_s} + \frac{[S]^2}{K_s^2} + \frac{2[S][I]}{\delta K_s K_i} + \frac{2[I]}{K_i} + \frac{[I]^2}{K_i^2}} \quad \text{equation 1.8}$$

$$\frac{\upsilon}{V_{max}} = \frac{\frac{[S]}{K_s} + \frac{[S]^2}{\alpha K_s^2}}{1 + \frac{2[S]}{K_s} + \frac{[S]^2}{\alpha K_s^2} + \frac{2[S][I]}{K_s K_i} + \frac{[I]}{K_i} + \frac{[S]^2[I]}{\alpha K_s^2 K_i}} \quad \text{equation 1.9}$$

$$\frac{\upsilon}{V_{max}} = \frac{\frac{[S]}{K_s} + \frac{[S]^2}{\alpha K_s^2} + \frac{[S][A]}{\alpha K_s K_a} + \frac{[S]^2[A]}{\alpha^2 K_s^2 K_a}}{1 + \frac{2[S]}{K_s} + \frac{[S]^2}{\alpha K_s^2} + \frac{2[S][A]}{\alpha K_s K_a} + \frac{[A]}{K_a} + \frac{[S]^2[A]}{\alpha^2 K_s^2 K_a}} \quad \text{equation 1.10}$$

$$\frac{\upsilon}{V_{max}} = \frac{\frac{2[S]}{K_s} + \frac{[S]^2}{\alpha K_s^2} + \frac{[I][S]}{K_i K_s}}{1 + \frac{2[S]}{K_s} + \frac{[S]^2}{\alpha K_s^2} + \frac{[I]}{K_i} + \frac{[I][S]}{K_i K_s} + \frac{2[I][S]}{\delta K_i K_s} + \frac{[I]^2}{\delta K_i^2} + \frac{[S]^2[I]}{\alpha\delta K_s^2 K_i} + \frac{[I]^2[S]}{\delta K_i^2 K_s}} \quad \text{equation 1.11}$$

Figure 1.13 Multisite kinetic equilibria models for heterotropic cooperativity (Taken from Kenworthy *et al*., 2001; Geletin *et al*., 2002:

A) A generic two-site model; Heterotropic inhibition or activation of a substrate showing hyperbolic kinetics (equation 1.7) and Heterotropic inhibition of a substrate with substrate inhibition kinetic (equation 1.8).

B) Three-site model; Heterotropic inhibition of a substrate showing sigmoidal kinetics (equation 1.9).

C) Three-site model; Heterotropic activation of a substrate showing sigmoidal kinetics (equation 1.10).

D) Three-site model; Partial inhibition of a substrate showing sigmoidal kinetics (equation 1.11).

Table 1.3 Multisite kinetic model interaction factors to describe the various modifications of CYP3A4 activity (Modified from Gelatin *et al*., 2002).

Kinetic models	Effect on CYP3A4	Interaction factors			Examples
		α	γ^a	δ	
Two-site model	Heterotropic activation	1	> 1	< 1	Quinidine effect on diclofenac (Ngui *et al.*, 2000) Quinidine effect on warfarin (Ngui *et al.*, 2001) Quinidine effect on filodipine and simvastatin (Galetin *et al.*, 2002)
Hyperbolic kinetics	Heterotropic inhibition	1	< 1	< 1	Haloperidol effect on filodipine and quinidine (Houston *et al.*, 2003)
	Partial inhibition	1	1	> 1	Testosterone effect on erythromycin (Wang *et al.*, 1997) Testosterone effect on terfenadine (Riedy *et al.*, 2000) Testosterone effect on midazolam (Riedy *et al.*, 2000; Houston *et al.*, 2003) Nifedipine effect on filodipine (Houston *et al.*, 2003)
Substrate inhibition	Heterotropic inhibition	1	$< 1^b$	< 1	Quinidine and haloperidol effect on nifedipine (Galetin *et al.*, 2002) Midazolam and filodipine effect on nifedipine (Houston *et al.*, 2003)
Three-site model	Heterotropic activation	< 1	> 1	$= \alpha$	Testosterone effect on diazepam (Kenworthy *et al.*, 2001)
Sigmoidal kinetics	Heterotropic inhibition	< 1	1	≤ 1	Diazepam effect on testosterone (Kenworthy *et al.*, 2001) Quinidine effect on testosterone (Galetin *et al.*, 2002)
	Partial inhibition	< 1	1	> 1	Haloperidol effect on testosterone (Galetin *et al.*, 2002)

[a] β (chang in K_p from SES) = 2 (equivalent binding site); [b] ($\beta < 1$ or $\beta = \alpha$)

1.2.5.4 Consequences of ignoring atypical kinetics

Although atypical behavior is commonly seen in kinetic profiles, it is not always taken into account by investigators. Several examples exist of standard Michaelis-Menten hyperbolic curves forced through the data rather than the adoption of more suitable models. Here, errors and consequences when applied to in vivo clearance prediction may be highly significant (Houston and Kenworthy, 2000; Houston and Galetin, 2005). In the case of autoactivation (i.e. sigmoidal kinetics; Fig.1.11B), either underestimation or overestimation of the clearance value may occur if a hyperbolic curve is forced through the data to obtain the parameters V_{max} and K_m to calculate the in vitro intrinsic clearance (CL_{int}). Typically, underestimation of the CL_{int} results. In this case, the CL_{max} when the enzyme is fully activated represents the alternative to CL_{int} for scaling of in vitro data and has been proposed as an alternate scaling strategy (Houston and Galetin, 2003). For substrate inhibition, substantial underestimation of V_{max} will result from ignoring the high concentration data points and forcing a hyperbolic curve through the remaining lower substrate concentration points. Furthermore, the K_m value will also be poorly estimated (Houston and Galetin, 2005). Thus, a full description of the profile (namely, the number and quality of the data points) is important if CL_{int} is to be calculated from the V_{max}/K_m.

Another important consideration is determination K_i values from inhibition studies. Normally, the K_i value is obtained from equations fitted to data that account for the effect of various concentrations of inhibitor, including the absence of inhibitor. However, insufficient data points to allow examination of the effects of atypical kinetic profiles may result in the calculation of an inaccurate K_i value (Houston and Kenworthy, 2000).

.

1.2.5.5 Analysis of enzyme inhibition data

Any substrate that reduces the velocity of an enzyme-catalyzed reaction can be considered to be an inhibitor (either irreversible or reversible inhibitor). Irreversible inhibitors usually react with the enzyme and change it chemically. These inhibitors modify key amino acid residues needed for enzymatic activity. In contrast, reversible inhibitors bind non-covalently and different types of inhibition are produced depending on whether these inhibitors bind the enzyme, the enzyme-substrate complex, or both. In this section, only reversible inhibition is reviewed. There are four types of reversible enzyme inhibitors (Segel, 1993; Ito *et al.*, 1998b; Marangoni, 2003).

A-1) Competitive inhibition

Competitive inhibition arises when the inhibitor competes with the drug for the same binding site within an enzyme protein (Fig.1.14).

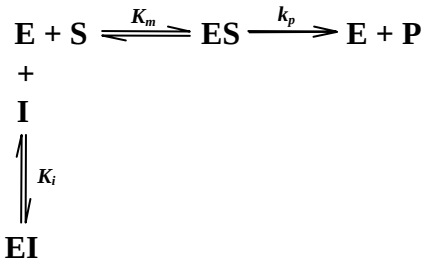

Figure 1.14 Representative diagram for competitive inhibition.

(Taken from Marangoni, 2003).

where E is the enzyme, S is the substrate, ES is the enzyme-substrate complex, P is the product, I is the inhibitor, and EI is the enzyme-inhibitor complex. The metabolic rate (ν) for this case is shown in summary Table 1.4. A competitive inhibitor acts only to increase the apparent K_s (i.e. there is an apparent decrease in the affinity of enzyme for substrate) for the substrate without affecting the V_{max} values.

A-2) Uncompetitive inhibition

In uncompetitive inhibition, an inhibitor binds reversibly to the ES complex yielding an inactive enzyme-substrate-inhibitor (ESI) complex (Fig.1.15). The inhibitor does not bind to the free enzyme.

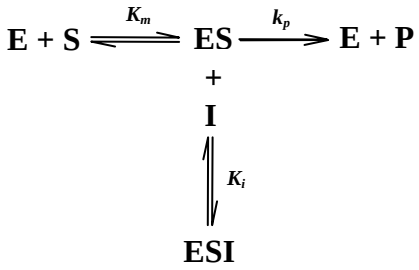

Figure 1.15 Representative diagram for uncompetitive inhibition.

(Taken from Marangoni, 2003).

This results in an apparent decrease in both V_{max} and K_s (Table 1.4). The apparent increase in affinity of the enzyme for substrate (i.e. a decrease in K_s) is due to unproductive substrate binding, resulting in a decrease in free enzyme concentration.

A-3) Noncompetitive inhibition

Non-competitive inhibition is a pattern of inhibition where the inhibitor binds to the same enzyme as the drug but the binding site is different, resulting in a conformational change in the protein (Fig.1.16).

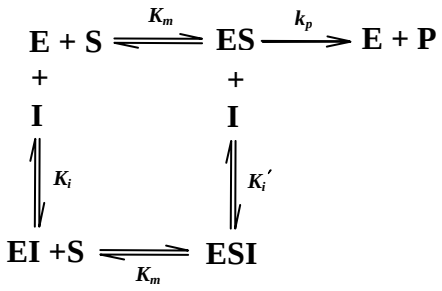

Figure 1.16 Representative diagram for noncompetitive inhibition.

(Taken from Marangoni, 2003).

It is assumed that the inhibitor binds to the free enzyme and the ES complex with the same affinity. An apparent decrease in V_{max} is observed while K_s remains unaffected (Table 1.4).

A-4) Linear mixed inhibition

This is a form of noncompetitive inhibition, where an inhibitor can interact with both the free enzyme and the ES complex at a site other than the active site (Fig.1.16). However, the binding of the inhibitor affects the binding of the substrate, and vice versa. Linear mixed inhibition includes all of the common types of inhibition as asymptotic or special cases, and it will therefore be taken as a general case. It is described by the rate equation:

$$\upsilon = \frac{V_{max} \times [S]}{[S](1 + \frac{[I]}{K_i'}) + K_m (1 + \frac{[I]}{K_i})} \qquad \text{equation 1.12}$$

where K_i is the dissociation constant of inhibitor to the enzyme and K_i' is the dissociation constant of inhibitor to the ES complex. An apparent decrease in V_{max} and an apparent increase in K_s when $K_i > K_i'$ is observed. In contrast, if $K_i < K_i'$, both V_{max} and K_m are decreased (Table 1.4). Although it is possible for mixed-type inhibitors to bind in the active site, this type of inhibition generally results from an allosteric effect where the inhibitor binds to a different site on an enzyme. Inhibitor binding to this allosteric site changes the conformation of the enzyme so that the affinity of the substrate for the active site is reduced.

Table 1.4 Summary of the rate equations describing reversible inhibition and the effects on apparent enzyme catalytic parameters (Modified from Bisswanger, 2008).

Inhibition types	**Rate equations**	**Effect on catalytic parameters**	
		$\mathbf{V_{max}}$	$\mathbf{K_s}$
Competitive	$\upsilon = \frac{V_{max} \times [S]}{[S] + K_m(1 + \frac{[I]}{K_i})}$	No effect ($\leftrightarrow$)	Increase ($\uparrow$)
Uncompetitive	$\upsilon = \frac{V_{max} \times [S]}{[S](1 + \frac{[I]}{K_i}) + K_m}$	Decrease ($\downarrow$)	Decrease ($\downarrow$)
Noncompetitive ($K_i = K_i'$)	$\upsilon = \frac{V_{max} \times [S]}{[S](1 + \frac{[I]}{K_i}) + K_m(1 + \frac{[I]}{K_i})}$	Decrease ($\downarrow$)	No effect ($\leftrightarrow$)
Linear mixed ($K_i > K_i'$)	$\upsilon = \frac{V_{max} \times [S]}{[S](1 + \frac{[I]}{K_i'}) + K_m(1 + \frac{[I]}{K_i})}$	Decrease ($\downarrow$)	Increase ($\uparrow$)
Linear mixed ($K_i < K_i'$)		Decrease ($\downarrow$)	Decrease ($\downarrow$)

υ: Velocity; V_{max}: Maximum velocity; [S]: Substrate concentration; [I]: Inhibitor concentration; K_m: Michaelis–Menten constant; K_i: Dissociation constant of inhibitor to the enzyme; K_i'; Dissociation constant of inhibitor to ES complex.

To determine visually the type of enzyme inhibition and the K_i values, Dixon plots (or direct linear plot) are often used. The effect on the rate of metabolism (υ) is determined at two or more substrate concentrations, and over a range of the inhibitor concentration. In a plot of $1/\nu$ against [I], data for each inhibitor concentration fall on straight lines and the apparent K_i value is obtained from the intercept of all lines. With competitive and mixed inhibition, the lines converge above the x axis and the value of inhibitor concentration where they intersect is $-K_i$ (Fig.1.17A). For non-competitive inhibition (Fig.1.17B), the lines intersect on the x axis and the value of inhibitor concentration where they intersect is $-K_i$. The lines are parallel in the case of uncompetitive inhibition (Fig.1.17C) (Cornish-Bowden, 1974; Segel, 1993; Bisswanger, 2008).

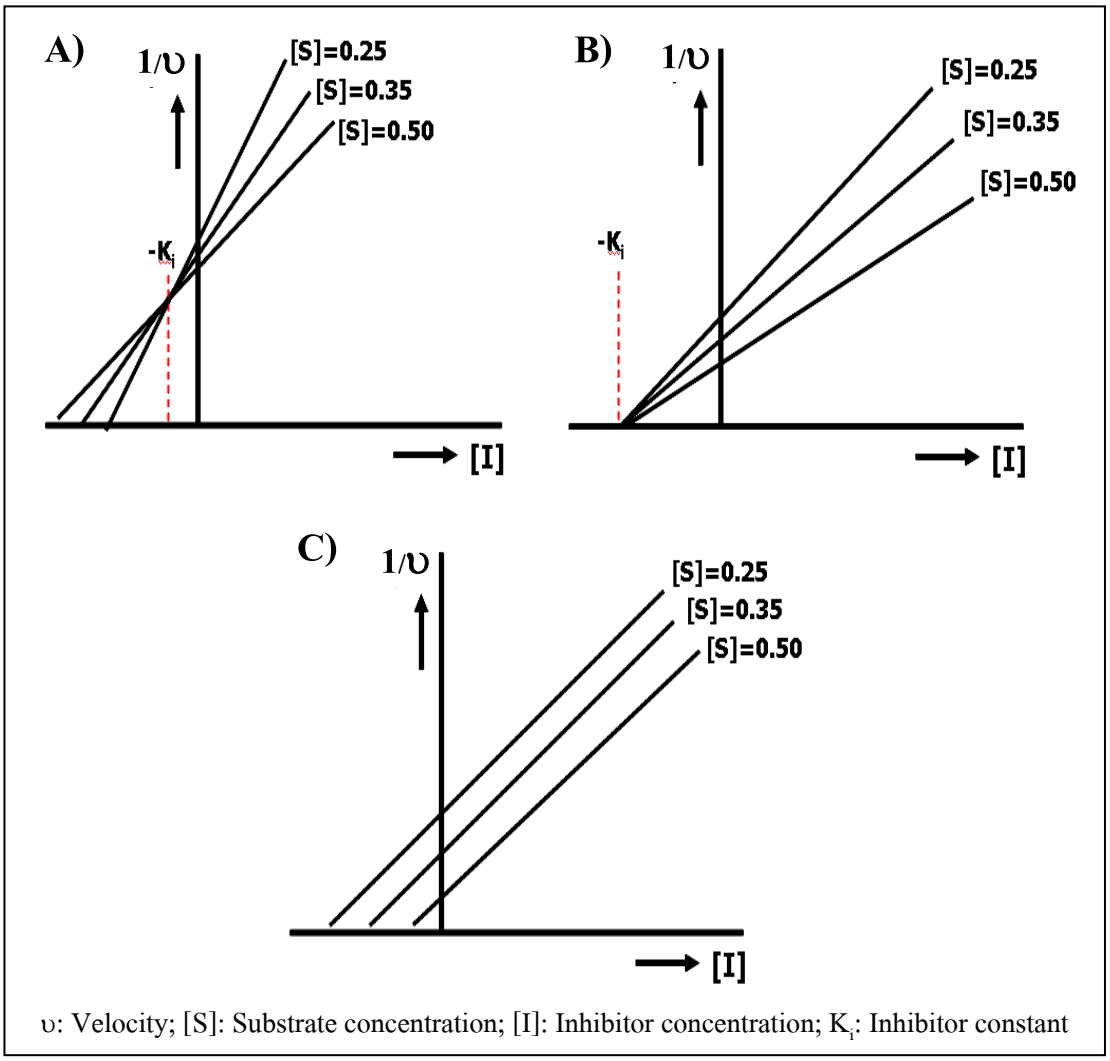

Figure 1.17 Representative Dixon plots for different mechanisms of inhibition (Modified from Segel, 1993):

A) Competitive and mixed inhibition.

B) Non-competitive inhibition.

C) Uncompetitive inhibition.

1.2.6 In vitro-in vivo extrapolation (IV-IVE)

The IV-IVE is an approach that predicts qualitative or quantitative aspects of human drug metabolism and kinetics in vivo. At the qualitative level, identification of the enzyme(s) responsible for the biotransformation of any given compound allows prediction of those factors (e.g. genetic polymorphism, DDIs) likely to influence metabolic clearance (Miners *et al*., 2010). Quantitative prediction most commonly involves the scaling of a CL_{int} calculated from the kinetic parameters (K_m, V_{max}) for formation of metabolite by enzyme sources (either by HLM or hepatocytes). The CL_{int} is then scaled up for whole liver by microsome yield (milligrams per gram of human liver) and liver weight (normally assumed as 1,500 g) to obtain a whole organ of the CL_{int} value, which is subsequently substituted to in vivo hepatic clearance (CL_H) using expressions for the mathematical models of the CL_H (well-stirred, parallel tube, or dispersion models) (Fig.1.18) (Pang and Rowland, 1977; Roberts and Rowland, 1986; Houston 1994; Iwatsubo *et al.*, 1997; Ito *et al.*, 1998b; Miners, 2002).

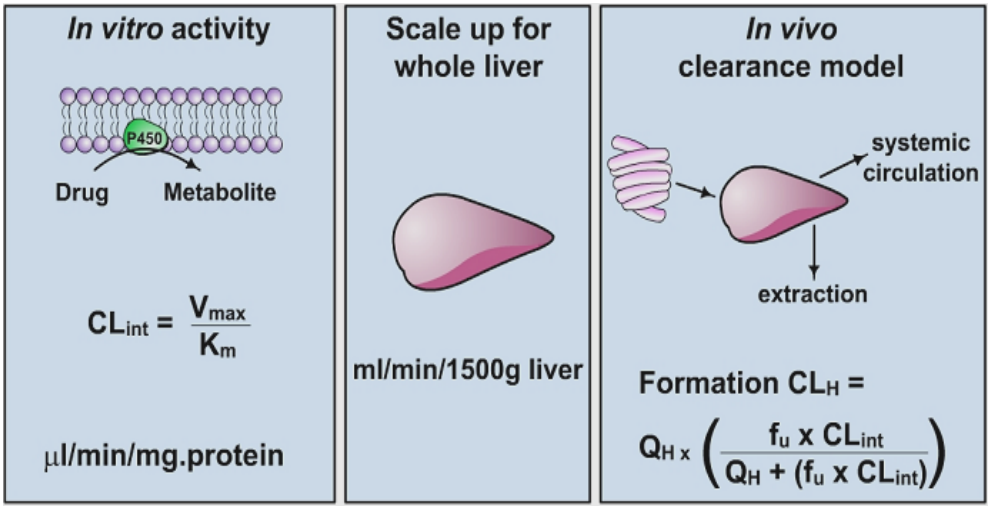

Figure 1.18 Scheme for the extrapolation of the intrinsic clearance (CL_{int}) calculated from human liver microsomal kinetic data to hepatic clearance (CL_H) in vivo (Taken from Miners *et al*., 2002).

1.2.6.1 Prediction of in vivo CL_H based on human liver microsomal kinetic data

A fundamental hypothesis of clinical pharmacokinetics is that a relationship exists between the pharmacological effects of a drug and the accessible concentrations of the drug in blood or plasma. This hypothesis has been documented for many drugs and is of benefit in the therapeutic management of patients. For some drugs, no clear or simple relationship has been found between pharmacological effect and concentration in plasma, whereas for other drugs, routine measurement of drug concentration is impractical as part of therapeutic monitoring. In most cases, the concentration of drug at its sites of action will be related to the concentration of drug in the systemic circulation. The pharmacological effect results may be a desired clinical effect, a toxic effect or, in some cases, an effect unrelated to therapeutic efficacy or toxicity. Clinical pharmacokinetics attempt to provide both a quantitative relationship between dose and effect and a framework within which to interpret measurement of concentration of drugs in biological fluids. The various physiological and pathophysiological variables that dictate adjustment of dosage often do so as a result of modification of pharmacokinetic parameter. The four most important pharmacokinetic parameters are clearance, volume of distribution, elimination half-life, and bioavailability (Buxton, 2006).

Clearance (CL) is the most important pharmacokinetic constant. It is defined as the proportionality factor relating the rate of drug elimination to the plasma concentration, or the volume of blood cleared irreversibly of drug per unit time. The CL may be viewed in another way, namely from the loss of drug across an organ(s) of elimination. This latter physiologic approach has a number of advantages, particularly in predicting and evaluating the effects of changes in blood flow, plasma protein binding, enzyme activity, or secretory activity on the elimination of a drug. The CL value can be considered in terms of the organs of elimination, namely hepatic clearance (CL_H), renal clearance (CL_R), pulmonary clearance, etc. The sum of the individual organ clearance values is equal to the systemic clearance (CL_S), which is whole body clearance (equation 1.13).

$$CL_S = CL_H + CL_R + CL_{other} \qquad \text{equation 1.13}$$

where CL_H is hepatic clearance, CL_R is renal clearance and CL_{Other} is clearance by all other routes. Although drug metabolism can take place in many organs, the liver has the greatest metabolic capacity and consequently has been the most thoroughly studied. The CL_H is often expressed as the blood flow rate multiplied by the extraction ratio (equation 1.14).

$$CL_H = Q_H \cdot E_H \qquad \text{equation 1.14}$$

where Q_H is the sum of hepatic portal and hepatic arterial blood flow (approximately 90 L/hr for a healthy adult) (Coleman, 2005) and E_H is the hepatic extraction ratio which represents the difference between the drug concentration in blood that enters the liver (C_a) and the concentration of drug in blood leaving the liver (C_v) according to the following equation:

$$E_H = \frac{(C_a - C_v)}{C_a} \qquad \text{equation 1.15}$$

The term of E_H is dimensionless and ranges between 0 and 1 (sometimes expressed as a percent). $E_H = 0$ means that the liver does not remove drug at all during perfusion, whereas $E_H = 1$ indicates the complete elimination of a drug from the blood by the liver during perfusion. In other words, E_H reflects the liver's efficiency in removing drug from the blood stream.

A-1) Hepatic clearance models

The IV-IVE approach is based on two essential steps (Fig.1.18). The initial step is conversion of the units of the CL_{int} to a parameter expressed in terms of total liver weight. The second step is incorporation other physiological processes (blood flow and blood protein binding) with the intrinsic metabolic stability of a drug to provide a whole liver CL_H (Houston 1994; Ito and Houston, 2004). Thus, the use of hepatic clearance models is an essential step in the scaling process and is used to relate the clearances obtained in vitro to the in vivo situation. There are three hepatic models which have been used: the well-stirred, parallel tube, and dispersion models (Ito and Houston, 2004). These models differ in their physiological interpretation of the way in which drugs interact in the liver (Pang and Rowland, 1977). Differences between these models have been extensively discussed and the application of different models to the same set of experimental data has been performed (Ito and Houston 2004). Result showed that different

models give acceptably similar clearance values. However, because well-stirred model is mathematically less cumbersome, it has been more widely applied in IV-IVE approach (Pelkonen and Turpeinen, 2007).

The well-stirred model assumes that the entire liver tissues including hepatocytes and the blood in the sinusoid, are well mixed so that drug molecules are distributed instantaneously and homogeneously within the liver. As a result, the drug concentration within the liver is assumed to be equal throughout the organ. In other words, the well-stirred model views the liver as a single compartment (anatomy of the liver) with complete mixing of blood (extent of blood mixing). Important assumptions for the well-stirred model for CL_H include (Pang and Rowland, 1977; Kwon, 2002): a) only unbound drug in blood is subject to elimination (metabolism and/or biliary excretion), b) no membrane transport barrier, c) no concentration gradient of the drug within the liver, d) concentration of the drug within the liver is equal to that in emergent venous blood, and e) linear kinetics.

The CL_H based on the well-stirred model is described as follows:

$$CL_H = \frac{Q_H \cdot f_u \cdot CL_{int}}{Q_H + f_u \cdot CL_{int}} \quad \text{equation 1.16}$$

where CL_{int} is the intrinsic clearance, a measure of the efficiency of the metabolic enzymes, and f_u is fraction unbound concentration in blood which is calculate by equation 1.17:

$$f_u = \frac{f_{u,p}}{R_B} \quad \text{equation 1.17}$$

where $f_{u,p}$ is the fraction of a drug unbound in plasma and R_B is the blood to plasma concentration ratio which is calculated by equation 1.18.

$$R_B = \frac{C_b}{C_p} \quad \text{equation 1.18}$$

where C_b and C_p are the drug concentrations in blood and plasma, respectively.

A-2) Determination of unbound concentration

In general, when drug enters into blood, most of the drug equilibrates rapidly with blood constituents such as blood cells, albumin, and α_1-acid glycoprotein. Binding of a drug to plasma and tissue proteins is a saturable process, and is generally considered reversible with rapid equilibrium within milliseconds. Albumin and α_1-acid glycoprotein are the two major proteins in plasma, with albumin being by far the most abundant (approximately 4% w/v) (Kwon, 2002). Three conventional methods are used for measuring the unbound drug concentration in plasma; equilibrium dialysis, ultrafiltration, and ultracentifugation (Oravcova *et al.*, 1996). Comparison of these methods is shown in Table 1.5. Of these, equilibrium dialysis and ultrafiltration are the most widely used because of their simplicity and general applicability to many different systems in vitro including plasma, serum, or tissue homogenate. However, equilibrium dialysis is often regarded as a "reference method" for the determination of drug protein binding, although this method has several problems which are summarized in Table.1.5. The adsorption of drugs to the surface of the dialysis device and dialysis membrane is a potential problem, particularly for highly lipophilic drugs: for example, for cyclosporin the use of steel chambers has been reported, instead of Teflon or Perspex cells which exhibit extensive adsorption (98%) of this compound (Henricsson, 1987). In addition, the observed unbound fraction may be overestimated as a result of slight leakage of protein into the dialysis apparatus, and thus the absence of drugs should be confirmed by protein assay in a validation study (Oravcova *et al*., 1996).

Equilibrium dialysis is based on the establishment of an equilibrium state between a protein compartment and buffer compartment (McLure *et al.*, 2000; Kwon, 2002). The equilibrium dialysis chamber for the binding compartment contains the drug and protein, from tissue homogenate, plasma, albumin etc. The other chamber contains buffer alone. Both chambers are separated by a semipermeable membrane which allows only low-molecular-weight ligands, such as drug molecules, to distribute between the two sides. Sodium or potassium phosphate buffers at pH 7.4 are most commonly used, although other buffers for some compounds are required due to the formation of insoluble salts or interactions with drug binding sites in protein molecules. When equilibrium is reached after incubation, only unbound drugs diffuse across the

semipermeable membrane. The fraction unbound of drug in incubation ($f_{u,inc}$) is calculated according to equation 1.19:

$$f_{u,inc} = \frac{C_b^*}{C_p^*} \qquad \text{equation 1.19}$$

where C_b^* and C_p^* denote the concentrations of compound in the dialysis chambers containing buffer and protein, respectively.

Table 1.5 Comparison of conventional separation methods (Modified from Oravcov *et al*., 1996 and Kwon, 2002).

	Equilibrium dialysis	**Ultrafiltration**	**Ultracentrifugation**
Advantages	- Temperature controlled - Thermodynamically sound - Considered as standard method	- Need small amount of sample (< 1 mL) - Fast (take ~ 30 min) - No buffer need - Commercially available kit - Disposable device - Small changes in drug concentration during filtration	- No Donnan effect - No nonspecific binding of drug to apparatus
Disadvantages	- Long time to reach equilibrium (up to 20 hr) - Need of buffer - Degradation of unstable compound - Donnan effect in buffer[a] - Volumn shift[b] - Dilution of drug[c] - pH change - Nonspecific binding to dialysis device and membrane	- Nonspecific binding of drug to plastic tube or ultrafiltration membrane - Volume of ultrafiltrate may not be sufficient for drug assay - Usually not temperature controlled - Constriction of membrane pores during ultrafiltration - Donnan effect	- Long time to reach equilibrium (12-15 hr) - Need large amount of sample (> 1 mL) - Usually not temperature controlled - Binding equilibrium may be altered during separation process (sedimentation, back diffusion) - Expensive equipment
Applications	- More suitable for highly protein bound drugs (> 98%)	- Suitable for fast screening when nonspecific binding is less than 10% - More applicable for highly concentrated protein solution or tissue homogenates	- An alternative method to eliminate the effect of nonspecific binding to dialysis apparatus

[a] The observation that charged molecules starting on one side of a semipermeable membrane sometimes will not evenly distribute themselves by diffusion on both sides of the membrane.

[b] Owing to the osmotic pressure difference between plasma (high) and buffer (low), water molecules from the buffer side are continuously moving into the plasma side during incubation, causing an increase in plasma volume and a decrease in buffer volume as compared to the original values.

[c] The initial concentration of drug in plasma decreases during incubcation as the plasma and the buffer equilibrate. Equilibrium dialysis may be inappropriate when there are significant changes in the extent of protein binding of a drug resulting from its dilution in plasma with buffer during equilibrium.

A-3) Reasons for the underestimation of in vivo CL_H

Although IV-IVE has an enormous potential, the promise is yet to be met. The use of HLM as the enzyme source generally results in underestimation of the in vivo CL_H. Several studies have compared observed and predicted in vivo CL_{int} values based on kinetic data generated using HLM and cryopreserved human hepatocytes. These datasets include drugs metabolized by CYP and UGTs (Ito and Houston, 2005; Riley *et al.*, 2005; Brown *et al.*, 2007). Riley *et al*. (2005) showed that underestimation of in vivo CL_{int} with HLM as the enzyme source is consistent with the underestimation of in vivo CL_H (Table 1.6).

Table 1.6 Correlation between predicted and observed in vivo $CL_{int,un}$ values for drugs metabolized CYP and UGT from some of studies (Modified from Riley *et al*., 2005).

Compounds	[a]In vivo $CL_{int,un}$ (mL/min/kg)		% Underestimation	References
	Predicted	Observed		
Amitriptyline	94.3	516.0	81.72	(Obach, 1999)
Diazepam	8.3	33.8	75.44	(Obach, 1999)
Diclofenac	190.9	1348.4	85.84	(Obach, 1999)
Ibuprofen	10.6	89.2	88.12	(Obach, 1999)
Imipramine	106.6	330.0	67.70	(Obach, 1999)
Metoprolol	6.8	20.2	66.34	(Obach, 1999)
Methoxsalen	43.0	1340.0	96.79	(Riley *et al.*, 2005)
Nilvadipine	3867	8123.4	52.40	(Naritomi *et al.*, 2001)
Omeprazole	101.0	502.7	79.91	(Naritomi *et al.*, 2001)
Phenacetin	9.9	212.5	95.34	(Riley *et al.*, 2005)
Phenytoin	0.5	4.0	87.50	(Carlile *et al.*, 1999)
Propranolol	16.3	284.5	94.27	(Riley *et al.*, 2005)
Quinidine	10.7	22.1	51.58	(Obach, 1999)
Verapamil	286.6	2926.0	90.21	(Obach, 1999)
Zolpidem	31	155.3	80.04	(Naritomi *et al.*, 2001)

[a] in vivo intrinsic clearance corrected for the fraction unbound in incubation

The reasons for the underestimation regarding to in vivo CL_{int} or in vivo CL_H are still unclear; however, there are numerous factors involved as discussed in the following sections. Underestimation arising from the IV-IVE approach may result from physiological scaling factors, non-specific and protein binding, inappropriate kinetic modeling in vitro, metabolism by extrahepatic tissues, etc. In addition, incubation components such as buffer type, pH and ionic strength, and the presence of activators, e.g. alamethicin, detergents, Mg^{2+} or other treatments (e.g. sonication), may result in variability (Miners *et al.*, 2004, 2006, and 2010).

a) Physiological scaling factor

In general, the CL_{int} obtained in vitro using microsomes fresh or cryopreserved hepatocytes, precision-cut liver slices or recombinant enzymes is converted to in vivo CL_H using physiological scaling factors. The physiological scaling factors for data from liver microsomes, hepatocytes, homogenates and liver slices are milligram of microsomal protein per gram of liver (MPPGL), number of hepatocytes per gram of liver (HPGL; hepatocellularity), milligram of homogenate protein per gram of liver (HomPGGL) or slice mass, respectively. A combination of MPPGL together with hepatic enzyme abundance is used to scale data from recombinantly expressed enzyme systems (Fig.1.19) (Barter *et al.*, 2007). Although several different enzyme sources may be used for IV-IVE, HLM is normally employed. Different values for MPPGL have been used over the years, many of them based on rat data. For example, the value of 45 mg/g commonly used for human MPPGL is determined originally from studies with rat hepatic microsomes (Houston, 1994). Recently, Barter *et al*. (2007) collated and analyzed data from a number of sources to provide weighted geometric mean values of human MPPGL of 32 mg/g (95% confidence interval in range 29–34 mg/g). Another publication gives a similar value (Hakooz *et al.*, 2006). Scaling of the liver unit value to the whole organ requires a value for liver weight. A value of 1,500 g in man has usually been employed, although there are recent meta-analyses on the liver size in different ethnic population (Murry *et al.*, 1995; Urata *et al.*, 1995; Heinemann *et al.*, 1999; Johnson *et al.*, 2005). Values derived from these studies are sufficiently similar to the above value so that scaling to the whole organ can reasonably be performed assuming the liver weight as 1,500 g (Pelkonen and Turpeinen, 2007).

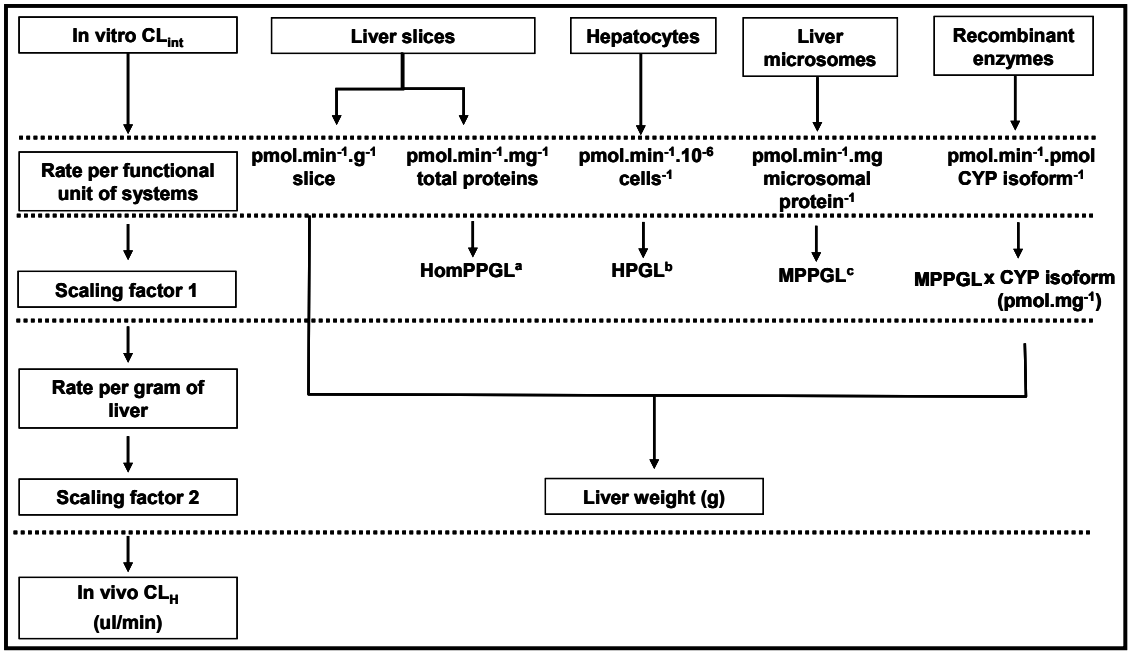

[a] Milligrams of homogenate protein per gram of liver, [b] Hepatocellularity per gram of liver, [c] Milligrams of microsomal protein per gram of liver.

Figure 1.19 Schematic representation of the scaling procedure using different in vitro systems. (Modified from Barter *et al*., 2007).

b) Nonspecific and protein binding

Nonspecific binding of substrate to incubation components, including microsomes, hepatocytes, or albumin added to incubation mixtures, is a very important factor in the calculation of kinetic constants for drug metabolism reactions in vitro. Failure to account for this phenomenon may lead to overestimation of K_m and, hence, underestimation of CL_{int} (Table 1.6) (Ito *et al.*, 1998a; Miners *et al.*, 2004). Some investigations have shown that the CL_{int} values of certain lipophilic amines (e.g. propranolol and imipramine) with high plasma protein binding or low unbound fractions in plasma ($f_{u,p} \leq 0.1$) are very poorly predicted (up to 100-fold). When plasma blood binding values are removed from hepatic models (well-stirred or parallel tube models) for these compounds, scaled-up values of CL_{int} are sometimes close to those measured in vivo (Obach, 1996, 1997). It is thus frequently assumed that non-specific binding in vitro and protein binding in vivo 'cancel out', and hence both terms are not uncommonly ignored in the

calculation of in vivo CL_H (Obach, 1999; Riley *et al.*, 2005; Miners *et al*., 2006). However, the two parameters are not related in a linear manner (Ito and Houston, 2005) and inclusion of both microsomal and plasma protein binding usually results in a better agreement between extrapolated and actual clearance values (Obach, 1999; Riley *et al.*, 2005; Miners *et al.*, 2006). Importantly, determination of fraction unbound of drug in a biological matrix (microsomal incubations, plasma etc.) can easily be measured by several methods as describe above and should therefore be accounted for in IV-IVE.

c) Incubation conditions

Difference of incubation conditions with HLM as the enzyme source may result in underestimation of CL_{int}, K_m and V_{max} values for glucuronidation. It can vary with buffer type, pH and ionic strength, and the presence of activators (e.g. alamethicin, detergents, Mg^{2+}) or other treatments (e.g. sonication) which release the 'latency' of microsomal UGTs (Boase and Miners, 2002; Soars *et al.*, 2003; Engtrakul *et al.*, 2005). Buffer type and strength for UGT assays with HLM as the enzyme source vary significantly among different laboratories. Several groups use phosphate buffers (Fisher *et al.*, 2000; Boase and Miners 2002; Court *et al.*, 2003), whereas others groups use sucrose buffer (Bock *et al.*, 1984; Soars *et al.*, 2001). Soars *et al*. (2003) showed that the formation of estradiol-3-glucuronide is up to 2.5-fold greater using HLM prepared in phosphate buffer compared with those prepared in sucrose with all other assay components held constant. In contrast, rates of AZT glucuronidation by HLM have been shown to be approximately doubled in the presence of carbonate buffer when compared to incubations performed in phosphate buffer (Engtrakul *et al.*, 2005), but the rate is no difference between phosphate and Tris-buffered incubations (Boase and Miners, 2002). Additionally, the pH and Mg^{2+} content of buffers may result in different rates of drug glucuronidation (Boase and Miners 2002; Soars *et al.*, 2003).

Activation by the membrane pore-forming peptide (alamethicin), sonication, or Brij 58 (polyoxyethylene monocetyl ether) have been shown to be necessary for optimum enhancement of microsomal UGT activity (Fisher *et al.*, 2000; Boase and Miners, 2002; Soars *et al.*, 2003). The consistently high levels of activation obtained using the alamethicin (Fig.1.20) and

its ease of use (50 μg/mg protein always gave maximal activation) provides a universal alternative to detergents for overcoming the latency of all UGT forms and achieving maximal glucuronidation activity in liver microsomes (Fisher *et al.*, 2000; Soars *et al.*, 2003). This latency arises from the location of the active site of UGTs within the lumen of the ER, such that the ER membrane presents a diffusional barrier for the access of substrates and cofactors to the enzyme (Meech and Mackenzie, 1997). Disruption of this barrier is required to overcome enzyme latency and obtain maximal glucuronidation activity in microsomal incubations.

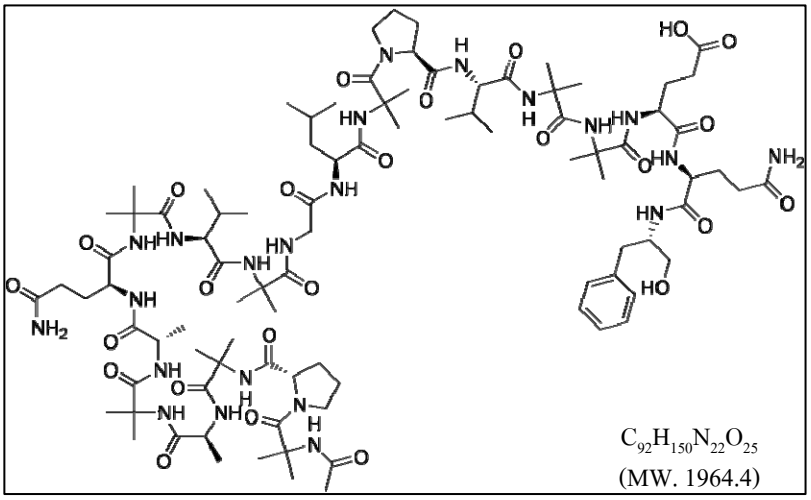

Figure 1.20 Structure of alamethicin

(Taken from Jones *et al*., 1980).

The mechanism of alamethicin insertion into the membrane to form well-defined pores has been elucidated (He *et al.*, 1996). Thus, the alamethicin allows free diffusion of substrates, cofactors, and products without affecting the gross membrane structure and intrinsic enzyme catalytic activity (Fisher *et al.*, 2000). In addition, enhancement the microsomal UGT activity may be seen with Mg^{2+} occurring in the presence of pores formed with alamethicin, when free diffusion of substrates and products occurs. Therefore, the Mg^{2+} appears to exert its effects directly on the actual catalytic activity of the UGTs increasing their catalytic activities (Fisher *et al.*, 2000; Boase and Miners 2002).

d) Extrahepatic metabolism

Underestimation of CL_{int} may also result from extrahepatic metabolisms. As mentioned previously, UGTs are expressed in tissue other than liver. Apart from the liver, UGT1A3, 1A9, and 2B7 are expressed in kidney and multiple forms are expressed throughout the GI tract (Tukey and Strassburg, 2000). Several lines of evidence showed that UGT activity is readily measurable in human kidney and GI tract and this has led to the proposal that these organs contribute significantly to the systemic clearance and first-pass extraction, respectively, of glucuronidated drugs (Soars *et al.*, 2001 and 2002; Miners *et al.*, 2004; Tsoutsikos *et al.*, 2004; Knights and Miners, 2010). Recently, evidence showed that the small intestine can contribute to first-pass metabolism in humans and thus lead to significant of extrahepatic drug glucuronidation (Soars *et al.*, 2002; Galetin *et al*., 2002). Ethinylestradiol is one example. The CL_{int} value is 2- to 3-fold greater with human intestinal microsome (HIM) than the CL_{int} determined with HLM. Similarly, small intestinal activity is higher than hepatic microsomal activity for the UGT1A1 probe estradiol (Czernik *et al.*, 2000; Fisher *et al.*, 2001). Additionally, glucuronidation by human kidney microsome (HKM) is predicted to be important in the metabolism of several compounds (Knights and Miners, 2010).

e) Atypical kinetic behaviors

There is also increasing evidence that many compounds metabolized by glucuronidation via UGT enzymes exhibit ‘atypical’ or non-Michaelis-Menten kinetic behavior (Miners *et al.*, 1988; Uchaipichat *et al.*, 2006a; Wong *et al.*, 2007). Atypical kinetics clearly impact on IV-IVE approaches which are assumed to be hyberbolic (Michaelis-Menten) kinetics. The consequences of ignoring atypical kinetic have been described as above.

1.2.6.2 Prediction of inhibitory interactions involving glucuronidated drugs from in vitro kinetic data

DDIs caused by inhibition of metabolic enzymes are common and clinically important. Despite the success of the IV-IVE approaches for drugs eliminated by CYP, few studies have investigated the reliability of extrapolating human liver microsomal kinetic data to an in vivo CL_H for drugs metabolized by glucuronidation. The UGTs is quantitatively the most important conjugation enzyme, and drugs from all therapeutic classes are eliminated by glucuronidation (Miners and Mackenzie, 1991). The effects of inhibition of drug metabolism on in vivo pharmacokinetics are highly variable and depend on the properties of the drug, the route of administration, etc. (Rowland and Matin, 1973; Tucker, 1992). Lack of a good understanding of the underlying inhibition mechanism may lead to inappropriate experimental design and inaccurate estimation of K_i values (Lin, 2000).

A-1) Equations for the quantitative prediction of in vivo DDIs

In human in vivo interaction studies, the degree of interaction is expressed as the ratio of the AUC in the presence and absence of an inhibitor (Miners *et al.*, 2010). The AUC ratio is related to the ratio of the CL_{int}. The degree of inhibition depends on the inhibition pattern when the substrate concentration is high. However, when the substrate concentration is much lower than K_m (K_m>>[S]), and the mechanism of inhibition (competitive or noncompetitive) is not relevant; therefore, the following equation (equation 1.20) is valid for both inhibition types (Tucker, 1992; Ito *et al.*, 1998b):

$$\text{AUC ratio} = \frac{\text{AUC (+inhibitor)}}{\text{AUC (control)}} = \frac{1}{\frac{f_m}{1+[I]/K_i} + \left(1 - f_m\right)} \qquad \text{equation 1.20}$$

where [I] is the concentration of inhibitor at the enzyme active site; f_m is the fraction of the dose metabolized by the enzyme and pathway of interest, and K_i is the inhibitor constant generated in vitro.

A-2) Estimation of inhibitor concentration at the enzyme active site

The accuracy of DDIs potential is optimized when [I] is taken as the maximum hepatic inlet concentration (I_{inlet}) (Miners *et al.*, 2010). Ito *et al*. (1998a) proposed an approach for predicting in vivo drug interaction potential using the concept of the unbound inhibitor hepatic inlet concentration ($I_{inlet,u}$), where the blood flow from the hepatic artery and portal vein meet. The $I_{inlet,u}$ of a given inhibitor during absorption can be expressed as a following equation.

$$I_{inlet,u} = f_u \times \left[I_{max} + \frac{k_a \times F_a \times Dose}{Q_H} \right] \qquad \text{equation 1.21}$$

where Q_H and f_u are the hepatic blood flow and the unbound fraction of inhibitors in blood, respectively. k_a and F_a represent the first-order absorption rate constant and the fraction of oral dose absorbed from the GI tract into the portal vein, respectively. During oral absorption, the concentration of inhibitor presented to hepatocytes via the portal vein is significantly higher than the systemic circulation, depending on the rate and extent of absorption. As indicated in the above equation, the first term of the equation, I_{max} (the maximum inhibitor concentration in the hepatic artery and portal vein), represents the contribution from systemic circulation, and the second term $[(k_a \times F_a \times Dose)/Q_H]$ is the contribution from the absorption. Because of practical limitations in the measurement of inhibitor concentration in the portal vein in humans, Ito *et al*. (1998b) also proposed that the k_a and F_a values can be used to estimate the inhibitor concentration in the portal vein. The parameters (I_{max}, F_a, and f_u) of inhibitors can be obtained from clinical studies, and the k_a values of inhibitors can be indirectly calculated from the time to maximum drug concentration (T_{max}) and absorption half life in plasma ($t_{1/2,ab}$). With this approach, there is an implicit assumption that a rapid equilibrium occurs between blood and hepatocytes. However, in vivo clinical studies frequently do not report k_a values; therefore, the theoretical maximum value of 0.1 min^{-1} is frequently used for k_a. Generally, the k_a value of the orally administered drug is maximum when the GI absorption of the drug is so rapid that the rate limiting step is the gastric emptying rate (Ito *et al.*, 1998b).

1.2.7 Albumin

Serum albumin is the most abundant blood plasma protein and is produced in the liver. It comprises a large proportion of all plasma proteins. Human serum albumin (HSA) accounts for approximately 60% of all human plasma proteins and circulates in the blood at a concentration of approximately 640 μM (or 4% w/v) (Zunszain *et al.*, 2003).

1.2.7.1 Structure of human serum albumin

The HSA (Fig.1.21) is a helical protein of 66 kDa which contains three homologous domains, I (residues 1-195), II (196-383), and III (384-585), each of which is composed of a and b subdomains (He and Carter, 1992). Although all three domains of the HSA molecule have similar three-dimensional structures, their assembly is highly asymmetric. Domain I and II are almost perpendicular to each other to form a T-shaped assembly in which the tail of subdomain IIA is attached to the interface region between subdomain IA and IB by hydrophobic interactions and hydrogen bonds (Sugio *et al.*, 1999; Zunszain *et al.*, 2003).

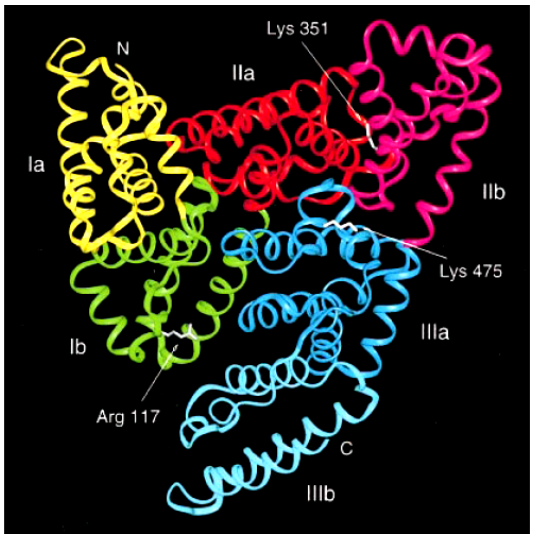

Figure 1.21 Crystal structure of human serum albumin.

(Taken from Sugio *et al*., 1999).

In contrast, domain III protrudes from subdomian IIB at an angel of about 45 °C to form a Y-shaped assembly for domains II and III. Domain III interacts only with subdomain IIB. These features make the HSA molecule heart-shaped (Sugio *et al.*, 1999; Zunszain *et al.*, 2003). In addition, several investigators have shown that HSA has a high affinity for a very wide range of substances, including metals such as Cu^{2+} and Zn^{2+}, fatty acids, and many drugs. The possible binding sites of long chain fatty acids are located at the surface of all three domains and Arg117, Lys351, and Lys365 may be binding sites for long chain fatty acids (Sugio *et al.*, 1999).

1.2.7.2 Function of albumin

Albumin is essential for maintaining the oncotic pressure in the vascular system. A decrease in oncotic pressure due to a low albumin levels allows fluid to leak out from the interstitial spaces into the peritoneal cavity, producing ascites. Albumin is also very important in the transportation of many substances such as drugs, lipids, hormones, and toxins that are bound to albumin in the bloodstream. Once the drug or other substance reaches the liver, it may dissociate from albumin and made less toxic by conversion to a water-soluble form that can be excreted.

1.2.7.3 Effect of albumin on in vitro kinetic parameters

Although predictivity using HLM as the enzyme source is good for some drugs metabolized by CYP, there is a general trend to underestimation of CL_H as mentioned above. Similarly, in vitro K_i values generated using HLM or recombinant human UGT2B7, underpredict the magnitude of inhibitory drug interactions (Rowland *et al.*, 2006; Uchaipichat *et al.*, 2006b). Results from previous studies have shown that addition of BSA to HLM incubations decreases the K_m and increases the in vitro CL_{int} for drugs metabolized by CYP2C9 (Tang *et al.*, 2002; Wang *et al.*, 2002; Zhou *et al.*, 2004). Improved predictivity of in vivo CL_{int} values occur for experiments conducted in the presence of BSA. Furthermore, the addition of 2% BSA to incubations of HLM and recombinant UGT2B7 increases the in vitro CL_{int} for LTG and AZT glucuronidation 7 to 10-fold and reduces the K_i (Rowland *et al.*, 2006; Uchaipichat *et al.*, 2006b).

Recently, it has been shown that several unsaturated long-chain fatty acids are present in HLM, human embryonic kidney (HEK293) cell lysates, and some albumin preparations (Rowland *et al.*, 2007). Oleic, linoleic, and arachidonic acids are the most prevalent (Rowland *et al.*, 2007). Studies have demonstrated previously that oleic, linoleic and arachidonic acids are substrates of UGT2B7 (Jude *et al.*, 2001; Turgeon *et al.*, 2003; Little *et al.*, 2004); therefore, fatty acid glucuronides can be formed during incubation and released during the course of incubation. Furthermore, these fatty acids have been shown to inhibit UGT2B7 activity, with arachidonic acid the most potent fatty acid inhibitor of UGT2B7 identified to date (Tsoutsikos *et al.*, 2004). Addition of BSA into incubations has the capacity to sequester inhibitory fatty acids, and subsequently reverses the inhibition (Rowland *et al.*, 2007). In contrast to BSA, UGT activity is not improved in the presence of HSA. Rowland *et al*. (2007) indicated that this may be due to the fatty acid content (oleic, linoleic, and arachidonic acids) of HSA preparations which are significantly higher than in BSA. Therefore, it is also likely that HSA contributes fatty acids to the incubation mixture. Because fatty acids can desorb from binding sites on albumin despite high binding affinities, fatty acid glucuronide formation is enhanced for incubations conducted in the presence of HSA (Hamilton, 2002; Rowland *et al.*, 2007).

1.2.8 Codeine

COD or 7, 8-didehydro-4,5-epoxy-3-methoxy-17-methyl-morphinan-6-ol mono-hydrate (Fig.1.22) is a naturally occurring opium alkaloid (Reynolds, 1996). It was first discovered as a natural constituent of opium in very small concentrations, in the range of 0.7%-2.5% by weight. Most COD found in pharmaceutical products today is synthetically produced via the methylation of morphine. COD effloresces slowly in dry air and is affected by light (William *et al.*, 2001).

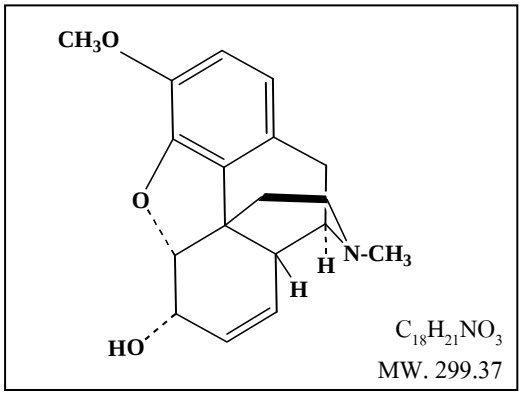

Figure 1.22 Chemical structure of codeine.

(Taken from Williams *et al*., 2001).

1.2.8.1 Pharmacodynamics

COD is mainly used as an analgesic, but is also employed as an antitussive agent and antidiarrhoeal (Eriksson *et al.*, 1982; Dollery, 1999). It is less potent than morphine, with a potency ratio of 1:10 (Wallenstein *et al.*, 1961). COD can be administered per orally (PO), subcutaneously (SC), intramuscularly (IM) and per rectally (PR). COD can not be safely administered by an IV injection as it may result in pulmonary oedema, facial swelling, release of histamine, and various cardiovascular effects (Parke *et al.*, 1992). COD is often used in combination with other drugs, for examples aspirin, paracetamol, NSAIDs and diphenhydramine in the treatment of mild to moderate pain. In neonates and children, it has been used in both acute and chronic painful conditions and particularly for post-operative and cancer pain (de Lima *et al.*, 1996). Its antitussive and constipating properties also mean that it is used in many cough, cold

and antidiarrhoeal remedies. However, both adult and pediatric clinical studies have demonstrated that the efficacy of COD is low and it has a ceiling effect at higher doses above which there is a marked increase in the incidence of side-effects (Quiding *et al.*, 1993; McEwan *et al.*, 2000).

A-1) Mechanism of actions

Analgesic effect: COD is a weak opioid agonist in the CNS. It has low affinity for the opioid receptor and the analgesic activity of COD is due to its conversion to morphine (Sindrup and Brosen, 1995; William *et al.*, 2001). Opioid agonist produces analgesia by binding to specific G protein-coupled receptors, mu (μ), kappa (κ), and delta (δ), located primarily in the brain and spinal cord regions involved in the transmission and modulation of pain. COD binds to the μ receptor like morphine but with a much lower affinity. It also binds to κ and δ receptors but again has a much lower affinity than morphine, though the difference is less marked (Neil, 1984). Opioids do not alter the pain threshold of afferent nerve endings to noxious stimuli, nor do they affect the conductance of impulses along peripheral nerves. Analgesia is mediated through changes in the perception of pain at the spinal cord and higher levels in the CNS. The stimulatory effects of opioids are the result of 'disinhibition' as the release of inhibitory neurotransmitters such as γ-aminobutyric acid (GABA) and acetylcholine is blocked. The exact mechanism how opioid agonists caused both inhibitory and stimulatory processes is not well understood. Possible mechanisms for these processes include differential susceptibility of the opioid receptor to desensitization or activation of more than one G-protein system or subunit (one excitatory and one inhibitory) by an opioid receptor.

Antitussive effect: The antitussive effect of COD is mediated through direct actions on receptors in the cough centre of the medulla. COD also has a drying effect on the respiratory tract and increases the viscosity of bronchial secretions. Cough suppression can be achieved at lower doses than those required to produce analgesia (Sindrup and Brosen, 1995).

A-2) Adverse effects and toxicity

Common adverse drug reactions associated with the use of COD include itching, nausea, vomiting, drowsiness, dry mouth, miosis, orthostatic hypotension, urinary retention and constipation (Eckhardt *et al.*, 1998). A potentially serious adverse drug reaction, as with other opioids, is respiratory depression which is dose-related. This effect is the mechanism for the potentially fatal consequences of overdose. Another adverse effect is the lack of sexual drive. COD toxicity may occur in overdose. The clinical course is complicated by shock, respiratory arrest and laboratory evidence of acute hepatic insufficiency. An initial slow rate of COD metabolism, possibly related to the hepatic damage, corresponds to prolonged respiratory depression (Huffman and Ferguson, 1975).

According to the incidence and role of COD in drug-related deaths in Victoria, Australia, a total of 107 cases were investigated over a 5-year period (Gerostamoulos *et al.*, 1996). There were six fatalities in which COD was considered the major poison and the remaining 101 cases involved a combination of COD and other drugs. The most common drugs have found in this group, other than COD, are acetaminophen (62%), diazepam (46%), salicylates (20%), and ethanol (25%). The association of other psychoactive drugs in these deaths made the contribution of COD is difficult to assess. Free COD concentrations > 0.4 mg/L and total COD concentrations > 2.0 mg/L may be sufficient to cause death in the absence of any other contributing factors.

More recently a case of drug-induced hypersensitivity syndrome which relates to COD has been reported (Enomoto *et al.*, 2004). A Japanese patient was prescribed COD phosphate 3 times daily and several other drugs for cold symptoms. About 20 days later, an erythematous, maculopapular rash appeared and progressed to erythroderma (a spiking fever). Laboratory examinations have showed atypical lymphocytosis, eosinophilia, and increased liver enzyme values. The platelet count slowly decreased after admission. However, although COD may rarely be associated with hypersensitivity syndrome, clinicians should be aware that the potentially fatal syndrome can be caused by various drugs.

1.2.8.2 Pharmacokinetics

COD is rapidly and well absorbed following PO administration, although approximately 50% undergoes presystemic metabolism in the gut and liver. Peak plasma concentration occurs after approximately 1 hr and the plasma half-life is 3-3.5 hr. Absorption is faster after IM injection, the time to peak plasma concentration is about 0.5 hr. The volume of distribution is 3.6 L/kg and the clearance is as high as 0.85 L/min (Dollery, 1999). COD has a medium to high hepatic extraction ratio (from 0.52 to 0.83) which is apparently dose-dependent (Christensen *et al.*, 1984). PR administration of COD has been recently introduced into pediatric practice. A study in healthy adult volunteers has showed no difference in COD bioavailability following PR or PO administration with a systemic availability of about 90% (Moolenaar *et al.*, 1983). Plasma protein binding is small (7-25%) (Moffat *et al.*, 1986). Elimination occurs mainly in renal as the unchanged drug, norcodeine, and free and conjugated morphine. Negligible amounts are excreted in the feces (Chen *et al.*, 1991; Vree *et al.*, 2000).

COD is considered a prodrug, since it is metabolized in vivo to morphine (Srinivasan *et al.*, 1997; Vree *et al.*, 2000). Roughly 5-10% of COD will be converted to morphine, with the remainder either free or conjugated to C6G (~80%) or converted to norcodeine (~10%) (Vree *et al.*, 2000). The metabolic pathway is presented in Figure 1.23.

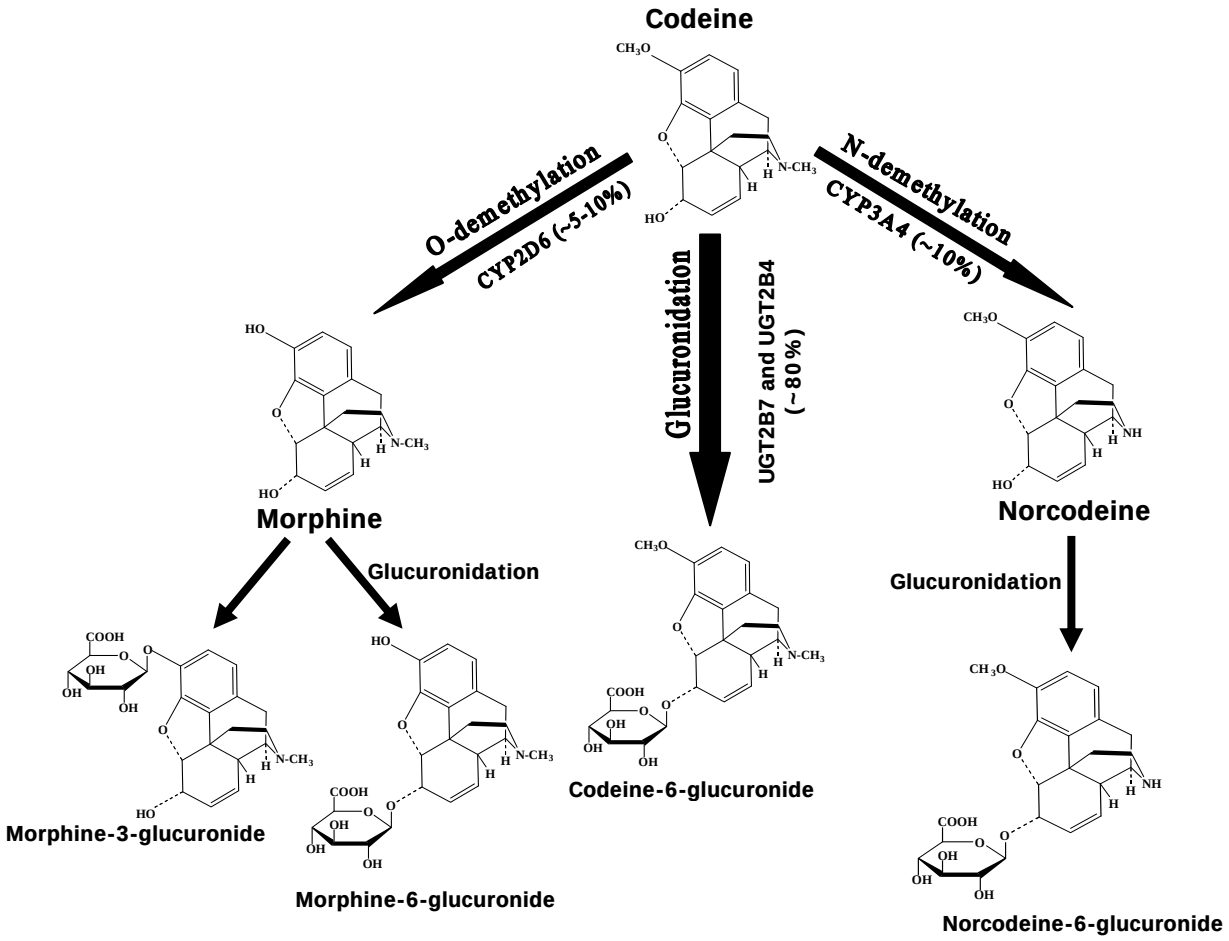

Figure 1.23 Metabolic pathway of codeine.

(Modified from Vree *et al*., 2000).

The major metabolic pathway of COD is the formation of the C6G metabolite by UGT2B7 and possibly UGT2B4 (Court *et al.*, 2003). The COD is metabolized to a minor extent via *O*-demethylation by CYP2D6 to morphine and via *N*-demethylation by CYP3A4 to norcodeine (Yue *et al.*, 1989; Chen *et al.*, 1991; Vree and Verwey-van Wissen, 1992). Norcodeine and morphine are subsequently glucuronidated to the corresponding 3-and 6-glucuronides. Only 10% of COD is not metabolized but is essential for its opioid activity (Vree and Verwey-van Wissen, 1992).

1.3 Objectives

This study aims to quantitatively predict the in vivo COD glucuronidation and inhibition using the in vitro kinetic parameters. The objectives are as follows:

1.3.1 To investigate whether the in vitro kinetic parameters (K_m, V_{max}, CL_{int}) determined for the COD glucuronidation, using HLM, predict the COD glucuronidation in vivo.

1.3.2 To determine the COD glucuronidation by recombinant UGT enzymes (viz. UGT2B4 and UGT2B7).

1.3.3 To investigate the effect of VPA on COD glucuronidation in HLM.

1.3.4 To predict the magnitude of inhibitory interaction of COD glucuronidation by FLZ, KTM, and KTZ in vivo.

1.3.5 To investigate the effect of exogenous albumin on the kinetics of COD glucuronidation and inhibition in vitro.

CHAPTER 2

METHODOLOGIES

2.1 Materials and chemicals

Codeine (COD), codeine-6-glucuronide (C6G), bovine serum albumin ('crude' BSA, 98-99% albumin, product number A7906), alamethicin (from *Trichoderma viride*), Uridine diphosphate glucuronic acid (UDPGA; trisodium salt), valproic acid (VPA), ketamine (KTM) and cellulose dialysis membrane (molecular weight cutoff 12,000 Da) were purchased from Sigma Aldrich (Sydney, Australia). Fluconazole (FLZ) was a gift from Pfizer Australia (Sydney, Australia). Ketoconazole (KTZ) was a gift from Janssen research foundation. Baculovirus-expressed UGT2B4, 2B7 and 2B15 enzymes were obtained from BD Gentest (Woburn, MA). Solvents and other reagents were of analytical reagent grade.

2.2 Methods

2.2.1 HLM and expression of recombinant UGT proteins

Human livers (HL 7, 10, 12, 13 and 40) were obtained from the human liver 'bank' of the Department of Clinical Pharmacology, Flinders Medical Centre. Approval was obtained from the Flinders Medical Centre Research Ethics Committee and from the donors' next-of-kin for the procurement and use of human liver tissue in xenobiotic metabolism studies. Microsomes were prepared by differential centrifugation, as described by Bowalgaha *et al*. (2005). Microsomal protein concentrations were determined by the method of Lowry *et al*. (1951) using BSA as standard. Prior to use in incubations, HLM was activated by the addition of the pore-forming peptide alamethicin (50 μg/mg of protein) with preincubation on ice for 30 min (Boase and Miners, 2002).

UGT1A1, 1A3, 1A4, 1A6, 1A7, 1A8, 1A9, 1A10, 2B4, 2B7, 2B10, 2B15, and 2B17 cDNAs were stably expressed in a HEK293 cell line, as described previously (Sorich *et al.*, 2002; Stone *et al.*, 2003; Uchaipichat *et al.*, 2004). Cells were separately transfected with the individual UGT cDNAs cloned into the pEF-IRES-puro6 expression vector. Transfected cells were incubated in Dulbecco's modified Eagle's medium, which contained puromycin (1.5 mg/L), 10% fetal calf serum and penicillin G sodium (100 U/mL)/streptomycin sulphate (100 μg/mL) in a humidified incubator with an atmosphere of 5% CO_2, at 37 °C. Following growth to at least 80% confluence, cells were harvested and washed with 0.1 M phosphate-buffered saline, pH 7.4. Cells were subsequently lysed by sonication using a sonicator (Heat Systems Ultrasonics, Plainsview, NY) set at microtip limit of 4, with four 1-s "bursts", separated by 3 min with cooling on ice. Lysed samples were centrifuged at 12,000 ×*g* for 1 min at 4 °C, and the supernatant fraction was removed and stored at -80 °C until use. Given the relatively low activity of UGT2B4, 2B7 and 2B15 expressed in HEK293 cells, Supersomes (BD Bioscience) expressing these enzymes were used in activity studies. The use of UGT2B enzymes from this source also allowed direct comparison of data from a previous study of COD glucuronidation (Court *et al*., 2003).

Expression of each UGT was demonstrated by immunoblotting with a commercial UGT1A antibody (BD Bioscience) and a nonselective UGT antibody (raised against purified mouse Ugt) according to Uchaipichat *et al*. (2004) and an antibody that recognizes UGT2B7 and UGT2B10 (Kerdpin *et al*., 2009). In addition, activity measurements were performed with the recombinant proteins. Activities of recombinant UGT1A1, 1A3, 1A6, 1A7, 1A8, 1A9, 1A10, 2B4, 2B7, 2B15, and 2B17 were confirmed using the nonselective 4-MU according to a previously published procedure (Rowland *et al*., 2007). UGT1A4 activity was demonstrated using TFP as the substrate (Uchaipichat *et al*., 2006b), while UGT2B10 activity was confirmed by measurement of cotinine glucuronidation (Kerdpin *et al*., 2009). Furthermore, the effect of alamethicin on COD glucuronidation enzyme was investigated by baculovirus-expressed UGT2B7 enzyme.

2.2.2 C6G glucuronidation assay

Incubation mixtures, in a total volume of 200 µL, contained phosphate buffer (0.1 M, pH 7.4), $MgCl_2$ (4 mM), UDPGA (5 mM), COD (0.025–10 mM) and activated HLM (1 mg/mL) or baculovirus-expressed UGT2B4 and 2B7 enzymes (1 mg/mL). Following a 5 min pre-incubation, reactions were initiated by the addition of UDPGA (5 mM) and performed at 37 °C in a shaking water bath for 60 min (HLM) and 120 min (UGT2B4 and 2B7). Reactions were terminated by the addition of 2.5 µL of 70% v/v perchloric acid ($HClO_4$) and cooling on ice for 20 min. Samples were subsequently centrifuged at 5,000 ×*g* for 10 min at 10 °C. A 120 µL aliquot of supernatant fraction was transferred to a 1.5-mL Eppendorf tube containing 2 µL of 4 M KOH, mixed, and centrifuged at 14,000 ×*g* for 5 min. Five microlitres of the supernatant fraction was injected directly into the HPLC column. For reactions carried out in the presence of BSA (2%), a lower range of COD concentration (0.025–3 mM) was employed as a consequence of the lower K_m in the presence of albumin (see Results). Incubation conditions were as described for reactions in the absence of BSA. Due to the higher protein concentration, reactions were terminated by addition of 8 µl of 70% $HClO_4$ and the supernatant fraction was treated with 6 µL of 4 M KOH.

C6G formation was not detected when UDPGA was incubated with lysate from untransfected HEK293 cells or control Supersomes. Similarly, there was no evidence for the formation of a glucoside conjugate when lysate from untransfected HEK293 cells or control Supersomes was incubated with UDP-glucose.

2.2.3 Quantification of C6G formation

HPLC was performed using an Agilent 1100 series instrument (Agilent Technologies, Sydney, Australia) fitted with a Security Guard C18 cartridge (4 × 3 mm; Phenomenex, Sydney, Australia) and a Synergi Hydro-RP C18 column (3 × 150 mm; 4 µm Phenomenex, Torrance, CA). The mobile phase consisted of 2 mM triethylamine (TEA) (pH adjusted to 2.7 with $HClO_4$) combined with 14% acetonitrile at a flow rate 1 mL/min. Column eluant was monitored by UV absorbance at 205 nm. Retention times of C6G and COD were 1.95 and 3.08 min, respectively (Fig.2.1 and Fig.2.2). C6G formation in incubation samples was quantified by comparison of peak areas to those of a COD standard curve prepared in phosphate

buffer (0.1 M, pH 7.4) over the concentration range 2-40 μM. The slope of the COD standard curve was comparable to that generated with an authentic standard of C6G (Fig.2.3). Linearity of product formation with respect to incubation time and microsomal protein concentration was determined at substrate concentrations of 0.5 and 10 mM. The formation of C6G was linear with incubation times to at least 100 min and microsomal protein concentrations to at least 1.25 mg/mL (Fig.2.4). Overall within day assay reproducibility was assessed by measuring C6G formation in 9 separate incubations of the same batch of pooled HLM. Coefficients of variation were 2.13% and 2.65% for the COD concentrations of 0.5 and 10 mM, respectively.

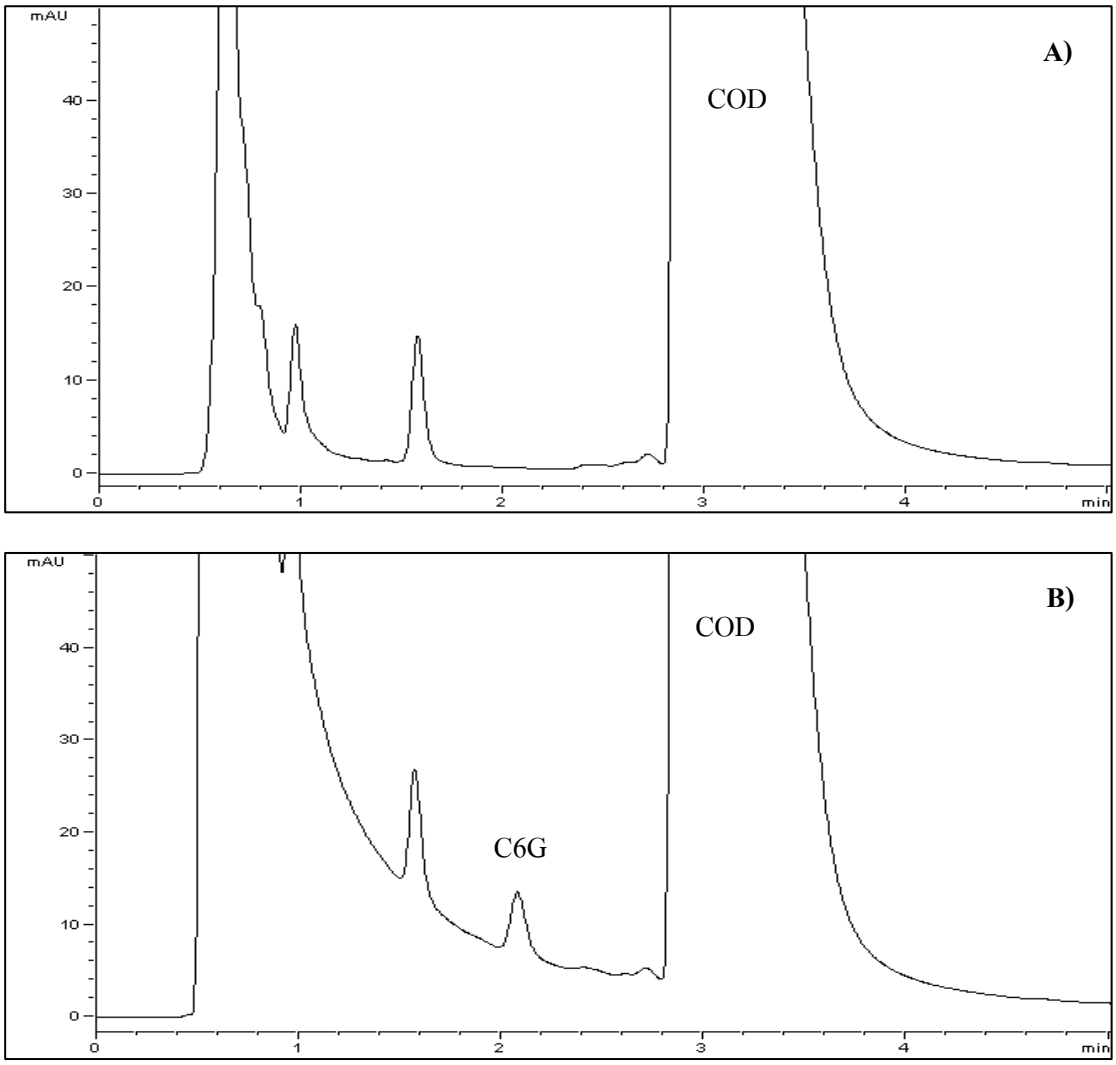

Figure 2.1 Representative HPLC chromatograms of codeine and codeine-6-glucuronide in human liver microsome: A) Codeine (5 mM) incubated with human liver microsomes (1 mg/mL) for 60 min in the absence of UDPGA; B) Codeine (5 mM) incubated with human liver microsomes (1 mg/mL) for 60 min in the presence of UDPGA.

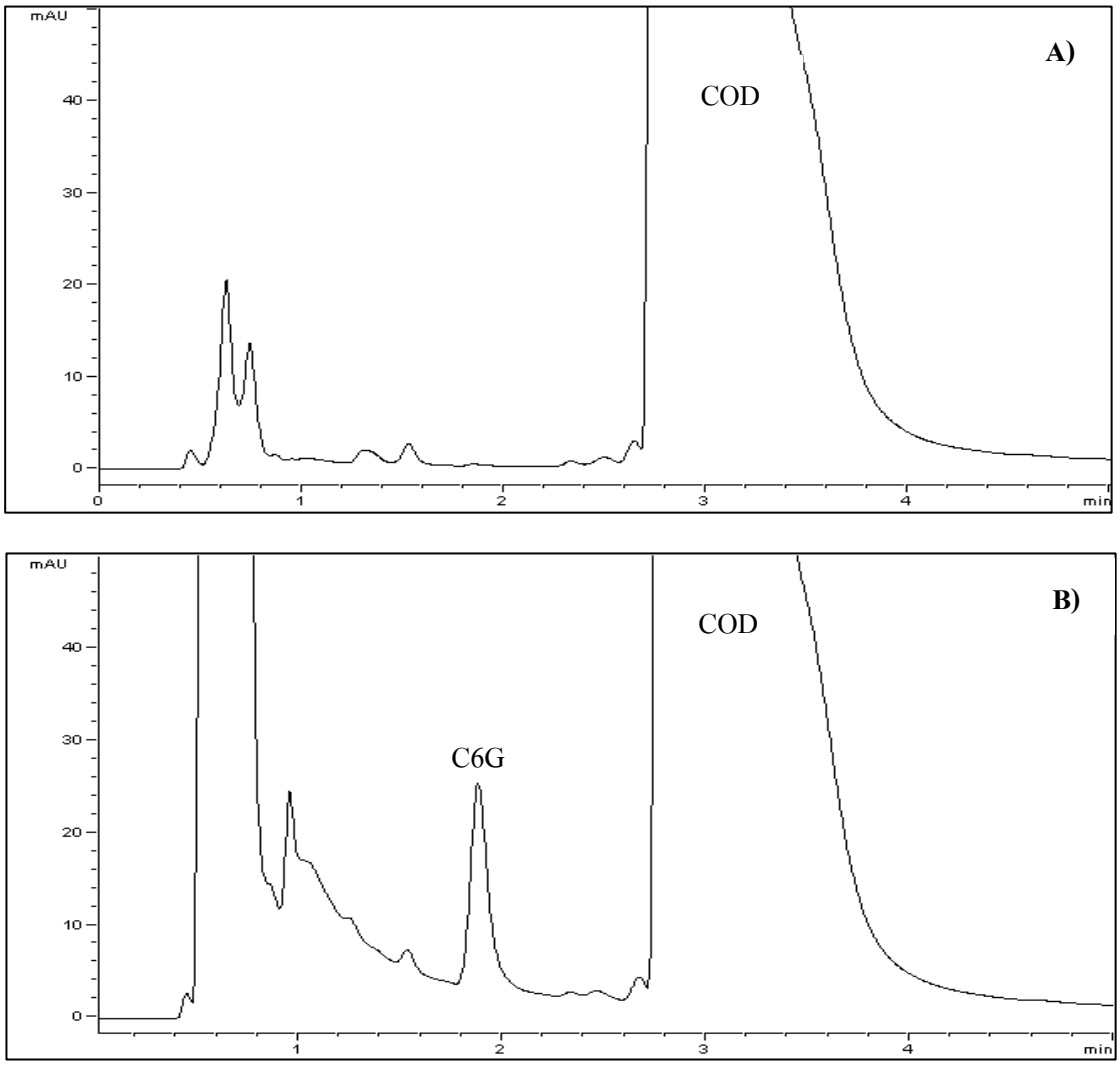

Figure 2.2 Representative HPLC chromatograms of codeine and codeine-6-glucuronide in baculovirus-expressed UGT2B7 enzyme: A) Codeine (5 mM) incubated with baculovirus-expressed UGT2B7 enzyme (1 mg/mL) for 120 min in the absence of UDPGA; B) Codeine (5 mM) incubated with baculovirus-expressed UGT2B7 enzyme (1 mg/mL) for 120 min in the presence of UDPGA.

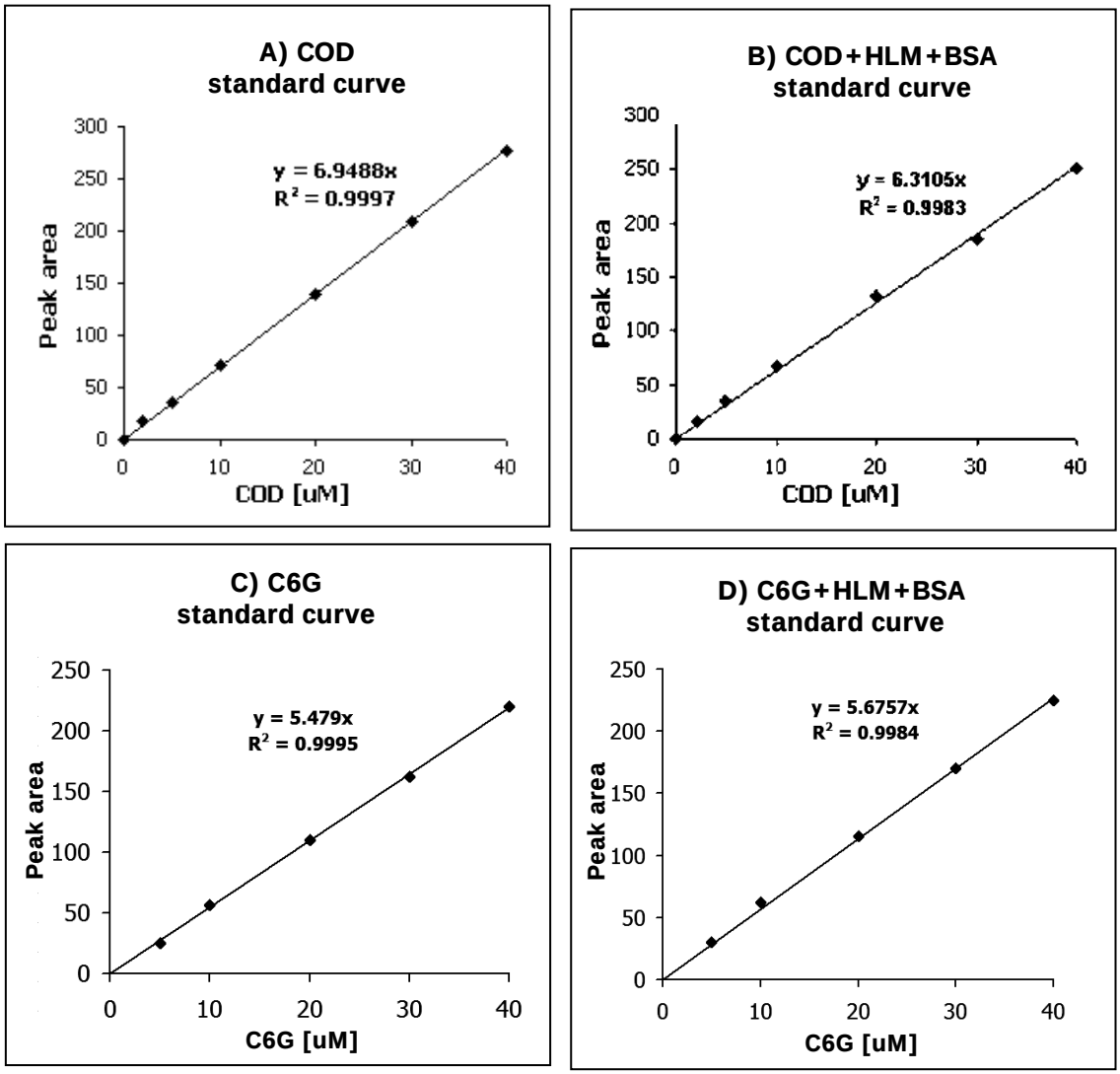

Figure 2.3 Representative codeine and codeine-6-glucuronide standard curves: Panels A,C) Prepared in phosphate buffer (0.1 M, pH 7.4); Panels B,D) Prepared in phosphate buffer (0.1 M, pH 7.4) with pooled human liver microsomes (1 mg/mL) and 2% (w/v) bovine serum albumin.

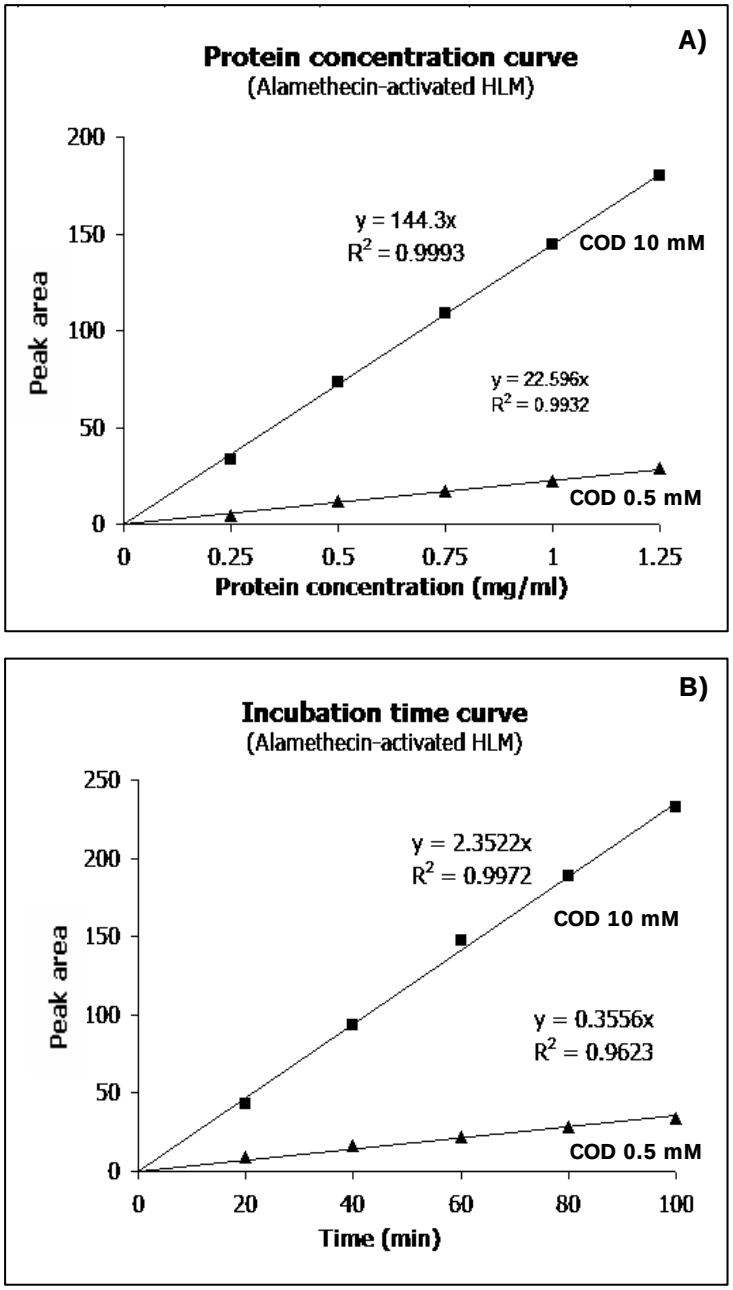

Figure 2.4 Relationships between codeine-6-glucuronide formation by alamethicin-activated human liver microsomes: Panel A) Protein concentration curve of codeine (0.5 and 10 mM) incubated with protein 0.25-1.25 mg/mL for 60 min; Panel B) Incubation time curve of codeine (0.5 and 10 mM) incubated with protein 1 mg/mL for 20-100 min.

2.2.4 COD glucuronidation of recombinant UGT enzymes

HEK293-expressed UGT enzymes (UGT 1A1, 1A3, 1A4, 1A6, 1A7, 1A8, 1A9, 1A10, 2B4, 2B7, 2B10, 2B15, and 2B17) activity screening studies were conducted at three COD concentrations (0.5, 2 and 10 mM), in the absence and presence 2% BSA, using the incubation and assay conditions described above. Due to the lower activity of recombinant UGT enzymes, the incubation mixture was modified by using 2 mg/mL for protein concentration and an incubation time of 120 min.

2.2.5 COD and inhibitor binding to HLM and BSA

The binding of COD and inhibitors (viz. KTM, KTZ and VPA) to HLM (1 mg/mL) or a combination of HLM (1 mg/mL) and 2% BSA was investigated using the equilibrium dialysis method reported previously by McLure *et al*. (2000). One side of the dialysis cell contained the drug in phosphate buffer (0.1 M, pH 7.4), while the other compartment contained a suspension of either pooled HLM (1 mg/mL) or a combination of 2% BSA and HLM (1 mg/mL) in phosphate buffer (0.1 M, pH 7.4). Drug binding was characterized at 5 or 6 concentrations over the ranges shown in Table 2.1: COD (25-10,000 μM); KTZ (2.5-250 μM); KTM (2-250 μM); and VPA (500-6,000 μM). The dialysis cell assembly was immersed in a water bath maintained at 37 °C and rotated at 12 rpm for 4-5 hr. Control experiments were performed with phosphate buffer or HLM, or a combination of 2% BSA with HLM on both sides of the cell, at low and high drug concentrations, to ensure that equilibrium was attained. A 200 μL aliquot was collected from each cell and treated with 500 μL of ice-cold methanol containing 4% glacial acid, or 800 μL of ice-cold acetonitrile (for samples containing KTZ). Samples were chilled on ice for 20 min and subsequently centrifuged at 13,000 ×*g* for 5 min at 4 °C. An aliquot of the supernatant fraction was analyzed by HPLC.

The HPLC system employed was as described previously for the measurement of C6G formation. Chromatography conditions for each analyte are detailed in Table 2.1. HPLC chromatograms of COD, KTM, KTZ and VPA are illustrated in Fig.2.5, 2.6, 2.7, and 2.8, respectively. Drug concentrations of dialysis samples recovered from each side of the cell were calculated by reference to peak areas of standard curves that spanned both the bound and unbound

concentrations of each compound. Standard curves of each drug were prepared in phosphate buffer (0.1 M, pH 7.4) alone or in combination with phosphate buffer (0.1 M, pH 7.4) and protein (HLM and BSA), and then treated in the same manner as dialysis samples (Fig.2.9-2.12). Binding to incubation components, calculated as the drug concentration in the buffer compartment divided by the drug concentration in the protein compartment, is expressed as the fraction unbound in incubations ($f_{u,inc}$). Microsomal and BSA binding data for FLZ have previously been reported by Uchaipichat *et al*. (2006a).

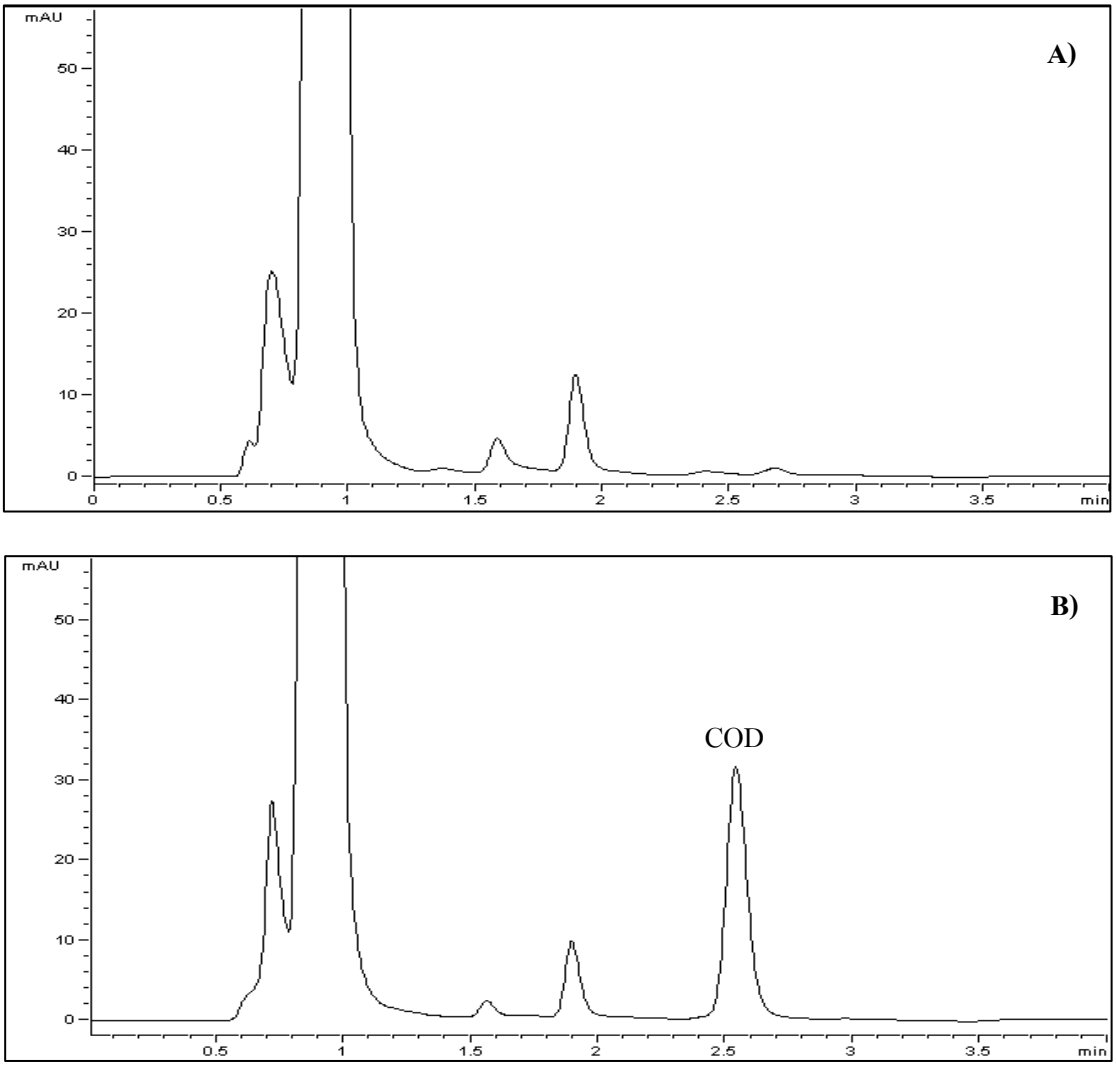

Figure 2.5 Representative HPLC chromatograms of codeine in equilibrium dialysis samples: A) Blank containing pooled human liver microsomes (1 mg/mL) in phosphate buffer (0.1 M, pH 7.4); B) Codeine (0.1 mM) in pooled human liver microsomes (1 mg/mL) in phosphate buffer (0.1 M, pH 7.4).

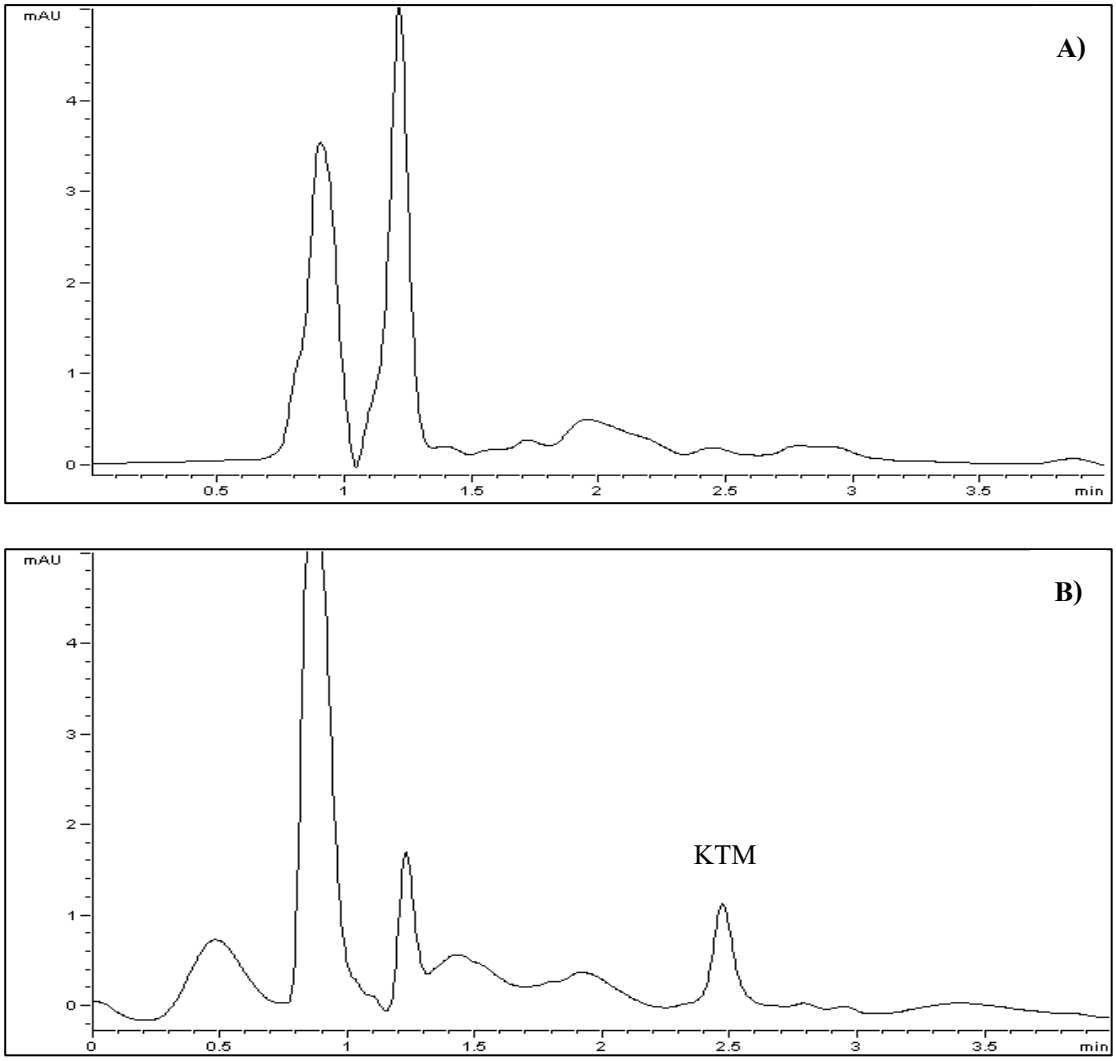

Figure 2.6 Representative HPLC chromatograms of ketamine in equilibrium dialysis samples: A) Blank containing pooled human liver microsomes (1 mg/mL) in phosphate buffer (0.1 M, pH 7.4); B) Ketamine (10 μM) in pooled human liver microsomes (1 mg/mL) in phosphate buffer (0.1 M, pH 7.4).

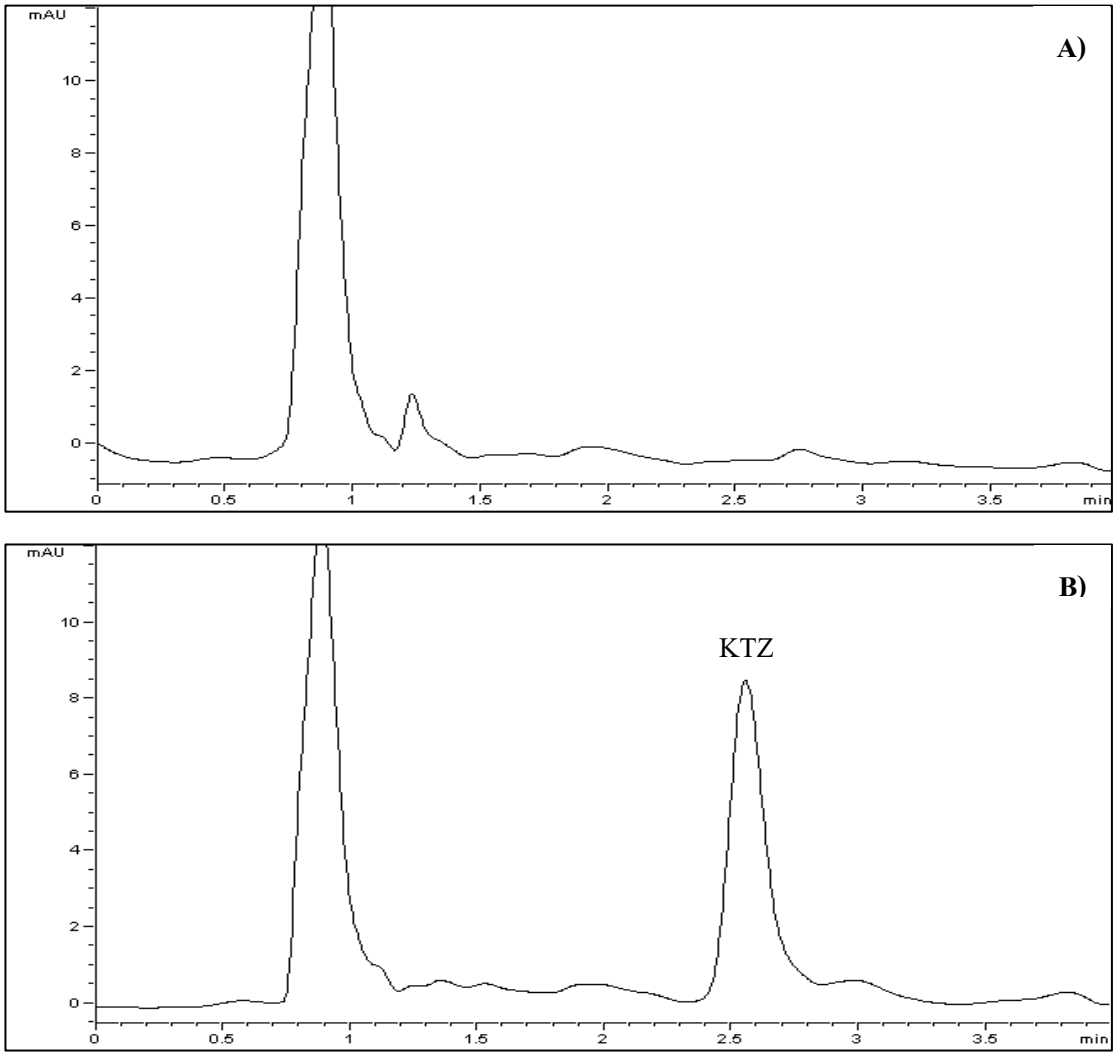

Figure 2.7 Representative HPLC chromatograms of ketoconazole in equilibrium dialysis samples: A) Blank containing pooled human liver microsomes (1 mg/mL) in phosphate buffer (0.1 M, pH 7.4); B) Ketoconazole (10 μM) in a combination of 2% (w/v) bovine serum albumin with pooled human liver microsomes (1 mg/mL).

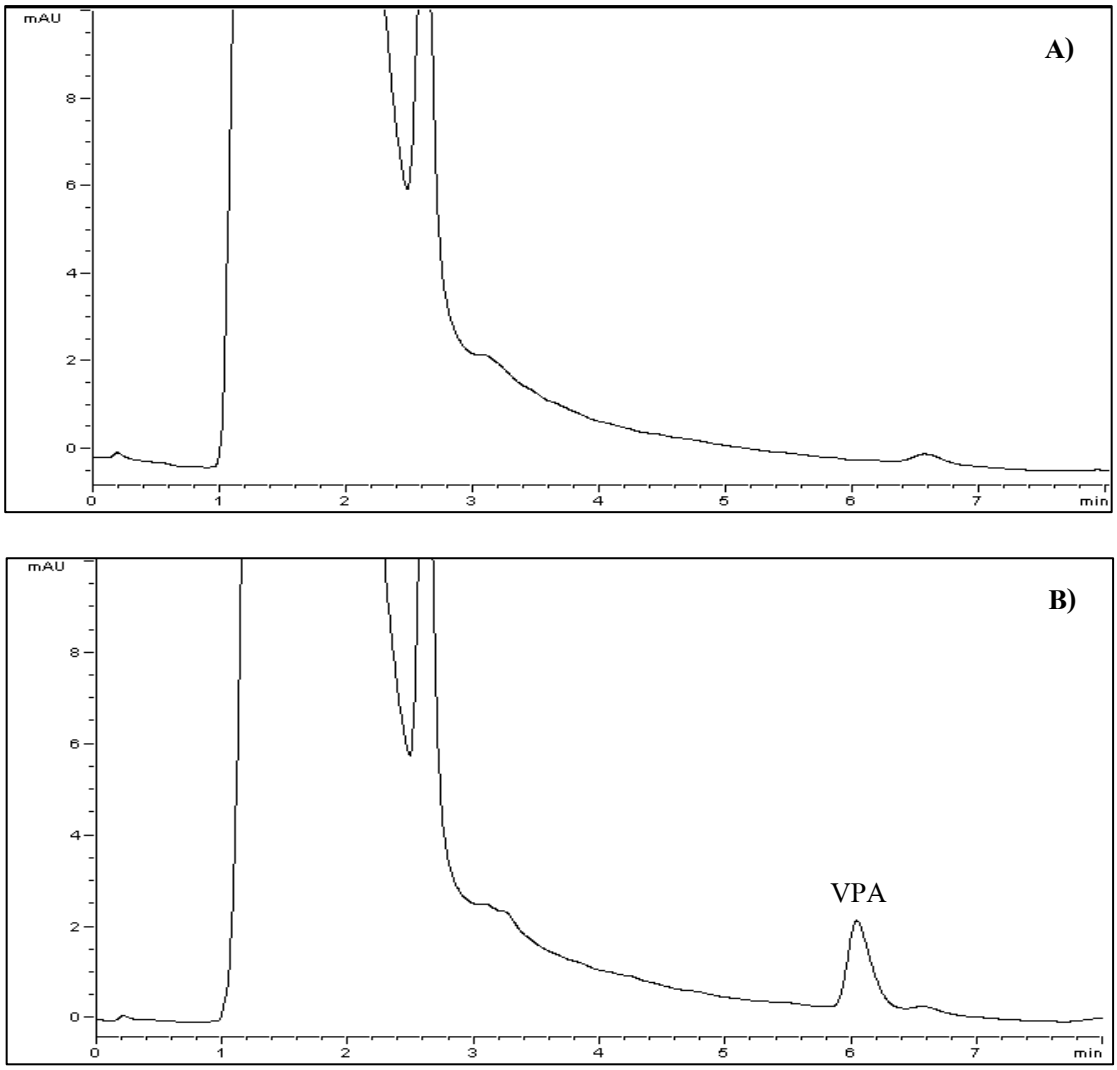

Figure 2.8 Representative HPLC chromatograms of valproic acid in equilibrium dialysis samples: A) Blank containing pooled human liver microsomes (1 mg/mL) in phosphate buffer (0.1 M, pH 7.4); B) Valproic acid (1 mM) in pooled human liver microsomes (1 mg/mL) in phosphate buffer (0.1 M, pH 7.4).

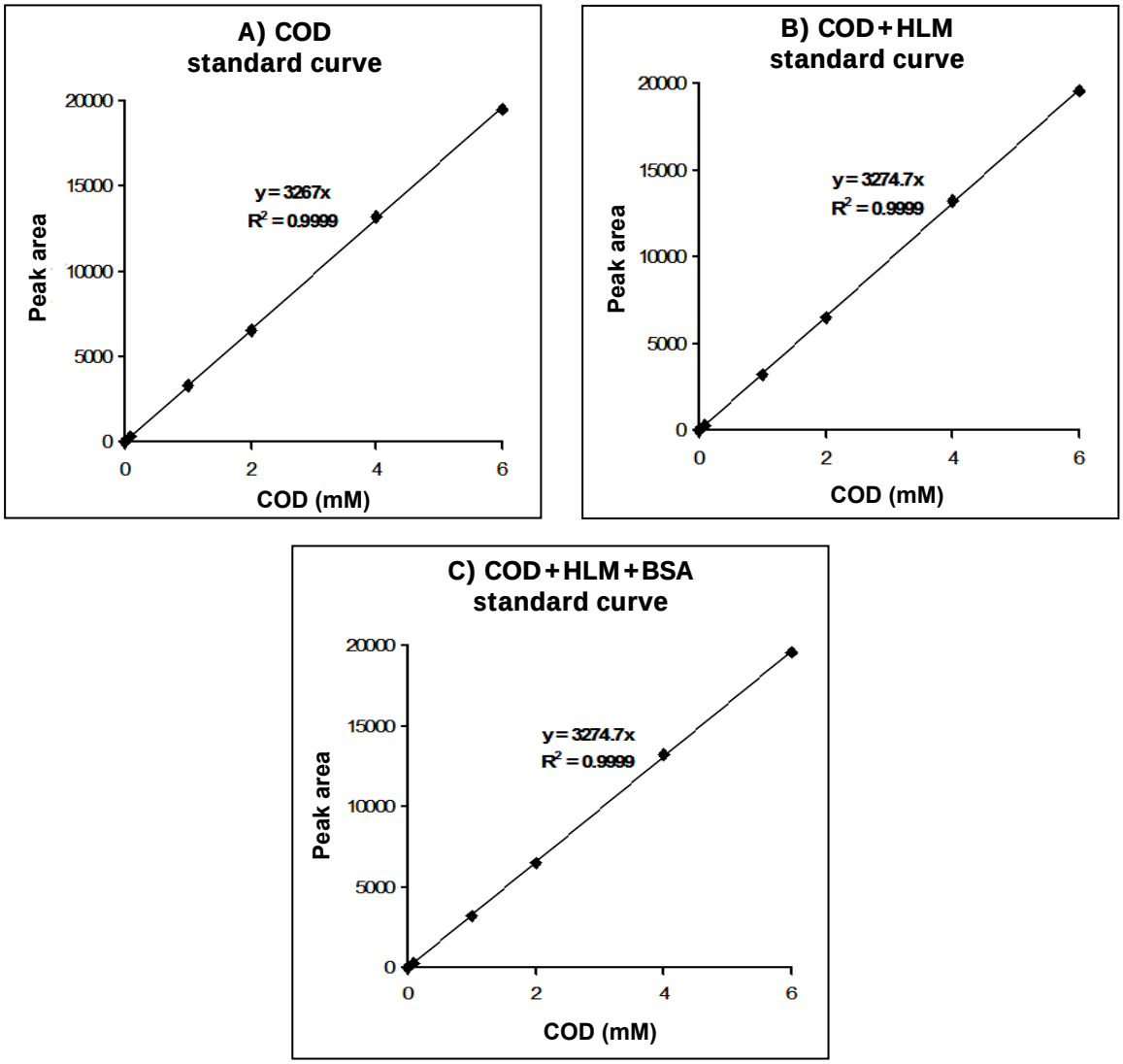

Figure 2.9 Representative codeine standard curves for equilibrium dialysis samples: Panel A) Phosphate buffer (0.1 M, pH 7.4) alone; Panel B) Phosphate buffer (0.1 M, pH 7.4) with pooled human liver microsomes (1 mg/mL); Panel C) Phosphate buffer (0.1 M, pH 7.4) with pooled human liver microsomes (1 mg/mL) and 2% (w/v) bovine serum albumin.

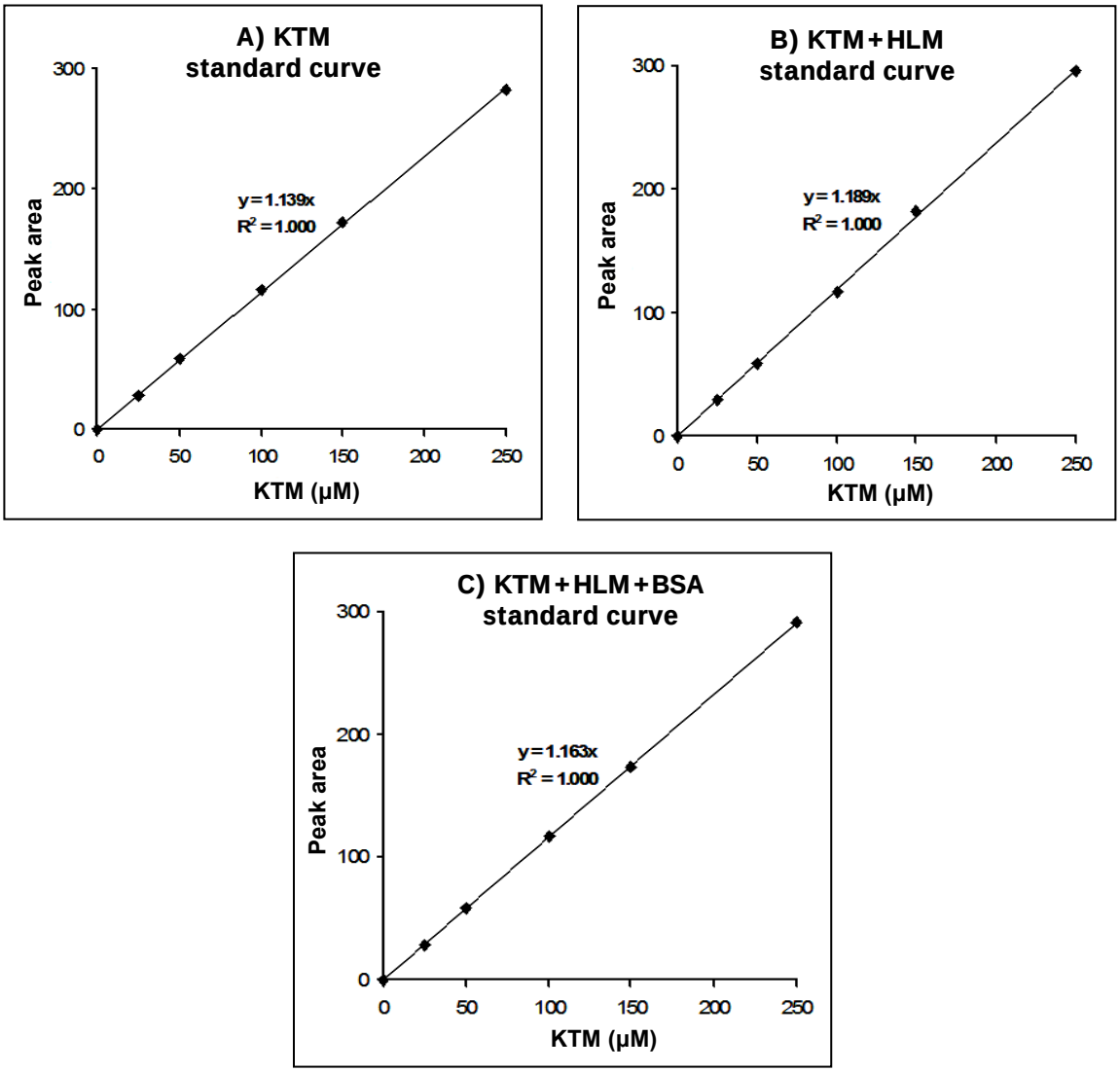

Figure 2.10 Representative ketamine standard curves for equilibrium dialysis samples: Panel A) Phosphate buffer (0.1 M, pH 7.4) alone; Panel B) Phosphate buffer (0.1 M, pH 7.4) with pooled human liver microsomes (1 mg/mL); Panel C) Phosphate buffer (0.1 M, pH 7.4) with pooled human liver microsomes (1 mg/mL) and 2% (w/v) bovine serum albumin.

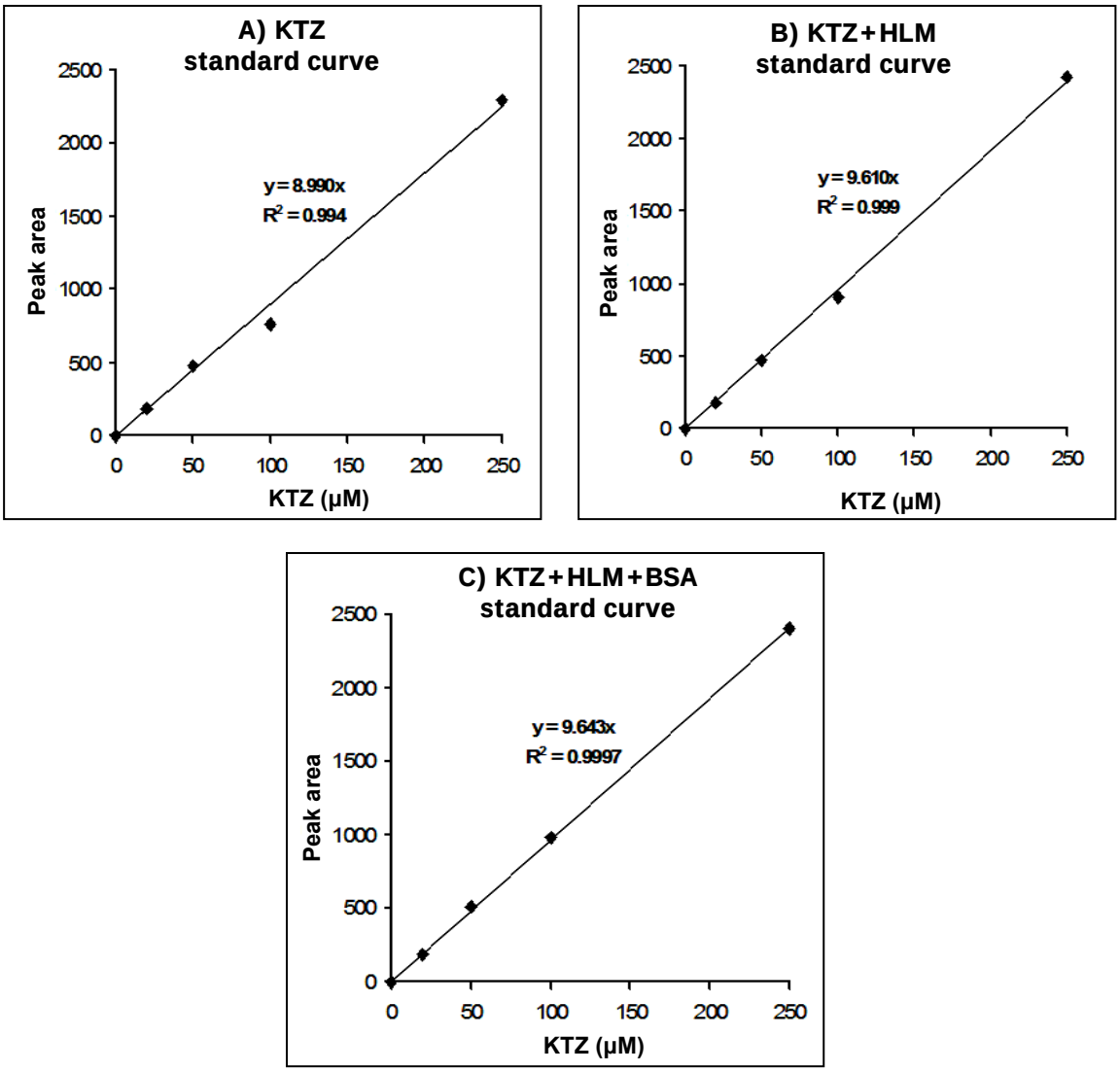

Figure 2.11 Representative ketoconazole standard curves for equilibrium dialysis samples: Panel A) Phosphate buffer (0.1 M, pH 7.4) alone; Panel B) Phosphate buffer (0.1 M, pH 7.4) with pooled human liver microsomes (1 mg/mL); Panel C) Phosphate buffer (0.1 M, pH 7.4) with pooled human liver microsomes (1 mg/mL) and 2% (w/v) bovine serum albumin.

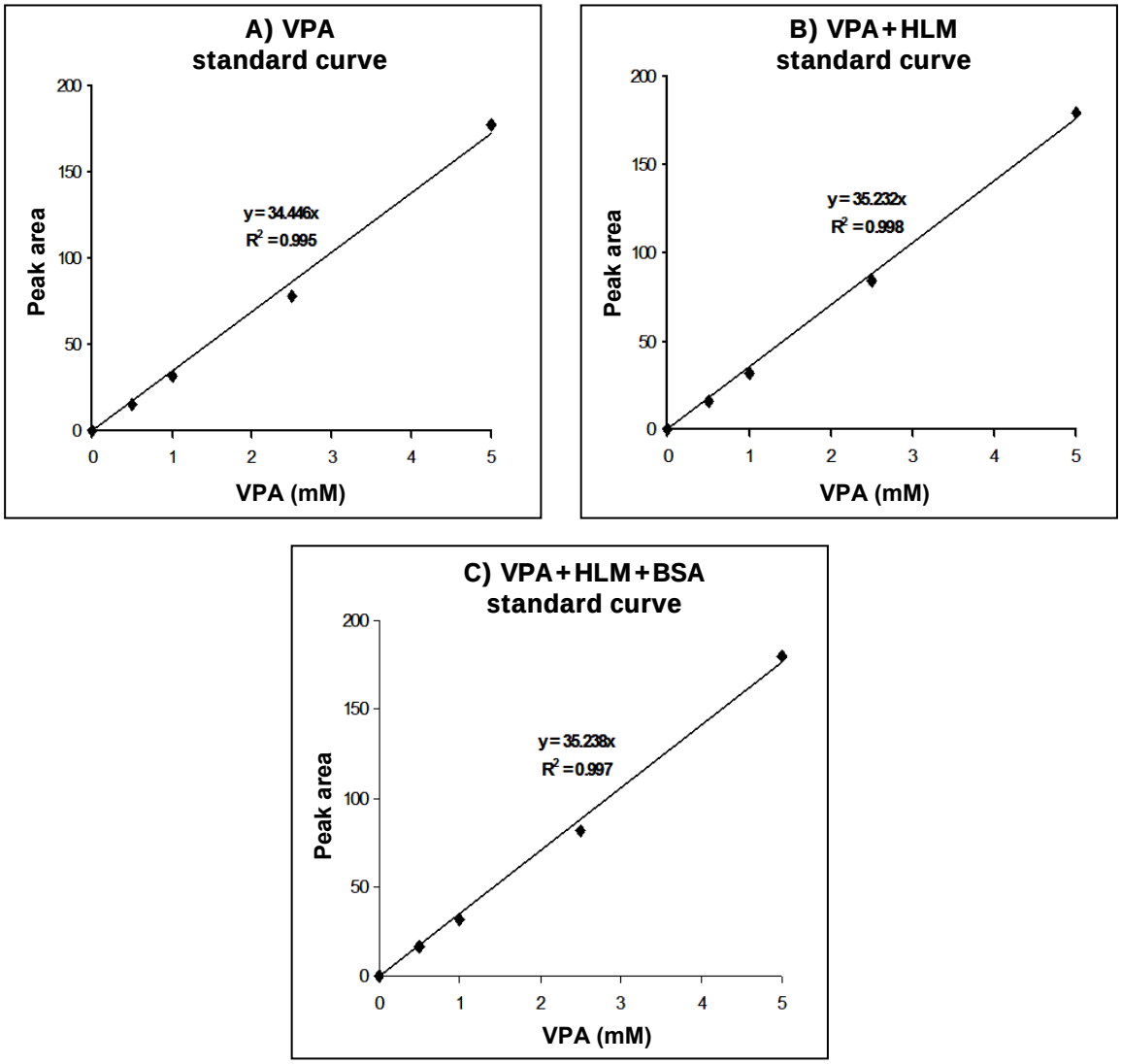

Figure 2.12 Representative valproic acid standard curves for equilibrium dialysis samples: Panel A) Phosphate buffer (0.1 M, pH 7.4) alone; Panel B) Phosphate buffer (0.1 M, pH 7.4) with pooled human liver microsomes (1 mg/mL); Panel C) Phosphate buffer (0.1 M, pH 7.4) with pooled human liver microsomes (1 mg/mL) and 2% (w/v) bovine serum albumin.

Table 2.1 HPLC conditions for the measurement of drug binding by equilibrium dialysis.

Drug	Concentration range	Column	Mobile phase	Detector wavelength (nm)	Flow rate (mL/min)	Retention time (min)	Calibration range
Codeine	**No BSA:** 0.1-10 mM **With BSA:** 0.25-3 mM	Synergi Hydro-RP C18 column (3 × 150 mm; 4 µm)	2 mM TEA (pH adjusted to 2.7 with $HClO_4$) combined with 14% acetonitrile	205	1	2.58	0.1-6 mM
Ketamine	**No BSA:** 10-250 µM **With BSA:** 2-50 µM	NovaPak C18 column (3.9 × 150 mm; 5 µm)	50%:50% mixtures of 30 mM phosphate buffer in TEA (pH 7.2) with acetonitrile	215	1	2.48	25-250 µM
Ketoconazole	**No BSA:** 10-250 µM **With BSA:** 10-250 µM	NovaPak C18 column (3.9 × 150 mm; 5 µm)	50%:50% mixtures of 30 mM phosphate buffer in TEA (pH 7.2) with acetonitrile	215	1	2.58	20-250 µM
Valproic acid	**No BSA:** 0.5-6 mM **With BSA:** 0.5-6 mM	Zorbax Eclipse XBD-C8 analytical column (4.6 × 150 mm; 5 µm)	55%:45% mixture of phosphate buffer (pH 3.1, 25 mM) with acetonitrile	210	1	6.12	0.5-5 mM

2.2.6 Inhibition of COD glucuronidation by inhibitors

Pooled HLM was prepared by mixing equal protein amounts from the five livers (H7, H10, H12, H13, and H40) used in the kinetic studies. The IC_{50} values for inhibition of COD glucuronidation were determined using the COD concentration corresponding to the apparent K_m value obtained from the kinetic studies of COD glucuronidation by HLM (i.e. 2 and 0.3 mM) in the absence and presence of BSA (2%), respectively. C6G activity was measured at five inhibitor concentrations ranging from 0.05-2.5 mM (FLZ); 0.05-1 mM (KTM); 0.05-1 mM (KTZ); and 1-20 mM (VPA) in the absence of BSA. In the presence of BSA, inhibitor concentrations were in the same range as those in the experiments without BSA except that the concentration range was 1-20 μM and 0.5-10 mM for KTM and VPA, respectively.

To determine the K_i value and inhibition mechanisms, four inhibitor concentrations in the range of 0.1-2.5 mM (FLZ); 25-250 μM (KTM); and 20-250 μM (KTZ) were used at each of three COD concentrations (1, 2, and 4 mM) in the absence of BSA. For incubations in the presence of BSA, the KTZ concentration range was similar to that in the absence of BSA, but the FLZ and KTM concentrations ranges were 0.05-1 mM and 2-20 μM, respectively and the three COD concentrations used were 0.15, 0.3, and 0.6 mM. FLZ and KTM were dissolved in water while KTZ and VPA were dissolved in methanol such that the final concentration of methanol added to incubations was 1% v/v which had a negligible effect on HLM (Uchaipichat *et al*., 2004). Where the binding was measurable, the concentration of each inhibitor was corrected by the $f_{u,inc}$ value to determine the IC_{50} and K_i values.

2.2.7 Data analysis

2.2.7.1 COD kinetic parameters

The kinetic data were presented as mean (±SD.) values derived from the experimental data. Kinetic constants for COD glucuronidation by HLM determined in the presence and absence of BSA were generated by fitting untransformed experimental data to the following equations.

The Michaelis–Menten equation (equation 2.1; Houston and Kenworthy, 2000):

$$\upsilon = \frac{V_{max} \times [S]}{K_m + [S]} \qquad \text{equation 2.1}$$

where υ is the rate of reaction, V_{max} is the maximum velocity, K_m is the Michaelis-Menten constant (substrate concentration at 0.5 V_{max}) and [S] is the substrate concentration.

The substrate inhibition equation (equation 2.2; Houston and Kenworthy, 2000):

$$\upsilon = \frac{V_{max}}{(1 + (K_m/[S]) + ([S]/K_{si}))} \qquad \text{equation 2.2}$$

where K_{si} is the constant describing the substrate inhibition interaction.

The Hill equation which describes sigmoidal kinetics (equation 2.3; Houston and Kenworthy, 2000):

$$\upsilon = \frac{V_{max} \times [S]^n}{S_{50}^n + [S]^n} \qquad \text{equation 2.3}$$

where the substrate concentration resulting in 50% of V_{max} (S_{50}) is analogous to K_m in the Michaelis-Menten equation, and n is the Hill coefficient.

In all cases, fitting was based on unbound substrate concentrations in incubations and performed with EnzFitter (Biosoft, Cambridge, UK). The CL_{int} for COD glucuronidation by HLM and recombinant UGT2B7 was determined as V_{max}/K_m in the case of Michaelis-Menten and substrate inhibition kinetics. For sigmoidal kinetic, the CL_{max} provides an estimate of the highest clearance attained, which is when the enzyme is fully activated before saturation occurs. The CL_{max} was determined as a following equation (Houston and Kenworthy, 2000).

$$CL_{max} = \frac{V_{max}}{S_{50}} \times \frac{(n-1)}{n(n-1)^{1/n}} \qquad \text{equation 2.4}$$

where V_{max} is the maximum velocity, S_{50} is the substrate concentration resulting in 50% of V_{max}, and n is the Hill coefficient.

The concentration of the inhibitor that is required to produce the IC_{50} was determined by using EnzFitter (Biosoft). The K_i value for determination the effect of each inhibitor on COD glucuronidation was determined by fitting the expressions for competitive, noncompetitive, and mixed inhibition to experimental data using EnzFitter (Biosoft). Goodness of fit to kinetic and inhibition mechanisms were assessed from the F statistic, r^2 values, parameter standard error (SE.) estimates and 95% confidence intervals. Kinetic constants are reported as the value ± SE. of the estimated parameters.

2.2.7.2 IV-IVE

A-1) Prediction of COD glucuronidation clearance

Microsomal COD glucuronidation intrinsic clearance by HLM is determined as units of µl/min/mg microsomal protein and subsequently converted to whole-liver CL_{int} ($CL_{int.liver}$) using scaling factors that correct for microsomal yield and liver weight according to the following equation:

$$CL_{int.liver} = \left[\frac{V_{max}(HLM)}{K_m(HLM)} \right] \times MPPGL \times LW \qquad \text{equation 2.5}$$

where MPPGL is the mass of microsomes per gram of human liver tissue taken as 38 mg/g corresponding to the geometric mean of the microsomal yield reported by Hakooz *et al*. (2006) and LW is the average weight of a huam liver (1,500 g). The result was multiplied by 0.00006 to express CL_{int} in L/hr. In vivo CL_H was predicted using the expression for the well-stirred model (Houston, 1994):

$$CL_H = \frac{Q_H \times f_u \times CL_{int}}{Q_H + f_u \times CL_{int}} \qquad \text{equation 2.6}$$

where f_u is fraction unbound in blood and Q_H is liver blood flow, assumed to be 90 L/hr. The fraction of drug unbound in blood was calculated as $f_u = f_{u,p} / R_B$, where R_B is the

blood to plasma concentration ratio and $f_{u,p}$ is the fraction unbound in plasma. For COD, $f_{u,p}$ was taken as 0.93 (Soars *et al*., 2002) and R_B as 1 (Carlile *et al*., 1999).

The In vivo CL_H value for COD glucuronidation was obtained from the literature. The mean COD systemic clearance is 44.95 L/hr per 70 kg (Bertz and Granneman, 1997; Vozeh, 1988). Because approximately 80% of COD was glucuronidated to C6G (Yue *et al*., 1991), therefore the plasma COD clearance by glucuronidation in vivo was taken as 35.96 L/hr per 70 kg.

A-2) Prediction of the inhibition of COD hepatic clearance

The extent of inhibition of COD hepatic clearance (determined as the ratio of the areas under the plasma COD concentration - time curves with and without inhibitor co-administration) was predicted using the equation for oral administration of an hepatically cleared drug (Miners *et al*., 2010);

$$\text{AUC ratio} = \frac{\text{AUC (+inhibitor)}}{\text{AUC (control)}} = \frac{1}{\frac{f_m}{1+[I]/K_i} + \left(1 - f_m\right)} \qquad \text{equation 2.7}$$

where [I] is the inhibitor concentration at the enzyme active site; f_m is the fraction of COD hepatic clearance via glucuronidation (taken here as 80%; Yue *et al*., 1991), and K_i is the inhibitor constant generated in vitro in the presence of BSA. The [I] value was taken as the maximum hepatic inlet concentration of the drug in vivo (Miners *et al*., 2010);

$$I_{inlet} = I_{max} + \frac{k_a \times F_a \times Dose}{Q_H} \qquad \text{equation 2.8}$$

where [I_{max}], k_a, F_a, and Q_H are the maximum total drug concentration in the systemic circulation associated with a given dose (Table 2.2), absorption rate constant, and fraction absorbed from the GI tract, and liver blood flow (taken as 90 L/hr or 1.5 L/min), respectively. The hepatic maximum unbound inlet concentration was calculated as the product of [$I_{inlet,max}$] and fraction unbound in plasma. Maximum hepatic inlet concentrations (total and unbound) were calculated from published pharmacokinetic data for FLZ (Sahai *et al*., 1994; Uchaipichat *et al*., 2006a). In contrast to FLZ, since KTM is administrated in favor of the IV route and there are no reliable estimates of k_a and F_a for KTZ, it was not possible to calculate $I_{inlet,max}$.

Thus, IV-IVE was based on reported the maximum concentration in plasma both total and unbound inhibitor concentrations for KTM (Clements ans Nimmo, 1981), and KTZ (Badcock *et al*., 1987; Daneshmend and Warnock, 1988).

Table 2.2 Pharmacokinetic parameters for the calculation the extent of inhibition of COD hepatic clearance based on the AUC ratio.

Parameters	Inhibitors		
	Fluconazole	**Ketamine**	**Ketoconazole**[a]
Route of administration	PO	IV	-
Molecular weight (g/mol)	306.27	237.73	531.43
Dose (mg/day)	400	18.70	200
Dose (μM)	1306	78.66	376.34
Plasma protein binding (%)	11	47	99
$f_{u,p}$	0.89	0.53	0.01
F_a	1	-	-
K_a (min^{-1})	0.1	-	-
I_{max} (μM)	77.70	0.45	3.20
K_i (μM)	202	3.51	0.66

[a] Calculation was based on reported the maximum concentration in plasma.

CHAPTER 3

RESULTS

3.1 Binding of COD and inhibitors to HLM and BSA

Nonspecific binding to HLM and binding to HLM plus BSA was characterized here for COD and the putative inhibitors KTZ, KTM and VPA (Table 3.1). Previous studies from this laboratory demonstrated that FLZ does not bind nonspecifically to HLM, and that binding of FLZ to HLM plus 2 % BSA is negligible (Uchaipichat *et al*., 2006a). The binding of COD and VPA to HLM alone was negligible across the concentration ranges investigated. The binding of COD to the mixture of HLM and BSA (2%) was also minor. KTM bound modestly to HLM plus BSA, although the binding of KTM to HLM alone was negligible. KTZ bound extensively to both HLM and to HLM plus BSA, with mean $f_{u,inc}$ values of 0.27 ± 0.01 and 0.09 ± 0.01, respectively. Consistent with a previous report (Rowland *et al*., 2006), the binding of VPA to the HLM/BSA mixture was concentration dependent; $f_{u,inc}$ values ranged from 0.29 at the lowest VPA concentration (0.5 mM) to 0.77 at the highest concentration (6 mM). Where observed, binding of inhibitors to HLM and to HLM plus BSA was accounted for in the calculation of IC_{50} and K_i values.

Table 3.1 Binding of codeine and inhibitors to human liver microsome (1 mg/ml) in the absence and presence of bovine serum albumin.

Drugs	Fraction unbound in incubations ($f_{u,inc}$)	
	HLM	**HLM plus 2% BSA**
Codeine	0.98 ± 0.013	0.96 ± 0.007
Fluconazole[a]	1.04 ± 0.020	0.92 ± 0.027
Ketamine	0.98 ± 0.019	0.79 ± 0.020
Ketoconazole	0.27 ± 0.005	0.09 ± 0.003
Valproic acid	0.99 ± 0.007	0.29-0.77[b]

Results are presented as fraction unbound ($f_{u,inc}$) ± SD.

[a] Data taken from Uchaipichat *et al*., 2006a.

[b] $f_{u,inc}$ concentration dependent in the range 0.5-6 mM.

3.2 C6G glucuronidation by HLM

Representative kinetic plots for C6G formation by HLM in the absence and presence of 2% BSA are shown in Fig.3.1, and derived kinetic constants are given in Table 3.2. C6G formation by HLM in the absence of BSA was well described by the Michaelis-Menten equation, whereas weak substrate inhibition (K_{si} approximately 40-times higher than K_m) was apparent for kinetic studies performed in the presence of BSA (2%). A transition from Michaelis Menten to weak substrate inhibition kinetics in the presence of BSA has been observed previously for AZT (Uchaipichat *et al*., 2006a), another UGT2B7 substrate. The addition of BSA to incubations resulted in an 8-fold reduction in K_m without an effect on V_{max} (Table 3.2). Microsomal CL_{int} increased in proportion to the change in K_m. Kinetic constants for COD glucuronidation by pooled HLM, prepared by mixing equal protein amounts of microsomes from the 5 separate livers, were similar to the mean data shown in Table 3.2; K_m and V_{max} values in the absence of BSA were 2.15 mM and 584 pmol/min.mg, while K_m, K_{si} and V_{max} values obtained for incubations supplemented with BSA (2%) were 0.23 mM, 8.15 mM, and 436 pmol/min.mg, respectively.

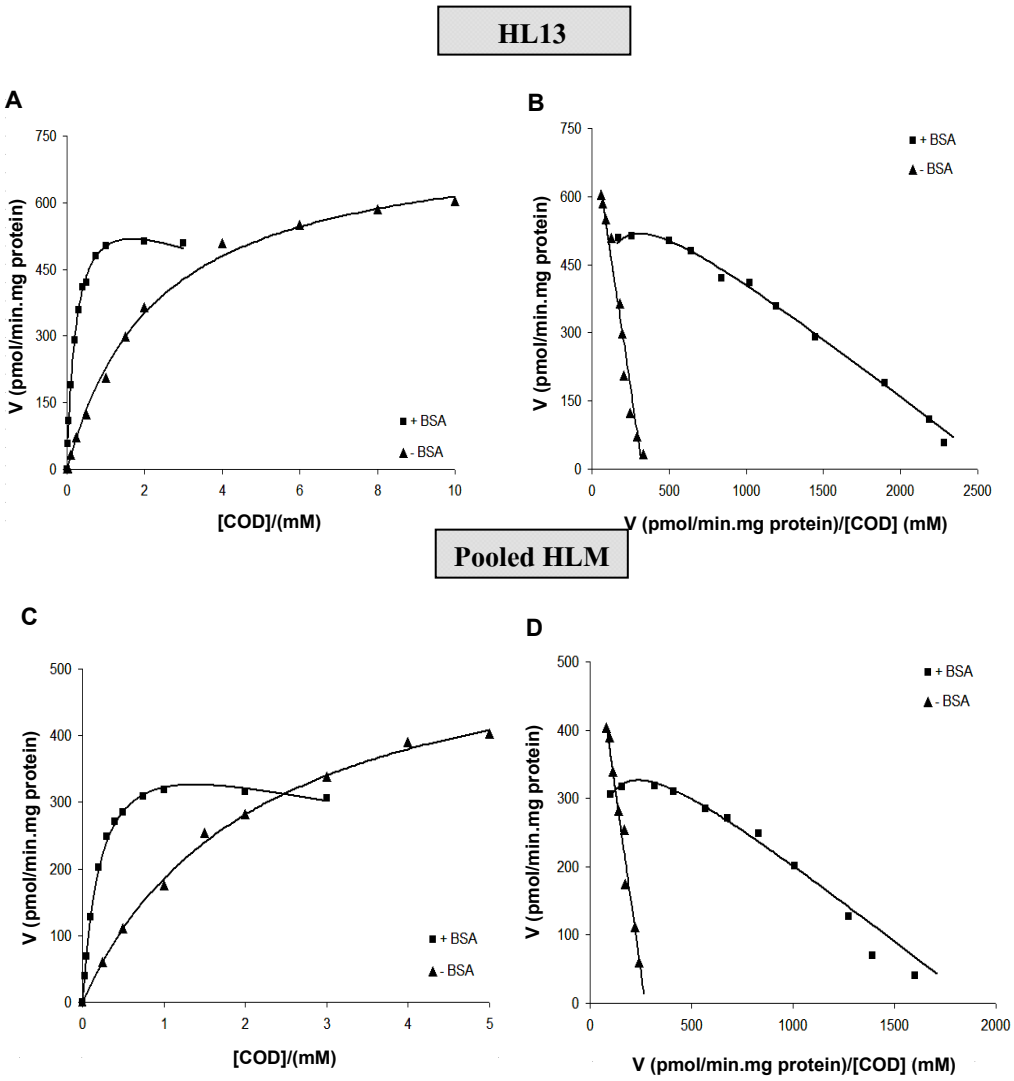

Figure 3.1 Kinetic plots for codeine 6-glucuronidation by microsomes from a representative human liver (HL13) and pooled human livers generated in the absence and presence of bovine serum albumin: Panels A and C) plots of the rate of product (C6G) formation versus substrate concentration; Panels B and D) Eadie-Hofstee plots. Points are experimentally derived values while curves are from model fitting.

Table 3.2 Derived kinetic parameters for codeine glucuronidation by human liver microsome determined in the absence and presence of bovine serum**.**

	Without BSA[a]			**With 2% BSA**[b]			
	K_m (mM)	V_{max} (pmol/min.mg)	CL_{int}[c] (µl/min/mg)	K_m (mM)	V_{max} (pmol/min.mg)	K_{si} (mM)	CL_{int}[c] (µL/min/mg)
HL7	2.35 ± 0.01	440 ± 1.2	0.19	0.32 ± 0.01	430 ± 9.7	8.20 ± 1.04	1.34
HL10	2.68 ± 0.02	312 ± 0.9	0.12	0.34 ± 0.01	303 ± 6.2	9.49 ± 1.19	0.89
HL12	3.13 ± 0.18	920 ± 20.8	0.29	0.28 ± 0.02	848 ± 23.8	14.42 ± 2.78	3.03
HL13	2.29 ± 0.12	754 ± 13.2	0.33	0.26 ± 0.001	680 ± 0.7	10.63 ± 0.12	2.62
HL40	1.16 ± 0.01	438 ± 0.5	0.38	0.24 ± 0.01	447 ± 6.6	14.46 ± 1.50	1.86
Mean ± SD.	2.32 ± 0.73	573 ± 253	0.26 ± 0.11	0.29 ± 0.04	541 ± 218	11.44 ± 2.87	1.95 ± 0.88
Pooled HLM	2.15 ± 0.13	584 ± 16	0.27	0.23 ± 0.01	436 ± 12	8.15 ± 1.03	1.90

Data presented as mean ± SE. of parameter fit.

[a] Kinetic constants derived from fitting with the Michaelis-Menten equation.

[b] Kinetic constants derived from fitting with the substrate inhibition equation.

[c] CL_{int} calculated as V_{max}/K_m for both Michaelis-Menten and substrate inhibition kinetics.

98

3.3 COD glucuronidation by recombinant UGTs

UGT1A1, 1A3, 1A4, 1A6, 1A7, 1A8, 1A9, 1A10, 2B4, 2B7, 2B10, 2B15, and 2B17 separately expressed in an HEK293 cell line were screened for C6G formation at three COD concentrations (0.5, 2, and 10 mM), both in the absence and presence BSA (2%). Although expression of all UGT enzymes was demonstrated by immunoblotting and activity measurements (data not shown), only UGT2B4 and UGT2B7 catalyzed the 6-glucuronidation of COD (Fig. 3.2). However, rates of C6G formation by these enzymes expressed in HEK293 cells were relatively low. Rates of COD glucuronidation by UGT2B4 at 10 mM was 2.1 pmol/min.mg in the absence of BSA and 1.7 and 1.3 pmol/min.mg at 2 and 10 mM COD concentrations in the presence of BSA, respectively. Respective rates of COD glucuronidation by UGT2B7 at COD concentrations of 0.5, 2 and 10 mM were 1.2, 2.8 and 4.2 pmol/min.mg in the absence of BSA, and 2.5, 3.1 and 4.6 pmol/min.mg in the presence of BSA. Compared to HEK293-expression, baculovius mediated expression in Sf9 cells UGTs showed higher UGT2B4 and UGT2B7 activities. Respective rates of C6G formation by baculovirus-expressed UGT2B4 at COD concentrations of 0.5, 2 and 10 mM were 6, 34 and 59 pmol/min.mg in the absence of BSA, and 23, 37 and 39 pmol/min.mg in the presence of BSA. With Sf9-expressed UGT2B7, respective rates of C6G formation at COD concentrations of 0.5, 2 and 10 mM were 13, 33 and 39 pmol/min.mg in the absence of BSA, and 36, 46 and 48 pmol/min.mg in the presence of BSA.

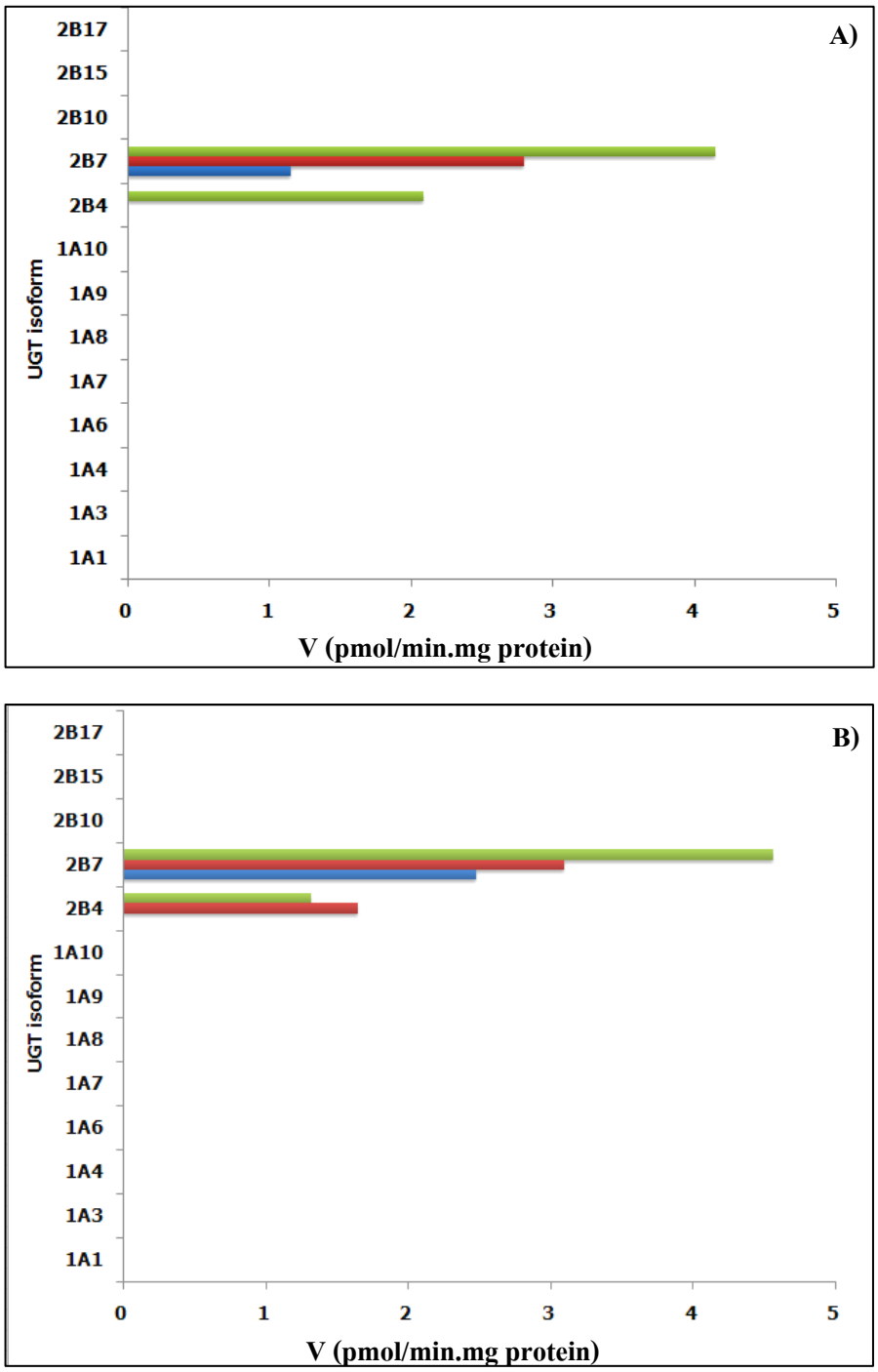

Figure 3.2 Representative the codeine glucuronidation by recombinant UGTs in HEK293-expression: Panel A) in the absence and Panel B) the presence bovine serum albumin. Codeine concentration; 0.5 mM (■), 2 mM ■), and 10 mM■).

3.4 COD glucuronidation by recombinant UGT2B4 and UGT2B7

In contrast to HLM, COD glucuronidation by baculovius-expressed UGT2B4 and UGT2B7 exhibited sigmoidal kinetics (Fig.3.3), which were modeled using the Hill equation. Addition of BSA to incubations resulted in approximate 8- and 4- fold reductions in the respective S_{50} values for UGT2B4 and UGT2B7 (Table 3.3). While the addition of BSA had no effect on the V_{max} and Hill coefficient for UGT2B7 catalyzed COD glucuronidation, the V_{max} and Hill coefficient obtained for UGT2B4 in the presence of BSA were decreased and increased, respectively, compared to experiments performed in the absence of albumin (Table 3.3).

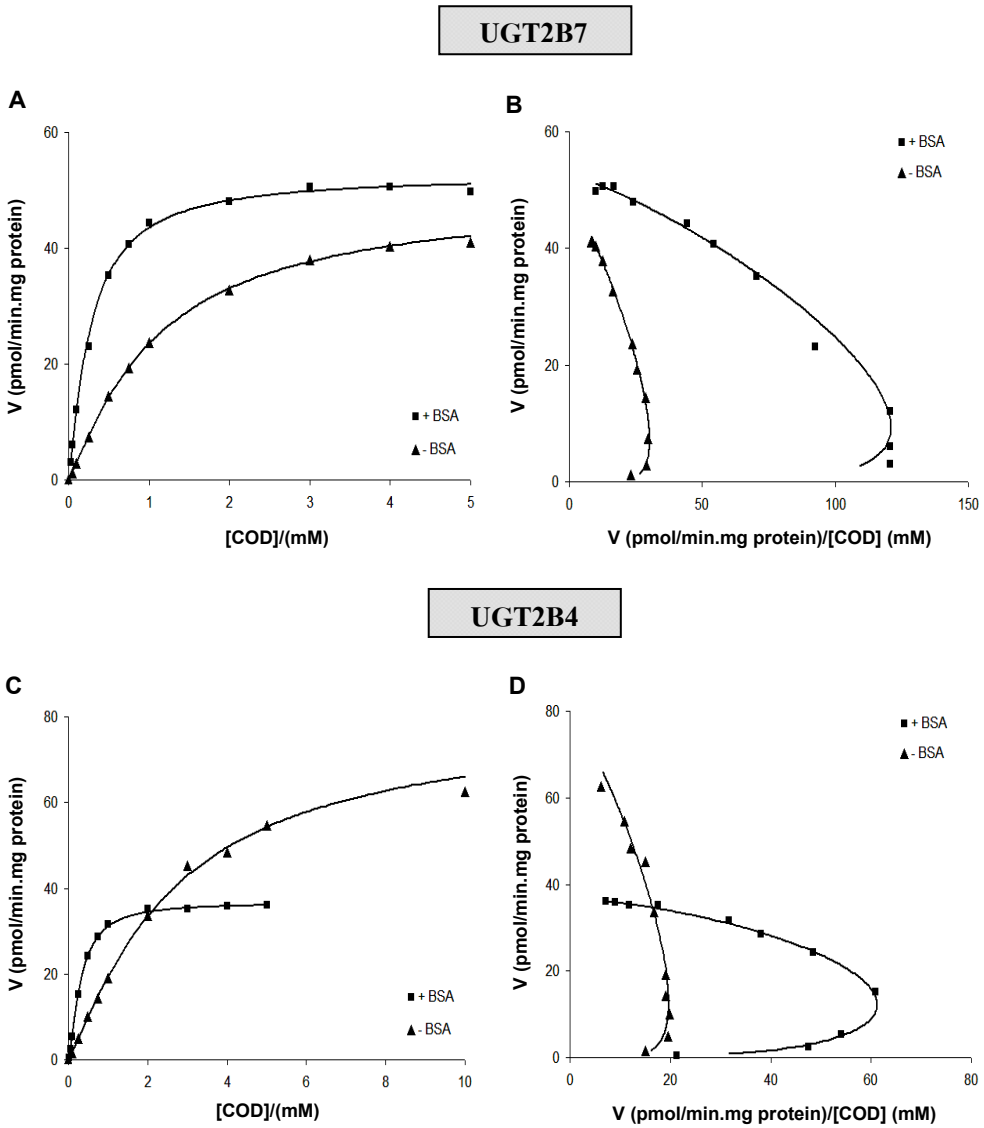

Figure 3.3 Kinetic plots for codeine 6-glucuronidation by baculovius-expressed UGT2B7 and UGT2B4 generated in the presence and absence of bovine serum albumin: Panels A and C) plots of the rate of product (C6G) formation versus substrate concentration; Panels B and D) Eadie-Hofstee plots. Points are experimentally derived values while curves are from model fitting.

Table 3.3 Derived kinetic parameters for codeine glucuronidation by baculovius-expressed UGT2B4 and UGT2B7 determined in the absence and presence of bovine serum albumin.

	Without BSA				**With 2% BSA**			
	S_{50} (mM)	V_{max} (pmol/min.mg)	n	CL_{max} [a] (µL/min/mg)	S_{50} (mM)	V_{max} (pmol/min.mg)	n	CL_{max} [a] (µL/min/mg)
UGT2B4	2.61 ± 0.001	79 ± 0.02	1.19 ± 0.001	0.02	0.32 ± 0.004	37 ± 0.16	1.50 ± 0.03	0.06
UGT2B7	1.07 ± 0.03	49 ± 0.63	1.17 ± 0.02	0.03	0.27 ± 0.01	53 ± 0.44	1.22 ± 0.03	0.12

Data presented as mean ± SE. of parameter fit.

Kinetic constants derived from fitting with the Hill equation.

[a] CL_{max} calculated as $\frac{V_{max}}{S_{50}} \times \frac{(n-1)}{n(n-1)^{1/n}}$

3.5 Inhibition of human liver microsomal COD glucuronidation

Experiments conducted to calculate IC_{50} and K_i values employed pooled HLM as the enzyme source, with and without 2% BSA. The effects of four concentrations of each putative inhibitor were assessed initially at the COD concentrations corresponding to the approximate mean K_m values for C6G formation in the absence (2 mM) and presence (0.3 mM) of 2% BSA (Table 3.4). Inhibitor binding to HLM and BSA was accounted for in the calculation of inhibition parameters (IC_{50} and K_i). FLZ and VPA were weak to moderate inhibitors of COD glucuronidation, with estimated IC_{50} values > 2 mM in the absence of BSA (Table 3.4). Potent inhibition was observed for KTM and KTZ, with IC_{50} values ranging from 4.5 to 70 μM. Addition of BSA (2%) to incubations typically resulted in an 8- to 12- fold reduction in the IC_{50} (Table 3.4). Based on data from the above inhibition screening studies, kinetic experiments were performed to determine K_i values for FLZ, KTM, and KTZ. Results are shown in Fig.3.4 as Dixon plots. Inhibition data for FLZ, KTM, and KTZ were well modeled using the expression for competitive inhibition of human liver microsomal COD glucuronidation. Consistent with the IC_{50} data, K_i values generated in the presence of BSA were lower (approximately 6- to 17- fold) compared to K_i obtained in the absence of albumin and potent inhibition of C6G formation was observed for KTM and KTZ (Table 3.5).

Table 3.4 IC_{50} values for inhibition of human liver microsomal codeine glucuronidation determined in the absence and presence of bovine serum albumin.

Inhibitors	**IC_{50} (μM)**	
	Without BSA	**With 2%BSA**
Fluconazole	2970 ± 16	371 ± 0.60[a]
	(50-2500 μM)	(46-2300 μM)[a]
Ketamine	70.1 ± 3.88	5.9 ± 0.31[a]
	(50-1000 μM)	(1.6-15.8 μM)[a]
Ketoconazole	17.2 ± 0.11[a]	2.0 ± 0.03[a]
	(4.5-270 μM)[a]	(1.5-90 μM)[a]
Valproic acid	4604 ± 509	580 ± 1.78[a]
	(1-20 mM)	(0.15-8.6 mM)[a]

Data given as IC_{50} ± SE. of parameter fit.

Concentration range of each inhibitor was shown in parenthesis.

[a] IC_{50} value is the unbound concentration in the incubation medium (i.e. corrected for binding to HLM and BSA).

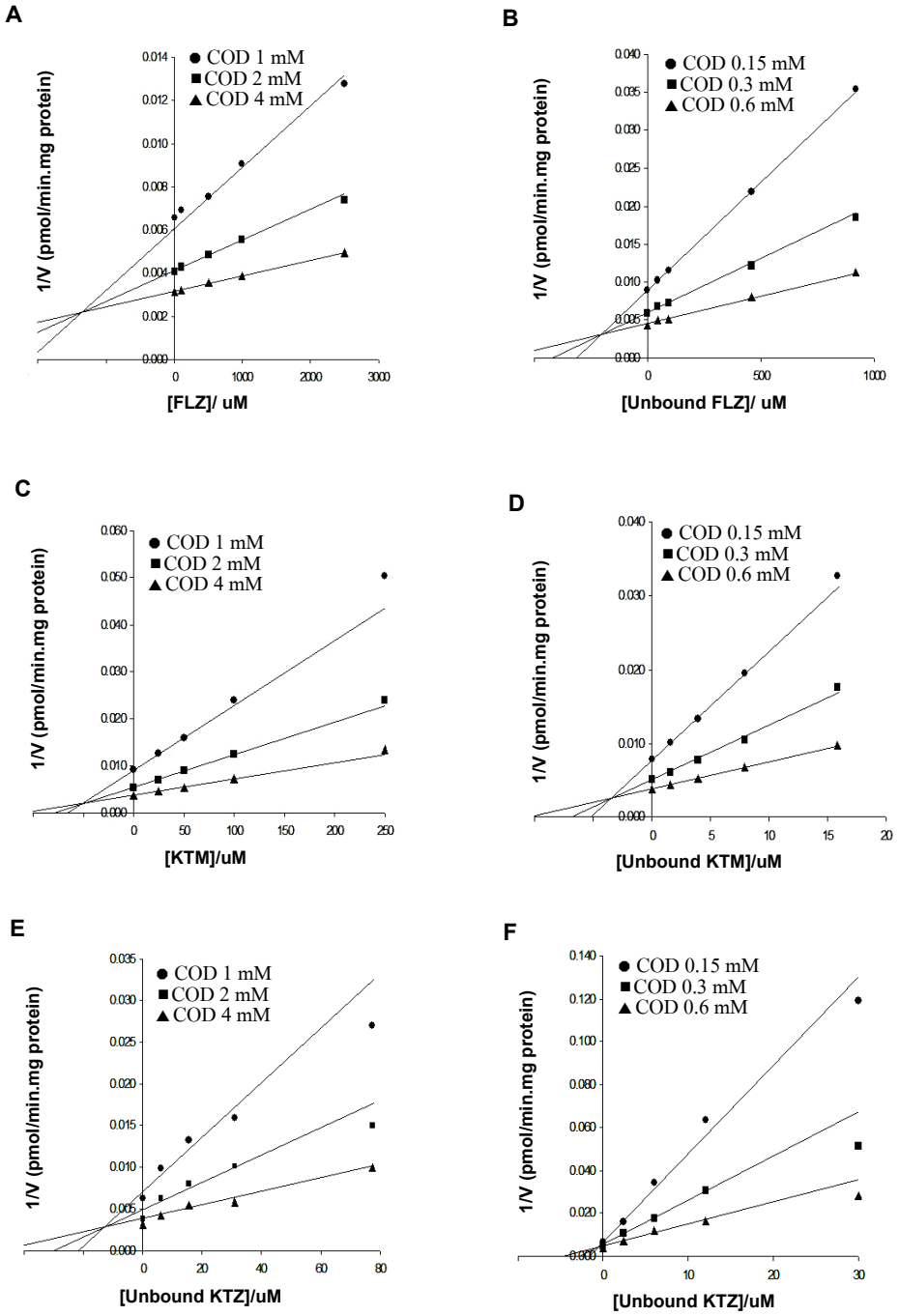

Figure 3.4 Dixon plots for fluconazole, ketamine, and ketoconazole inhibition of codeine 6-glucuronidation by pooled human liver microsomes generated in the absence (panels A, C, and E) and presence (panels B, D, and F) of bovine serum albumin. Inhibitor concentrations are corrected for binding to human liver microsomes and bovine serum albumin (i.e. unbound concentration in the incubation medium).

Table 3.5 K_i values for the inhibition of human liver microsomal codeine glucuronidation determined in the absence and presence of bovine serum albumin.

Inhibitors	**K_i (μM)**	
	Without BSA	**With 2%BSA**
Fluconazole	1341 ± 0.04	202 ± 0.001[a]
Ketamine	52 ± 0.75	3.51 ± 0.09[a]
Ketoconazole	11.3 ± 1.5[a]	0.66 ± 0.01[a]

K_i ± SE. of parameter fit.

Data were best fitted with the expression for competitive inhibition.

[a] K_i value based on the unbound concentration in the incubation medium (i.e. corrected for binding to HLM and BSA).

3.6 Effect of VPA on COD glucuronidation in HLM

The effects of VPA on the kinetics of COD glucuronidation are presented in Fig.3.5 and Table 3.6. The effect of VPA on COD glucuronidation was investigated in pooled HLM over the COD concentration range 0.25-5 mM. In the absence of BSA (2%), COD glucuronidation by HLM was best modeled with the Michaelis-Menten equation, whereas kinetic data were consistent with weak substrate inhibition for incubations performed in the presence of BSA. In both the absence and presence of BSA, addition of VPA changed the kinetics of C6G formation to sigmoidal. The sigmoidal kinetics were best fitted with the Hill equation. The K_m (or S_{50}) values for COD glucuronidation were increased 4.8- to 7.7-fold with increasing VPA concentration. The K_m (or S_{50}) values increased from 2.04 mM (no VPA) to 9.82 mM (at the highest concentration of VPA, 6 mM), and from 0.18 mM (no VPA) to 1.39 mM (at the highest unbound concentrations of VPA of 2.14 mM) in the absence and presence of BSA, respectively. However, V_{max} values and the Hill coefficient for COD glucuronidation were essentially unchanged by VPA.

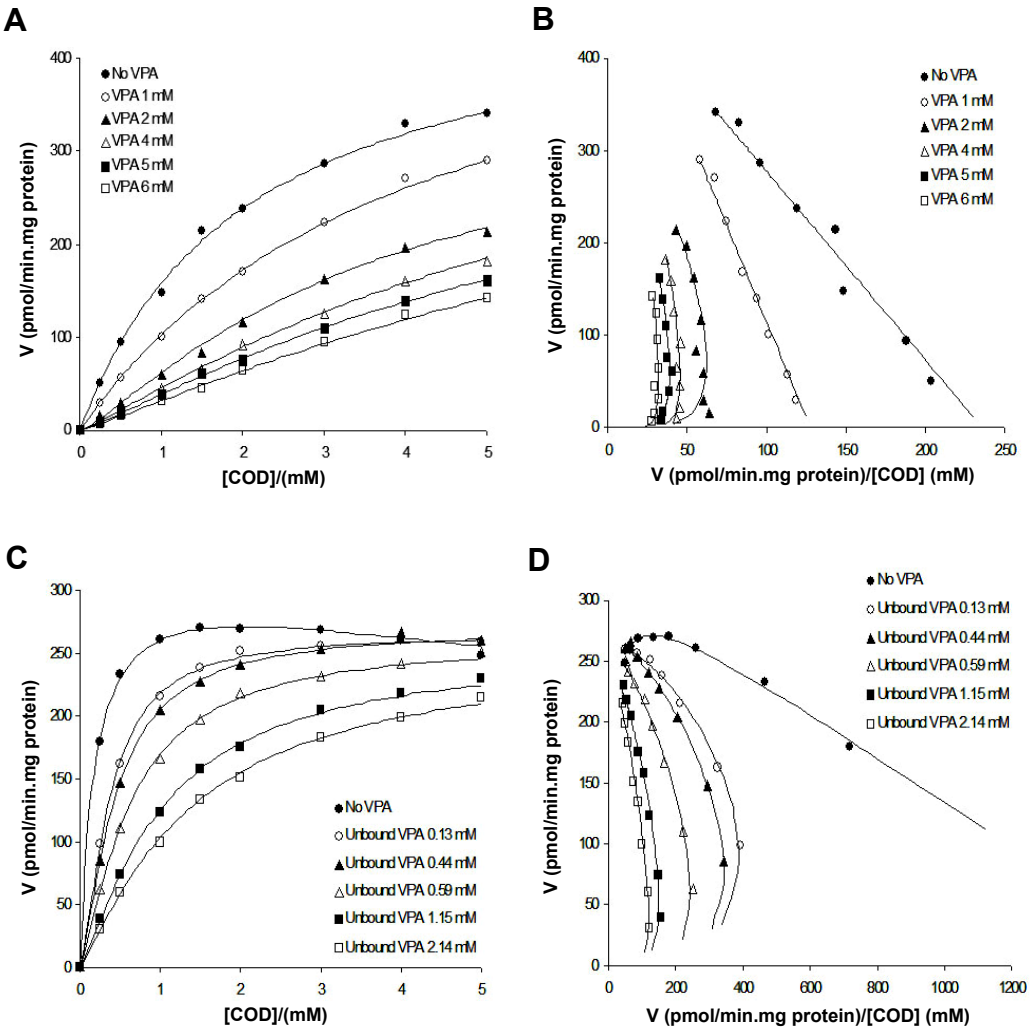

Figure 3.5 Kinetic plots of codeine 6-glucuronidation by pooled human liver microsomes in the presence of increasing valproic acid concentration in the absence (Panel A and B) and presence (Panel C and D) of bovine serum albumin. Panel A and C, plots of the rate of product (C6G) formation versus substrate concentration; panel B and D, and Eadie–Hofstee plots.

Table 3.6 Derived kinetic parameters for codeine glucuronidation with increasing concentrations of valproic acid in the absence and presence of bovine serum albumin.

	Without BSA[a]					**With 2% BSA**[a]			
[VPA] mM	Kinetic equations	K_m or S_{50} (mM)	V_{max} (pmol/min.mg)	n	[Unbound VPA] mM	Kinetic equations	K_m or S_{50} (mM)	V_{max} (pmol/min.mg)	n
0 mM[b]	MM	2.04 ± 0.004	482 ± 0.37	-	0 mM[d]	SI	0.18 ± 0.01	319 ± 5.20	-
1 mM[b]	MM	4.17 ± 0.003	532 ± 0.22	-	0.13 mM[c]	Hill	0.36 ± 0.01	266 ± 2.52	1.50 ± 0.07
2 mM[c]	Hill	3.48 ± 0.03	356 ± 1.66	1.25 ± 0.02	0.44 mM[c]	Hill	0.44 ± 0.02	270 ± 3.81	1.39 ± 0.08
4 mM[c]	Hill	6.50 ± 0.53	435 ± 19.38	1.15 ± 0.03	0.59 mM[c]	Hill	0.63 ± 0.02	262 ± 3.46	1.30 ± 0.06
5 mM[c]	Hill	5.94 ± 0.40	361 ± 19.38	1.19 ± 0.03	1.15 mM[c]	Hill	1.02 ± 0.03	255 ± 2.97	1.26 ± 0.04
6 mM[c]	Hill	9.82 ± 0.65	446 ± 17.34	1.13 ± 0.02	2.14 mM[c]	Hill	1.39 ± 0.01	256 ± 0.92	1.18 ± 0.01

[a] Data presented as mean ± SE. of parameter fit; [b] Michaelis-Menten equation (MM); [c] Hill equation (Hill); [d] Substrate inhibition (SI) with K_{si} = 23.56 ± 2.36 mM; S_{50}: Substrate concentration resulting in 50% of V_{max}; K_m: Michaelis-Menten constant; V_{max}: Maximum of velocity; K_{si}: Constant describing the substrate inhibition interaction; n: Hill coefficient.

3.7 Effect of alamethicin on COD glucuronidation by baculovirus-expressed UGT2B7 enzyme

The effect of alamethicin on C6G formation was investigated in the absence of BSA (2%) by baculovirus-expressed UGT2B7 enzyme (Fig.3.6). In the absence of alamethicin, COD glucuronidation was fitted with Sigmoidal kinetic with V_{max} = 46.43 ± 0.43 pmol/min/mg, S_{50} = 1.09 ± 0.02 mM, and Hill coefficient (n) = 1.22 ± 0.02. Although the rate of C6G formation was changed to the generic two-site model for incubation pre-incubated with alamethicin, effect on V_{max} (37.30 ± 1.17 pmol/min/mg) and K_s (1.26 ± 0.41 mM) values were not observed when compared with the rates measured in the absence of alamethicin.

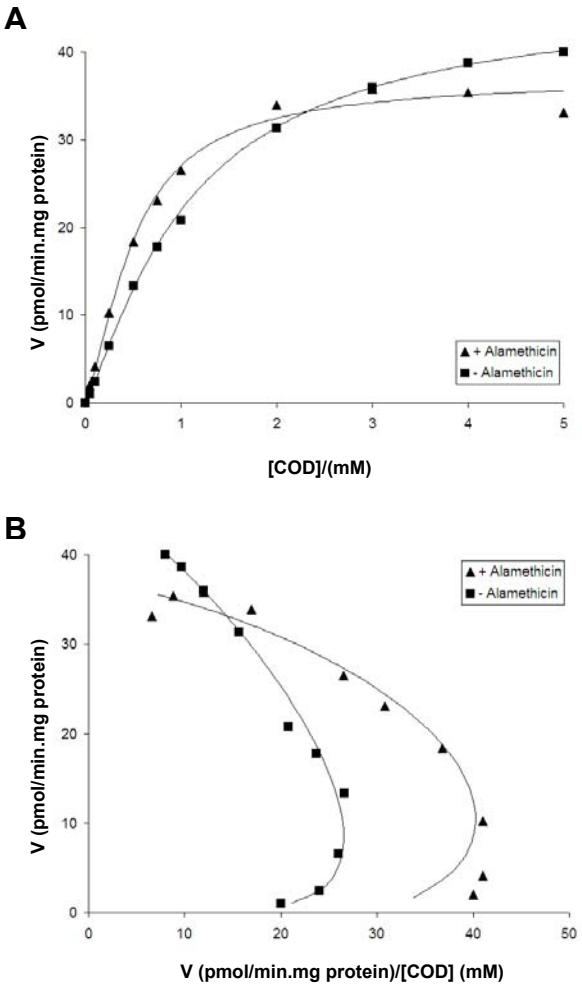

Figure 3.6 Kinetic plots for codeine 6-glucuronidation in the absence of bovine serum albumin by baculovius-expressed UGT2B7 generated in the absence and presence of alamethicin: Panels A) plots of the rate of product (C6G) formation versus substrate concentration; Panels B) Eadie-Hofstee plots. Points are experimentally derived values while curves are from model fitting.

3.8 Prediction of COD glucuronidation clearance

For IV-IVE of the COD glucuronidation kinetic data, in vitro CL_{int} values obtained from hepatic microsomes were extrapolated to in vivo blood CL_H values using the well-stirred model as described in data analysis. In the absence of BSA, the mean (±SD.) predicted CL_H value for COD elimination via glucuronidation was 0.82 ± 0.34 L/hr. This was increased 7-fold, to 5.82 ± 2.72 L/hr, in the presence of BSA. As above mentioned in data analysis, the mean observed in vivo CL_H value is 35.9 L/hr. Therefore, the predicted CL_H value in the absence of BSA was lower than the known CL_H value (by 44-fold). Addition of BSA (2%) improved the prediction of CL_H, but this parameter was still underestimated by approximately 6-fold. The derived kinetic parameters by IV-IVE were shown in Table 3.7.

Table 3.7 Derived kinetic parameters of prediction of codeine glucuronidation clearance in the absence and presence of bovine serum albumin.

Parameters	**Without BSA**	**With 2% BSA**
Mean CL_{int} (µl/min/mg)	0.26 ± 0.11	1.95 ± 0.88
Mean $CL_{int.liver}$ (ml/min/kg)	0.89 ± 0.37	6.66 ± 3.01
Mean CL_H (L/hr)	0.82 ± 0.34	5.80 ± 2.72
Fold of underestimation[a]	44	6

Data were presented as mean ± SD.

[a] Predicted CL_H value by IV-IVE compared to the observed in vivo CL_H value (35.9 L/hr).

3.9 Prediction of inhibition of COD hepatic clearance

Predicted changes in the AUC for COD when coadministered with FLZ and KTZ are given in Table 3.8. Based on total inhibitor concentration in blood for the doses indicated in Table 3.8, predicted AUC ratios were increased 1.10-, 1.60-, and 2.97-fold with KTM, FLZ and KTZ, respectively. When considered in terms of unbound inhibitor concentration in blood, no interaction was predicted with KTM and KTZ. The predicted change in the AUC ratio based on unbound FLZ concentration did not change appreciably given the minor plasma protein binding of this compound.

Table 3.8 Predicted increase in the area under the codeine plasma concentration-time from co-administration of fluconazole, ketamine, and ketoconazole.

Drugs (in vitro dose)[a]	**Predicted fold increase in AUC ratio based on:**	
	Total inhibitor concentration[b]	Unbound inhibitor concentration[b]
Fluconazole (400 mg/day[c])	1.60	1.54
Ketamine (18.7 mg/day[d])	1.10	1.05
Ketoconazole (200 mg/day[e])	2.97	1.04

[a] Dose calculated as free base where drug administered as a salt.

[b] Hepatic maximum input concentration, except for KTM and KTZ (maximum plasma concentration; see Methods).

[c] Sahai *et al*. (1994).

[d] Clements and Nimmo (1981).

[e] Badcock *et al*. (1987).

CHAPTER 4

DISCUSSIONS

COD is an opioid drug used to treat mild to moderate pain. COD exerts its therapeutic effects through the formation of morphine. Approximately 5-10% of the COD dose is converted to morphine by CYP2D6 catalysed *O*-demethylation. The major metabolic pathway of COD is the formation of C6G (Yue *et al*., 1991).

Initial studies aimed to characterize the effect of BSA on COD glucuronidation by HLM and confirm the contributions of UGT2B4 and UGT2B7 to C6G formation. C6G formation in the absence of BSA exhibited Michaelis-Menten kinetics. Kinetic constants derived here in the absence of BSA were similar to those reported previously by Court *et al*. (2003). Addition of BSA (2%) to incubations resulted in an 8-fold reduction in K_m without an effect on V_{max}. A similar affect has been reported for the glucuronidation of AZT by HLM, where the K_m value was decreased by approximately 10 to 13-fold. Consequently, there was a 10 to 15-fold increase in CL_{int} (Uchaipichat *et al*., 2006b; Rowland *et al*., 2007). An increase in microsomal CL_{int} (2 to 13-fold) of other UGT2B7 substrates (viz. diclofenac, gemfibrozil, ketoprofen, and naloxone) has also recently been observed in the presence of BSA (Kilford *et al*., 2009). These data confirm that K_m or microsomal CL_{int} values for UGT2B7 substrates are typically overestimated by approximately an order of magnitude when HLM are used as the enzyme source in the absence of albumin supplementation. The mechanism of the albumin on improving the kinetic parameter with a reduction in the "apparent" K_m has been proposed recently. It involved sequestration of long-chain unsaturated fatty acids (arachidonic, linoleic, oleic) released from the microsomal membrane during the course of an incubation and acted as potent competitive inhibitors of UGT2B7 (Rowland *et al*., 2007, 2008a,b). The screening of 13 recombinant UGT enzymes expressed in HEK293 cell demonstrated that only UGT2B4 and UGT2B7 contributed the C6G formation. This result was also consistent with previous published data that investigated in baculovirus-expressed UGT enzymes (Court *et al*., 2003). However the rates of C6G formation in HEK293-expression were approximately 10-fold lower than in baculovirus-expression.

Although it is acknowledged that UGT expression may differ from enzyme to enzyme and between expression systems, the use of positive controls precluded absent activity as a reason for the inability of UGTs other than 2B4 and 2B7 to form C6G.

In contrast to the Michaelis-Menten (or weak substrate inhibition) kinetics observed for C6G formation by HLM, COD glucuronidation by UGT2B4 and UGT2B7 exhibited sigmoidal kinetics. Differences in kinetic behavior between HLM and recombinant UGTs have been observed in other studies. Naproxen acyl glucuronidation by HLM exhibited biphasic kinetics. In contrast, the conversion of naproxen to naproxen acyl glucuronide was best described by the Michaelis-Menten equation for UGT1A3, UGT1A6, and UGT2B7, the Hill equation with negative cooperativity for UGT1A9, and the substrate inhibition equation for UGT1A10. Similarly, desmethylnaproxen phenolic glucuronidation by HLM showed apparent biphasic kinetics, while negative cooperative and Michaelis–Menten kinetics were observed with UGT1A9 and UGT1A10, respectively (Bowalgaha *et al*., 2005). Reasons for the inter-system differences remain unknown, but may reflect membrane effects on protein function (Miners *et al*., 2006). The difference in the kinetic model (sigmoidal versus hyperbolic) between present and previously (Court *et al*., 2003) reported data for UGT2B7 may arise from our use of more points at lower substrate concentrations, which favors detection of sigmoidal kinetics.

In addition, to confirm the effect of alamethicin on different enzyme sources, preincubation of Supersomes expressing UGT2B7 was investigated. The result showed that alamethicin has no effect on COD glucuronidation, both in the absence and presence of BSA (data not shown). Kaivosaari *et al*. (2008) have similarly demonstrated that alamethicin is without affect on the activity of UGT1A4 expressed in baculovirus infected insect cells. In contrast to recombinant UGT2B7 expressed in insect cells, pretreatment of HLM with alamethicin results in a 2 to 3-fold increase in microsomal UGT2B7 activity, as evidenced here by effects on C6G formation and in previous studies with AZT, morphine, diclofenac, gemfibrozil, ketoprofen, and naloxone (Fisher *et al*., 2000; Boase and Miners, 2002; Kilford *et al*., 2009). Similarly, the rates of glucuronidation of estradiol and acetaminophen which are relatively selective probes for human UGT1A1 and UGT1A6 were increased by approximately 2- to 3-fold with alamethicin-treated microsomes (Fisher *et al*., 2000). These results demonstrate that the alamethicin appears to increase human liver microsomal UGT enzyme activity in a substrate-independent fashion,

presumably by facilitating entry of substrate and UDPGA into, and the diffusion of conjugate and UDP out of, the lumen of the ER (Fisher *et al*., 2000).

S_{50} values for COD glucuronidation by both UGT2B4 and UGT2B7 were reduced by BSA, and the S_{50} values generated in the presence of BSA were close in value. However, in contrast to HLM and UGT2B7, the V_{max} for UGT2B4 was also reduced by BSA. In general, identification of the UGT enzyme responsible for the glucuronidation of a compound in vitro referred to as "reaction phenotyping" may be underpinned by several approaches: (1) a reduction in glucuronidation of the test compound by individual UGT-enzyme–selective inhibitors; (2) screening for glucuronidation by a battery of recombinant UGTs, together with comparison of K_m values for glucuronidation by the recombinant enzyme and HLM; (3) competitive inhibition of the glucuronidation of a UGT-enzyme–selective substrate by the test compound, with K_i matching K_m; and (4) a significant correlation between the rates of glucuronidation of the test compound and a UGT-enzyme–selective substrate in microsomes from a panel of livers (Miners *et al*., 2006, 2010).

Although, this study indicated that the UGT2B4 and UGT2B7 contribute the C6G formation, a significant enzyme between UGT2B4 and UGT2B7 is not unclear. While it is not possible to determine the relative contribution of UGT enzymes to a metabolic pathway in the absence of relative protein expression data, it is noteworthy that UGT2B4 mRNA expression in human liver exceeds that of UGT2B7 9-fold (Ohno and Nakajin, 2009). Collectively, these data suggest a significant, perhaps major, contribution of UGT2B4 to human liver microsomal COD glucuronidation. This contrasts to the very minor or negligible contribution of UGT2B4 to AZT and morphine (3- and 6-) glucuronidation (Court *et al*., 2003; JO Miners, unpublished data). However, data of the competitive inhibition and a significant correlation of the rates of COD glucuronidation and the selective substrates of UGT2B4 and UGT2B7 in pooled HLM should be investigated in further study to confirm a significant contribution of UGT2B4.

Drugs previously identified as potential UGT2B7 inhibitors in either in vitro or in vivo studies (viz. FLZ, KTM, KTZ and VPA) were screened for inhibition of human liver microsomal COD glucuronidation. IC_{50} values generated for FLZ, KTM, and KTZ in the presence of BSA were in the ranges of plasma and/or hepatic input concentrations observed for therapeutic doses in vivo. Thus, K_i values were determined for these compounds. As with the IC_{50}'s, K_i values

generated from incubations supplemented with BSA (and corrected for binding to HLM and albumin) were 6.6- to 17-fold lower than the corresponding parameters determined in the absence of BSA. A similar effect of BSA was observed in studies of the FLZ - AZT and VPA – LTG interactions in vitro (Rowland *et al*., 2006; Uchaipichat *et al*., 2006a) and confirm that, like the K_m, K_i values for UGT2B7 inhibitors are overestimated when BSA is not present in incubations of HLM.

K_i values obtained here for FLZ (from incubations with and without BSA) inhibition of human liver microsomal COD glucuronidation were approximately 30% higher than the corresponding K_i reported for inhibition of AZT glucuronidation (Uchaipichat *et al*., 2006b). Moreover, the K_i value determined here for KTZ inhibition of COD glucuronidation also differs from inhibition studies with the predominantly UGT2B7 substrate morphine, which reported less potent inhibition (Takeda *et al*., 2006). While this may be due in part to the differing contributions of UGT2B4 and UGT2B7 to COD and morphine (3- and 6-) glucuronidation, binding to HLM was not accounted for in the morphine inhibition studies and effects of BSA were not investigated. Inhibition of human liver microsomal morphine glucuronidation by KTM has been recently investigated (Miners JO; unpublished data). The reported K_i value for KTM inhibition of morphine-6-glucuronide formation in the absence and presence of 2% BSA were 35 and 5 μM, respectively which is consistent with the K_i values obtained from this study.

Based on total inhibitor concentration in blood, extrapolation of the K_i values for FLZ, KTM and KTZ predicted 1.60, 1.10 and 2.97 fold increases, respectively in the AUC ratio for COD when co-administered with each inhibitor at the doses shown in Table 3.7. When considered in terms of unbound inhibitor concentration in blood, the inhibition potential of FLZ and KTM was unaltered. Although there is no consensus whether DDI potential should be predicted based on total or unbound concentration of the perpetrator drug in plasma, optimum predictivity of the magnitude of inhibitory interactions involving both CYP and UGT substrates is achieved when total maximum hepatic input concentration is employed in equation 2.8(Ito and Houston, 2004; Brown *et al*., 2005; Rowland *et al*., 2006; Uchaipchat *et al*., 2006b; Miners *et al*., 2010). According to Ito and colleague (2004), various inhibitor concentrations calculated for use in the prediction of in vivo drug–drug interactions showed that the total hepatic input concentration of inhibitor together with in vitro K_i values is the most successful method for

identifying inhibitory DDIs. On this basis, significant DDIs involving inhibition of COD glucuronidation by FLZ, KTM and KTZ would be predicted in vivo.

Like the prediction of DDI potential, IV-IVE may be employed to determine in vivo CL_H and extraction ratio from the experimentally measured microsomal intrinsic clearance, calculated as $CL_{int} = V_{max}/K_m$ (see Miners *et al*., 2006 and 2010 for approach). Estimates of CL_H for COD clearance via hepatic glucuronidation were derived with the equation for the well stirred model of the CL_H using scaling factors given in Rowland *et al*. (2008b), 0.93 as the fraction of COD unbound in blood, and the mean K_m and V_{max} values generated here for human liver microsomal COD glucuronidation. The predicted CL_H values were 0.82 L/hr and 5.74 L/hr for kinetic constants obtained in the absence and presence of BSA, respectively. The approximate 7-fold increase in predicted CL_H from in vitro CL_{int} values determined from incubations supplemented with BSA is consistent with previous studies kinetic studies of UGT1A9, UGT2B7 and CYP2C9 substrates conducted in this and other studies (Rowland *et al*., 2007; 2008a and b; Kilford *et al*., 2009). Despite this, the predicted CL_H from experiments performed in the presence of BSA still under-predicts the known in vivo CL_H for COD via glucuronidation (ca. 36 L/hr). The data are consistent with the 2- to 5- fold under-prediction observed for the predicted in vivo clearances of UGT2B7 substrates from in vitro data obtained in the presence of BSA (Rowland *et al*., 2007; Kilford *et al*., 2009), but contrasts to the near exact prediction of in vivo CL_H for the UGT1A9 substrate propofol and the CYP2C9 substrate phenytoin when in vitro kinetic data generated in the presence of BSA are used for IV-IVE (Rowland *et al*., 2008 and b). Since it is believed that the K_m value obtained from experiments with HLM supplemented with BSA reflects 'true' hepatocellular K_m (Rowland *et al*., 2007), other factors such as under-prediction of V_{max}, extra-hepatic glucuronidation or uptake barriers presumably contribute to the accuracy of in vivo clearance prediction for moderately polar UGT2B7 substrates.

In addition, this work showed a complex kinetic interaction between UGT2B7 substrates. In both the absence and presence of BSA, addition of VPA changed the kinetics of C6G formation from the Michaelis-Menten or weak substrate inhibition to sigmoidal kinetics with increasing of K_m (or S_{50}) values by approximately 4.8- to 7.7-fold. This data was consistent with the existence of two "catalytic" sites for AZT, 4-MU, and 1-NP within the UGT2B7 substrate binding domain (Uchaipichat *et al*., 2008). The inhibition mechanism was a competitive

inhibition, as evidenced by decreased substrate binding affinity (i.e., increased K_m or S_{50}) without a change in V_{max}. In addition, however, the observation of sigmoidal kinetics in the presence of VPA suggests the existence of cooperative binding of the second substrate molecule occurring in the presence of VPA. It is further assumed that VPA binds to a distinct effector site, which results in the complex C6G glucuronidation kinetics observed in the presence of modifier.

CHAPTER 5

CONCLUSIONS

In summary, IV-IVE predicts significant DDIs arising from inhibition of COD metabolic clearance via glucuronidation by coadministered FLZ and KTZ, but not KTM. Available evidence is generally consistent with superior pain relief from COD in CYP2D6 EMs, and absent or minor COD analgesia in PMs (Somogyi *et al*., 2007). Conversely, the relative conversion of COD to morphine is approximately 2 to 3-fold higher in CYP2D6 UMs compared to EMs and this may result in an exaggerated response, including sedation and respiratory depression. Thus, it may be speculated that inhibition of COD glucuronidation by coadministered drugs, for examples FLZ and KTZ, will potentially result in enhanced and prolonged analgesia due to increased formation of morphine. Furthermore, marked inhibition of the glucuronidation of high dose COD could conceivably result in morphine and COD toxicity. In addition, this work showed a complex kinetic interaction between UGT2B7 substrates. The observation of sigmoidal kinetics in the presence of VPA suggests the existence of cooperative binding of the second substrate molecule occurring in the presence of VPA. It is further assumed that VPA binds to a distinct effector site, which results in the complex C6G glucuronidation kinetics observed in the presence of modifier.

BIBLIOGRAPHIES

Atkins WM (2005). Non-Michaelis-Menten kinetics in cytochrome P450-catalyzed reactions. *Annu Rev Pharmacol Toxicol* 45: 291-310.

Badcock NR, Bartholomeusz FD, Frewin DB, Sansom LN, and Reid JG (1987). The pharmacokinetics of ketoconazole after chronic administration in adults. *Eur J Clin Pharmacol* 33(5): 531-534.

Barbier O, Turgeon D, Girard C, Green MD, Tephly TR, Hum DW, and Belanger A (2000). 3'-azido-3'-deoxythimidine (AZT) is glucuronidated by human UDP-glucuronosyltransferase 2B7 (UGT2B7). *Drug Metab Dispos* 28(5): 497-502.

Barter ZE, Bayliss MK, Beaune PH, Boobis AR, Carlile DJ, Edwards RJ, Houston JB, Lake BG, Lipscomb JC, Pelkonen OR, Tucker GT, and Rostami-Hodjegan A (2007). Scaling factors for the extrapolation of in vivo metabolic drug clearance from in vitro data: reaching a consensus on values of human microsomal protein and hepatocellularity per gram of liver. *Curr Drug Metab* 8(1): 33-45.

Benoit-Biancamano MO, Connelly J, Villeneuve L, Caron P, and Guillemette C (2009). Deferiprone glucuronidation by human tissues and recombinant UDP glucuronosyltransferase 1A6: an in vitro investigation of genetic and splice variants. *Drug Metab Dispos* 37(2): 322-329.

Bernard O and Guillemette C (2004). The main role of UGT1A9 in the hepatic metabolism of mycophenolic acid and the effects of naturally occurring variants. *Drug Metab Dispos* 32(8): 775-778.

Bertz RJ and Granneman GR (1997). Use of in vitro and in vivo data to estimate the likelihood of metabolic pharmacokinetic interactions. *Clin Pharmacokinet* 32(3): 210-258.

Bhasker CR, McKinnon W, Stone A, Lo AC, Kubota T, Ishizaki T, and Miners JO (2000). Genetic polymorphism of UDP-glucuronosyltransferase 2B7 (UGT2B7) at amino acid 268: ethnic diversity of alleles and potential clinical significance. *Pharmacogenetics* 10(8): 679-685.

Bisswanger H. Enzyme kinetics: principles and methods. (2^{nd} ed). Weinheim: WILEY-VCH Verlag GmbH & Co. KGaA; 2008.

Boase S and Miners JO (2002). In vitro-in vivo correlations for drugs eliminated by glucuronidation: investigations with the model substrate zidovudine. *Br J Clin Pharmacol* 54(5): 493-503.

Bock KW, Lilienblum W, and von Bahr C (1984). Studies of UDP-glucuronyltransferase activities in human liver microsomes. *Drug Metab Dispos* 12(1): 93-97.

Bosma PJ, Seppen J, Goldhoorn B, Bakker C, Oude Elferink RP, Chowdhury JR, Chowdhury NR, and Jansen PL (1994). Bilirubin UDP-glucuronosyltransferase 1 is the only relevant bilirubin glucuronidating isoform in man. *J Biol Chem* 269(27): 17960-17964.

Bowalgaha K, Elliot DJ, Mackenzie PI, Knights KM, and Miners JO (2007). The glucuronidation of Delta4-3-Keto C19- and C21-hydroxysteroids by human liver microsomal and recombinant UDP-glucuronosyltransferases (UGTs): 6alpha- and 21-hydroxyprogesterone are selective substrates for UGT2B7. *Drug Metab Dispos* 35(3): 363-370.

Bowalgaha K, Elliot DJ, Mackenzie PI, Knights KM, Swedmark S, and Miners JO (2005). S-Naproxen and desmethylnaproxen glucuronidation by human liver microsomes and recombinant human UDP-glucuronosyltransferases (UGT): role of UGT2B7 in the elimination of naproxen. *Br J Clin Pharmacol* 60(4): 423-433.

Breton C and Imberty A (1999). Structure/function studies of glycosyltransferases. *Curr Opin Struct Biol* 9(5): 563-571.

Breton C, Snajdrova L, Jeanneau C, Koca J, and Imberty A (2006). Structures and mechanisms of glycosyltransferases. *Glycobiology* 16(2): 29R-37R.

Brown HS, Griffin M, and Houston JB (2007). Evaluation of cryopreserved human hepatocytes as an alternative in vitro system to microsomes for the prediction of metabolic clearance. *Drug Metab Dispos* 35(2): 293-301.

Brown HS, Ito K, Galetin A, and Houston JB (2005). Prediction of in vivo drug-drug interactions from in vitro data: impact of incorporating parallel pathways of drug elimination and inhibitor absorption rate constant. *Br J Clin Pharmacol* 60(5): 508-518.

Burchell B, Nebert DW, Nelson DR, Bock KW, Iyanagi T, Jansen PL, Lancet D, Mulder GJ, Chowdhury JR, Siest G, and et al. (1991). The UDP glucuronosyltransferase gene

superfamily: suggested nomenclature based on evolutionary divergence. *DNA Cell Biol* 10(7): 487-494.

Buxton ILO. Pharmacokinetics and pharmacodynamics: the dynamics of drug absorption, distribution, action, and elimination. In: Beunton LL, Lazo JS, and Parker KL, editors. Goodman & Gilman's : the pharmacological basis of therapeutics. (11th ed). New York: McGraw-Hill Companies; 2006. pp. 1-40.

Campbell JA, Davies GJ, Bulone V, and Henrissat B (1997). A classification of nucleotide-diphospho-sugar glycosyltransferases based on amino acid sequence similarities. *Biochem J* 326 (Pt 3): 929-939.

Campbell JA, Davies GJ, Bulone VV, and Henrissat B (1998). A classification of nucleotide-diphospho-sugar glycosyltransferases based on amino acid sequence similarities. *Biochem J* 329 (Pt 3): 719.

Carlile DJ, Hakooz N, Bayliss MK, and Houston JB (1999). Microsomal prediction of in vivo clearance of CYP2C9 substrates in humans. *Br J Clin Pharmacol* 47(6): 625-635.

Carrier JS, Turgeon D, Journault K, Hum DW, and Belanger A (2000). Isolation and characterization of the human UGT2B7 gene. *Biochem Biophys Res Commun* 272(2): 616-621.

Chen ZR, Somogyi AA, Reynolds G, and Bochner F (1991). Disposition and metabolism of codeine after single and chronic doses in one poor and seven extensive metabolisers. *Br J Clin Pharmacol* 31(4): 381-390.

Christensen CB, Jansen JA, Ravn-Jonsen A, and Reiff L (1984). Metabolism of 14C-codeine in the isolated, perfused rat liver. *Acta Pharmacol Toxicol (Copenh)* 54(2): 134-140.

Clements JA and Nimmo WS (1981). Pharmacokinetics and analgesic effect of ketamine in man. *Br J Anaesth* 53(1): 27-30.

Coffman BL, Kearney WR, Goldsmith S, Knosp BM, and Tephly TR (2003). Opioids bind to the amino acids 84 to 118 of UDP-glucuronosyltransferase UGT2B7. *Mol Pharmacol* 63(2): 283-288.

Coffman BL, Kearney WR, Green MD, Lowery RG, and Tephly TR (2001). Analysis of opioid binding to UDP-glucuronosyltransferase 2B7 fusion proteins using nuclear magnetic resonance spectroscopy. *Mol Pharmacol* 59(6): 1464-1469.

Coffman BL, King CD, Rios GR, and Tephly TR (1998). The glucuronidation of opioids, other xenobiotics, and androgens by human UGT2B7Y(268) and UGT2B7H(268). *Drug Metab Dispos* 26(1): 73-77.

Coleman MD. Human drug metabolism: an introduction. Chichester: John Wiley & Sons Ltd; 2005.

Cornish-Bowden A (1974). A simple graphical method for determining the inhibition constants of mixed, uncompetitive and non-competitive inhibitors. *Biochem J* 137(1): 143-144.

Court MH (2005). Isoform-selective probe substrates for in vitro studies of human UDP-glucuronosyltransferases. *Methods Enzymol* 400: 104-116.

Court MH, Duan SX, Guillemette C, Journault K, Krishnaswamy S, Von Moltke LL, and Greenblatt DJ (2002). Stereoselective conjugation of oxazepam by human UDP-glucuronosyltransferases (UGTs): S-oxazepam is glucuronidated by UGT2B15, while R-oxazepam is glucuronidated by UGT2B7 and UGT1A9. *Drug Metab Dispos* 30(11): 1257-1265.

Court MH, Krishnaswamy S, Hao Q, Duan SX, Patten CJ, Von Moltke LL, and Greenblatt DJ (2003). Evaluation of 3'-azido-3'-deoxythymidine, morphine, and codeine as probe substrates for UDP-glucuronosyltransferase 2B7 (UGT2B7) in human liver microsomes: specificity and influence of the UGT2B7*2 polymorphism. *Drug Metab Dispos* 31(9): 1125-1133.

Coutinho PM, Deleury E, Davies GJ, and Henrissat B (2003). An evolving hierarchical family classification for glycosyltransferases. *J Mol Biol* 328(2): 307-317.

Czernik PJ, Little JM, Barone GW, Raufman JP, and Radominska-Pandya A (2000). Glucuronidation of estrogens and retinoic acid and expression of UDP-glucuronosyltransferase 2B7 in human intestinal mucosa. *Drug Metab Dispos* 28(10): 1210-1216.

Daneshmend TK, and Warnock DW (1988). Clinical pharmacokinetics of ketoconazole. *Clin Pharmacokinet* 14(1): 13-34.

de Lima J, Lloyd-Thomas AR, Howard RF, Sumner E, and Quinn TM (1996). Infant and neonatal pain: anaesthetists' perceptions and prescribing patterns. *Bmj* 313(7060): 787.

Di Marco A, D'Antoni M, Attaccalite S, Carotenuto P, and Laufer R (2005). Determination of drug glucuronidation and UDP-glucuronosyltransferase selectivity using a 96-well radiometric assay. *Drug Metab Dispos* 33(6): 812-819.

Dollery C. Therapeutic drugs. 2nd ed. Edinburgh: Churchill Livingstone; 1999. C317-320.

Eckhardt K, Li S, Ammon S, Schanzle G, Mikus G, and Eichelbaum M (1998). Same incidence of adverse drug events after codeine administration irrespective of the genetically determined differences in morphine formation. *Pain* 76(1-2): 27-33.

Engtrakul JJ, Foti RS, Strelevitz TJ, and Fisher MB (2005). Altered AZT (3'-azido-3'-deoxythymidine) glucuronidation kinetics in liver microsomes as an explanation for underprediction of in vivo clearance: comparison to hepatocytes and effect of incubation environment. *Drug Metab Dispos* 33(11): 1621-1627.

Enomoto M, Ochi M, Teramae K, Kamo R, Taguchi S, and Yamane T (2004). Codeine phosphate-induced hypersensitivity syndrome. *Ann Pharmacother* 38(5): 799-802.

Eriksson MB, Lindahl S, and Nyquist JK (1982). Experimental cutaneous pain thresholds and tolerance in clinical analgesia with epidural morphine. *Acta Anaesthesiol Scand* 26(6): 654-657.

Finel M and Kurkela M (2008). The UDP-glucuronosyltransferases as oligomeric enzymes. *Curr Drug Metab* 9(1): 70-76.

Fisher MB, Campanale K, Ackermann BL, VandenBranden M, and Wrighton SA (2000). In vitro glucuronidation using human liver microsomes and the pore-forming peptide alamethicin. *Drug Metab Dispos* 28(5): 560-566.

Fisher MB, Paine MF, Strelevitz TJ, and Wrighton SA (2001). The role of hepatic and extrahepatic UDP-glucuronosyltransferases in human drug metabolism. *Drug Metab Rev* 33(3-4): 273-297.

Galetin A, Clarke SE, and Houston JB (2002). Quinidine and haloperidol as modifiers of CYP3A4 activity: multisite kinetic model approach. *Drug Metab Dispos* 30(12): 1512-1522.

Galetin A, Clarke SE, and Houston JB (2003). Multisite kinetic analysis of interactions between prototypical CYP3A4 subgroup substrates: midazolam, testosterone, and nifedipine. *Drug Metab Dispos* 31(9): 1108-1116.

Gasche Y, Daali Y, Fathi M, Chiappe A, Cottini S, Dayer P, and Desmeules J (2004). Codeine intoxication associated with ultrarapid CYP2D6 metabolism. *N Engl J Med* 351(27): 2827-2831.

Gerostamoulos J, Burke MP, and Drummer OH (1996). Involvement of codeine in drug-related deaths. *Am J Forensic Med Pathol* 17(4): 327-335.

Ghosal A, Yuan Y, Hapangama N, Su AD, Alvarez N, Chowdhury SK, Alton KB, Patrick JE, and Zbaida S (2004). Identification of human UDP-glucuronosyltransferase enzyme(s) responsible for the glucuronidation of 3-hydroxydesloratadine. *Biopharm Drug Dispos* 25(6): 243-252.

Ghosh SS, Sappal BS, Kalpana GV, Lee SW, Chowdhury JR, and Chowdhury NR (2001). Homodimerization of human bilirubin-uridine-diphosphoglucuronate glucuronosyltransferase-1 (UGT1A1) and its functional implications. *J Biol Chem* 276(45): 42108-42115.

Gonzalez FJ, and Tukey RH. Goodman & Gilman's : the pharmacological basis of therapeutics. In: Beunton LL, Lazo JS, and Parker KL, editors. Drug metabolism. (11th ed). New York: McGraw-Hill Companies; 2006. pp. 71-92.

Guengerich FP (2008). Cytochrome p450 and chemical toxicology. *Chem Res Toxicol* 21(1): 70-83.

Hakooz N, Ito K, Rawden H, Gill H, Lemmers L, Boobis AR, Edwards RJ, Carlile DJ, Lake BG, and Houston JB (2006). Determination of a human hepatic microsomal scaling factor for predicting in vivo drug clearance. *Pharm Res* 23(3): 533-539.

Hamilton JA (2002). How fatty acids bind to proteins: the inside story from protein structures. *Prostaglandins Leukot Essent Fatty Acids* 67(2-3): 65-72.

He K, Ludtke SJ, Heller WT, and Huang HW (1996). Mechanism of alamethicin insertion into lipid bilayers. *Biophys J* 71(5): 2669-2679.

He XM and Carter DC (1992). Atomic structure and chemistry of human serum albumin. *Nature* 358(6383): 209-215.

Heinemann A, Wischhusen F, Puschel K, and Rogiers X (1999). Standard liver volume in the Caucasian population. *Liver Transpl Surg* 5(5): 366-368.

Henricsson S (1987). A new method for measuring the free fraction of cyclosporin in plasma by equilibrium dialysis. *J Pharm Pharmacol* 39(5): 384-385.

Holford NH and Sheiner LB (1981). Understanding the dose-effect relationship: clinical application of pharmacokinetic-pharmacodynamic models. *Clin Pharmacokinet* 6(6): 429-453.

Holford NHG. Pharmacokinetics & pharmacodynamics: dose selection & the time course of drug action. In: Katzung BG, editor. Basic & clinical pharmacology. (9th ed). New York: The McGraw-Hill Companies; 2004. pp. 34-50.

Houston JB (1994). Utility of in vitro drug metabolism data in predicting in vivo metabolic clearance. *Biochem Pharmacol* 47(9): 1469-1479.

Houston JB and Galetin A (2003). Progress towards prediction of human pharmacokinetic parameters from in vitro technologies. *Drug Metab Rev* 35(4): 393-415.

Houston JB and Galetin A (2005). Modelling atypical CYP3A4 kinetics: principles and pragmatism. *Arch Biochem Biophys* 433(2): 351-360.

Houston JB and Kenworthy KE (2000). In vitro-in vivo scaling of CYP kinetic data not consistent with the classical Michaelis-Menten model. *Drug Metab Dispos* 28(3): 246-254.

Houston JB, Kenworthy KE, and Galetin A. 'Typical and atypical enzyme kinetics'. In: Fisher M, Lee J, and Obach S, editors. Drug Metabolizing Enzymes: Cytochrome P450 and Other Enzymes in Drug Discovery and Development. Lausanne: Fontis Media; 2003.

Huffman DH and Ferguson RL (1975). Acute codeine overdose: correspondence between clinical course and codeine metabolism. *Johns Hopkins Med J* 136(4): 183-186.

Ikushiro S, Emi Y, and Iyanagi T (1997). Protein-protein interactions between UDP-glucuronosyltransferase isozymes in rat hepatic microsomes. *Biochemistry* 36(23): 7154-7161.

Innocenti F, Iyer L, Ramirez J, Green MD, and Ratain MJ (2001). Epirubicin glucuronidation is catalyzed by human UDP-glucuronosyltransferase 2B7. *Drug Metab Dispos* 29(5): 686-692.

Itaaho K, Mackenzie PI, Ikushiro S, Miners JO, and Finel M (2008). The configuration of the 17-hydroxy group variably influences the glucuronidation of beta-estradiol and epiestradiol by human UDP-glucuronosyltransferases. *Drug Metab Dispos* 36(11): 2307-2315.

Ito K, Brown HS, and Houston JB (2004). Database analyses for the prediction of in vivo drug–drug interactions from in vitro data. *Br J Clin Pharmacol* 57(4): 473–486.

Ito K and Houston JB (2004). Comparison of the use of liver models for predicting drug clearance using in vitro kinetic data from hepatic microsomes and isolated hepatocytes. *Pharm Res* 21(5): 785-792.

Ito K and Houston JB (2005). Prediction of human drug clearance from in vitro and preclinical data using physiologically based and empirical approaches. *Pharm Res* 22(1): 103-112.

Ito K, Iwatsubo T, Kanamitsu S, Nakajima Y, and Sugiyama Y (1998a). Quantitative prediction of in vivo drug clearance and drug interactions from in vitro data on metabolism, together with binding and transport. *Annu Rev Pharmacol Toxicol* 38: 461-499.

Ito K, Iwatsubo T, Kanamitsu S, Ueda K, Suzuki H, and Sugiyama Y (1998b). Prediction of pharmacokinetic alterations caused by drug-drug interactions: metabolic interaction in the liver. *Pharmacol Rev* 50(3): 387-412.

Iwatsubo T, Hirota N, Ooie T, Suzuki H, Shimada N, Chiba K, Ishizaki T, Green CE, Tyson CA, and Sugiyama Y (1997). Prediction of in vivo drug metabolism in the human liver from in vitro metabolism data. *Pharmacol Ther* 73(2): 147-171.

Jin CJ, Miners JO, Burchell B, and Mackenzie PI (1993). The glucuronidation of hydroxylated metabolites of benzo[a]pyrene and 2-acetylaminofluorene by cDNA-expressed human UDP-glucuronosyltransferases. *Carcinogenesis* 14(12): 2637-2639.

Johnson TN, Tucker GT, Tanner MS, and Rostami-Hodjegan A (2005). Changes in liver volume from birth to adulthood: a meta-analysis. *Liver Transpl* 11(12): 1481-1493.

Jones LR, Maddock SW, and Besch HR, Jr. (1980). Unmasking effect of alamethicin on the (Na+,K+)-ATPase, beta-adrenergic receptor-coupled adenylate cyclase, and cAMP-dependent protein kinase activities of cardiac sarcolemmal vesicles. *J Biol Chem* 255(20): 9971-9980.

Jude AR, Little JM, Czernik PJ, Tephly TR, Grant DF, and Radominska-Pandya A (2001). Glucuronidation of linoleic acid diols by human microsomal and recombinant UDP-glucuronosyltransferases: identification of UGT2B7 as the major isoform involved. *Arch Biochem Biophys* 389(2): 176-186.

Kaivosaari S, Toivonen P, Aitio O, Sipila J, Koskinen M, Salonen JS, and Finel M (2008). Regio- and stereospecific N-glucuronidation of medetomidine: the differences between UDP glucuronosyltransferase (UGT) 1A4 and UGT2B10 account for the complex kinetics of human liver microsomes. *Drug Metab Dispos* 36(8): 1529-1537.

Kaji H and Kume T (2005). Regioselective glucuronidation of denopamine: marked species differences and identification of human udp-glucuronosyltransferase isoform. *Drug Metab Dispos* 33(3): 403-412.

Kasai N, Sakaki T, Shinkyo R, Ikushiro S, Iyanagi T, Ohta M, and Inouye K (2005). Metabolism of 26,26,26,27,27,27-F6-1 alpha,23S,25-trihydroxyvitamin D3 by human UDP-glucuronosyltransferase 1A3. *Drug Metab Dispos* 33(1): 102-107.

Kenworthy KE, Clarke SE, Andrews J, and Houston JB (2001). Multisite kinetic models for CYP3A4: simultaneous activation and inhibition of diazepam and testosterone metabolism. *Drug Metab Dispos* 29(12): 1644-1651.

Kerdpin O, Elliot DJ, Mackenzie PI, and Miners JO (2006). Sulfinpyrazone C-glucuronidation is catalyzed selectively by human UDP-glucuronosyltransferase 1A9. *Drug Metab Dispos* 34(12): 1950-1953.

Kerdpin O, Mackenzie PI, Bowalgaha K, Finel M, and Miners JO (2009). Influence of N-terminal domain histidine and proline residues on the substrate selectivities of human UDP-glucuronosyltransferase 1A1, 1A6, 1A9, 2B7, and 2B10. *Drug Metab Dispos* 37(9): 1948-1955.

Kilford PJ, Stringer R, Sohal B, Houston JB, and Galetin A (2009). Prediction of drug clearance by glucuronidation from in vitro data: use of combined cytochrome P450 and UDP-glucuronosyltransferase cofactors in alamethicin-activated human liver microsomes. *Drug Metab Dispos* 37(1): 82-89.

King CD, Rios GR, Green MD, and Tephly TR (2000). UDP-glucuronosyltransferases. *Curr Drug Metab* 1(2): 143-161.

Kirchheiner J, Schmidt H, Tzvetkov M, Keulen JT, Lotsch J, Roots I, and Brockmoller J (2007). Pharmacokinetics of codeine and its metabolite morphine in ultra-rapid metabolizers due to CYP2D6 duplication. *Pharmacogenomics J* 7(4): 257-265.

Knights KM and Miners JO (2010). Renal UDP-glucuronosyltransferases and the glucuronidation of xenobiotics and endogenous mediators. *Drug Metab Rev* 42(1): 60-70.

Korzekwa KR, Krishnamachary N, Shou M, Ogai A, Parise RA, Rettie AE, Gonzalez FJ, and Tracy TS (1998). Evaluation of atypical cytochrome P450 kinetics with two-substrate models: evidence that multiple substrates can simultaneously bind to cytochrome P450 active sites. *Biochemistry* 37(12): 4137-4147.

Krishnaswamy S, Duan SX, Von Moltke LL, Greenblatt DJ, and Court MH (2003). Validation of serotonin (5-hydroxtryptamine) as an in vitro substrate probe for human UDP-glucuronosyltransferase (UGT) 1A6. *Drug Metab Dispos* 31(1): 133-139.

Kubota T, Lewis BC, Elliot DJ, Mackenzie PI, and Miners JO (2007). Critical roles of residues 36 and 40 in the phenol and tertiary amine aglycone substrate selectivities of UDP-glucuronosyltransferases 1A3 and 1A4. *Mol Pharmacol* 72(4): 1054-1062.

Kurkela M, Garcia-Horsman JA, Luukkanen L, Morsky S, Taskinen J, Baumann M, Kostiainen R, Hirvonen J, and Finel M (2003). Expression and characterization of recombinant human UDP-glucuronosyltransferases (UGTs). UGT1A9 is more resistant to detergent inhibition than other UGTs and was purified as an active dimeric enzyme. *J Biol Chem* 278(6): 3536-3544.

Kwon Y. Handbook of essential pharmacokinetics: pharmacodynamics and drug metabolism for industrial scientists New York: Kluwer Academic Publishers; 2002.

Lepine J, Bernard O, Plante M, Tetu B, Pelletier G, Labrie F, Belanger A, and Guillemette C (2004). Specificity and regioselectivity of the conjugation of estradiol, estrone, and their catecholestrogen and methoxyestrogen metabolites by human uridine diphospho-glucuronosyltransferases expressed in endometrium. *J Clin Endocrinol Metab* 89(10): 5222-5232.

Lesk AM (1995). NAD-binding domains of dehydrogenases. *Curr Opin Struct Biol* 5(6): 775-783.

Li D, Fournel-Gigleux S, Barre L, Mulliert G, Netter P, Magdalou J, and Ouzzine M (2007). Identification of aspartic acid and histidine residues mediating the reaction mechanism and the substrate specificity of the human UDP-glucuronosyltransferases 1A. *J Biol Chem* 282(50): 36514-36524.

Li Q, Lou X, Peyronneau MA, Straub PO, and Tukey RH (1997). Expression and functional domains of rabbit liver UDP-glucuronosyltransferase 2B16 and 2B13. *J Biol Chem* 272(6): 3272-3279.

Lin JH (2000). Sense and nonsense in the prediction of drug-drug interactions. *Curr Drug Metab* 1(4): 305-331.

Lin Y, Lu P, Tang C, Mei Q, Sandig G, Rodrigues AD, Rushmore TH, and Shou M (2001). Substrate inhibition kinetics for cytochrome P450-catalyzed reactions. *Drug Metab Dispos* 29(4 Pt 1): 368-374.

Liston HL, Markowitz JS, and DeVane CL (2001). Drug glucuronidation in clinical psychopharmacology. *J Clin Psychopharmacol* 21(5): 500-515.

Little JM, Kurkela M, Sonka J, Jantti S, Ketola R, Bratton S, Finel M, and Radominska-Pandya A (2004). Glucuronidation of oxidized fatty acids and prostaglandins B1 and E2 by human hepatic and recombinant UDP-glucuronosyltransferases. *J Lipid Res* 45(9): 1694-1703.

Lowry OH, Rosebrough NJ, Farr AL, and Randall RJ (1951). Protein measurement with the Folin phenol reagent. *J Biol Chem* 193(1): 265-275.

Mackenzie P, Little JM, and Radominska-Pandya A (2003). Glucosidation of hyodeoxycholic acid by UDP-glucuronosyltransferase 2B7. *Biochem Pharmacol* 65(3): 417-421.

Mackenzie PI (1990). Expression of chimeric cDNAs in cell culture defines a region of UDP glucuronosyltransferase involved in substrate selection. *J Biol Chem* 265(6): 3432-3435.

Mackenzie PI, Bock KW, Burchell B, Guillemette C, Ikushiro S, Iyanagi T, Miners JO, Owens IS, and Nebert DW (2005). Nomenclature update for the mammalian UDP glycosyltransferase (UGT) gene superfamily. *Pharmacogenet Genomics* 15(10): 677-685.

Mackenzie PI, Owens IS, Burchell B, Bock KW, Bairoch A, Belanger A, Fournel-Gigleux S, Green M, Hum DW, Iyanagi T, Lancet D, Louisot P, Magdalou J, Chowdhury JR, Ritter JK, Schachter H, Tephly TR, Tipton KF, and Nebert DW (1997). The UDP glycosyltransferase gene superfamily: recommended nomenclature update based on evolutionary divergence. *Pharmacogenetics* 7(4): 255-269.

Madadi P, Ross CJ, Hayden MR, Carleton BC, Gaedigk A, Leeder JS, and Koren G (2009). Pharmacogenetics of neonatal opioid toxicity following maternal use of codeine during breastfeeding: a case-control study. *Clin Pharmacol Ther* 85(1): 31-35.

Marangoni AG. Enzyme kinetics: A Modern Approach. New Jersey: John Wiley & Sons, Inc.; 2003.

McEwan A, Sigston PE, Andrews KA, Hack HA, Jenkins AM, May L, Llewelyn N, and MacKersie A (2000). A comparison of rectal and intramuscular codeine phosphate in children following neurosurgery. *Paediatr Anaesth* 10(2): 189-193.

McLure JA, Miners JO, and Birkett DJ (2000). Nonspecific binding of drugs to human liver microsomes. *Br J Clin Pharmacol* 49(5): 453-461.

Meech R and Mackenzie PI (1997). UDP-glucuronosyltransferase, the role of the amino terminus in dimerization. *J Biol Chem* 272(43): 26913-26917.

Meech R and Mackenzie PI (1998). Determinants of UDP glucuronosyltransferase membrane association and residency in the endoplasmic reticulum. *Arch Biochem Biophys* 356(1): 77-85.

Meech R, Yogalingam G, and Mackenzie PI (1996). Mutational analysis of the carboxy-terminal region of UDP-glucuronosyltransferase 2B1. *DNA Cell Biol* 15(6): 489-494.

Miley MJ, Zielinska AK, Keenan JE, Bratton SM, Radominska-Pandya A, and Redinbo MR (2007). Crystal structure of the cofactor-binding domain of the human phase II drug-metabolism enzyme UDP-glucuronosyltransferase 2B7. *J Mol Biol* 369(2): 498-511.

Miners JO (2002). Evolution of drug metabolism: hitchhiking the technology bandwagon. *Clin Exp Pharmacol Physiol* 29(11): 1040-1044.

Miners JO, Knights KM, Houston JB, and Mackenzie PI (2006). In vitro-in vivo correlation for drugs and other compounds eliminated by glucuronidation in humans: pitfalls and promises. *Biochem Pharmacol* 71(11): 1531-1539.

Miners JO, Lillywhite KJ, Matthews AP, Jones ME, and Birkett DJ (1988). Kinetic and inhibitor studies of 4-methylumbelliferone and 1-naphthol glucuronidation in human liver microsomes. *Biochem Pharmacol* 37(4): 665-671.

Miners JO and Mackenzie PI (1991). Drug glucuronidation in humans. *Pharmacol Ther* 51(3): 347-369.

Miners JO, Mackenzie PI, and Knights KM (2010). The prediction of drug-glucuronidation parameters in humans: UDP-glucuronosyltransferase enzyme-selective substrate and inhibitor probes for reaction phenotyping and in vitro-in vivo extrapolation of drug clearance and drug-drug interaction potential. *Drug Metab Rev* 42(1): 189-201.

Miners JO, Smith PA, Sorich MJ, McKinnon RA, and Mackenzie PI (2004). Predicting human drug glucuronidation parameters: application of in vitro and in silico modeling approaches. *Annu Rev Pharmacol Toxicol* 44: 1-25.

Moffat AC, Jackson JV, Moss MS, and Widdop B. Clarke's isolation and identification of drugs: in pharmaceuticals, body fluids, and post-mortem material. 2nd ed. London: The Pharmaceutical Press; 1986. 490–491.

Moolenaar F, Grasmeijer G, Visser J, and Meijer DK (1983). Rectal versus oral absorption of codeine phosphate in man. *Biopharm Drug Dispos* 4(2): 195-199.

Mulichak AM, Losey HC, Walsh CT, and Garavito RM (2001). Structure of the UDP-glucosyltransferase GtfB that modifies the heptapeptide aglycone in the biosynthesis of vancomycin group antibiotics. *Structure* 9(7): 547-557.

Murry DJ, Crom WR, Reddick WE, Bhargava R, and Evans WE (1995). Liver volume as a determinant of drug clearance in children and adolescents. *Drug Metab Dispos* 23(10): 1110-1116.

Naritomi Y, Terashita S, Kimura S, Suzuki A, Kagayama A, and Sugiyama Y (2001). Prediction of human hepatic clearance from in vivo animal experiments and in vitro metabolic studies with liver microsomes from animals and humans. *Drug Metab Dispos* 29(10): 1316-1324.

Neil A (1984). Affinities of some common opioid analgesics towards four binding sites in mouse brain. *Naunyn Schmiedebergs Arch Pharmacol* 328(1): 24-29.

Ngui JS, Chen Q, Shou M, Wang RW, Stearns RA, Baillie TA, and Tang W (2001). In vitro stimulation of warfarin metabolism by quinidine: increases in the formation of 4'- and 10-hydroxywarfarin. *Drug Metab Dispos* 29(6): 877-886.

Ngui JS, Tang W, Stearns RA, Shou M, Miller RR, Zhang Y, Lin JH, and Baillie TA (2000). Cytochrome P450 3A4-mediated interaction of diclofenac and quinidine. *Drug Metab Dispos* 28(9): 1043-1050.

Nishiyama T, Kobori T, Arai K, Ogura K, Ohnuma T, Ishii K, Hayashi K, and Hiratsuka A (2006). Identification of human UDP-glucuronosyltransferase isoform(s) responsible for the C-glucuronidation of phenylbutazone. *Arch Biochem Biophys* 454(1): 72-79.

Obach RS (1996). The importance of nonspecific binding in in vitro matrices, its impact on enzyme kinetic studies of drug metabolism reactions, and implications for in vitro-in vivo correlations. *Drug Metab Dispos* 24(10): 1047-1049.

Obach RS (1997). Nonspecific binding to microsomes: impact on scale-up of in vitro intrinsic clearance to hepatic clearance as assessed through examination of warfarin, imipramine, and propranolol. *Drug Metab Dispos* 25(12): 1359-1369.

Obach RS (1999). Prediction of human clearance of twenty-nine drugs from hepatic microsomal intrinsic clearance data: An examination of in vitro half-life approach and nonspecific binding to microsomes. *Drug Metab Dispos* 27(11): 1350-1359.

Ohno S, Kawana K, and Nakajin S (2008). Contribution of UDP-glucuronosyltransferase 1A1 and 1A8 to morphine-6-glucuronidation and its kinetic properties. *Drug Metab Dispos* 36(4): 688-694.

Ohno S and Nakajin S (2009). Determination of mRNA expression of human UDP-glucuronosyltransferases and application for localization in various human tissues by real-time reverse transcriptase-polymerase chain reaction. *Drug Metab Dispos* 37(1): 32-40.

Oravcova J, Bohs B, and Lindner W (1996). Drug-protein binding sites. New trends in analytical and experimental methodology. *J Chromatogr B Biomed Appl* 677(1): 1-28.

Ouzzine M, Antonio L, Burchell B, Netter P, Fournel-Gigleux S, and Magdalou J (2000). Importance of histidine residues for the function of the human liver UDP-glucuronosyltransferase UGT1A6: evidence for the catalytic role of histidine 370. *Mol Pharmacol* 58(6): 1609-1615.

Owens IS and Ritter JK (1992). The novel bilirubin/phenol UDP-glucuronosyltransferase UGT1 gene locus: implications for multiple nonhemolytic familial hyperbilirubinemia phenotypes. *Pharmacogenetics* 2(3): 93-108.

Pang KS and Rowland M (1977). Hepatic clearance of drugs. I. Theoretical considerations of a "well-stirred" model and a "parallel tube" model. Influence of hepatic blood flow, plasma

and blood cell binding, and the hepatocellular enzymatic activity on hepatic drug clearance. *J Pharmacokinet Biopharm* 5(6): 625-653.

Parke TJ, Nandi PR, Bird KJ, and Jewkes DA (1992). Profound hypotension following intravenous codeine phosphate. Three case reports and some recommendations. *Anaesthesia* 47(10): 852-854.

Pelkonen O and Turpeinen M (2007). In vitro-in vivo extrapolation of hepatic clearance: biological tools, scaling factors, model assumptions and correct concentrations. *Xenobiotica* 37(10-11): 1066-1089.

Picard N, Ratanasavanh D, Premaud A, Le Meur Y, and Marquet P (2005). Identification of the UDP-glucuronosyltransferase isoforms involved in mycophenolic acid phase II metabolism. *Drug Metab Dispos* 33(1): 139-146.

Quiding H, Lundqvist G, Boreus LO, Bondesson U, and Ohrvik J (1993). Analgesic effect and plasma concentrations of codeine and morphine after two dose levels of codeine following oral surgery. *Eur J Clin Pharmacol* 44(4): 319-323.

Radominska-Pandya A, Czernik PJ, Little JM, Battaglia E, and Mackenzie PI (1999). Structural and functional studies of UDP-glucuronosyltransferases. *Drug Metabolism Reviews* 31(4): 817-899.

Radominska-Pandya A, Little JM, and Czernik PJ (2001). Human UDP-glucuronosyltransferase 2B7. *Curr Drug Metab* 2(3): 283-298.

Radominska-Pandya A, Ouzzine M, Fournel-Gigleux S, and Magdalou J (2005). Structure of UDP-glucuronosyltransferases in membranes. *Methods Enzymol* 400: 116-147.

Reynolds JEF. Martindale: the complete drug reference. 31st ed. UK: The Royal Pharmaceutical Society, Pharmaceutical Publications Department; 1996.

Riedy M, Wang JY, Miller AP, Buckler A, Hall J, and Guida M (2000). Genomic organization of the UGT2b gene cluster on human chromosome 4q13. *Pharmacogenetics* 10(3): 251-260.

Riley RJ, McGinnity DF, and Austin RP (2005). A unified model for predicting human hepatic, metabolic clearance from in vitro intrinsic clearance data in hepatocytes and microsomes. *Drug Metab Dispos* 33(9): 1304-1311.

Ritter JK (2000). Roles of glucuronidation and UDP-glucuronosyltransferases in xenobiotic bioactivation reactions. *Chem Biol Interact* 129(1-2): 171-193.

Ritter JK, Chen F, Sheen YY, Lubet RA, and Owens IS (1992). Two human liver cDNAs encode UDP-glucuronosyltransferases with 2 log differences in activity toward parallel substrates including hyodeoxycholic acid and certain estrogen derivatives. *Biochemistry* 31(13): 3409-3414.

Roberts MS and Rowland M (1986). Correlation between in-vitro microsomal enzyme activity and whole organ hepatic elimination kinetics: analysis with a dispersion model. *J Pharm Pharmacol* 38(3): 177-181.

Rowland A, Elliot DJ, Knights KM, Mackenzie PI, and Miners JO (2008a). The "albumin effect" and in vitro-in vivo extrapolation: sequestration of long-chain unsaturated fatty acids enhances phenytoin hydroxylation by human liver microsomal and recombinant cytochrome P450 2C9. *Drug Metab Dispos* 36(5): 870-877.

Rowland A, Elliot DJ, Williams JA, Mackenzie PI, Dickinson RG, and Miners JO (2006). In vitro characterization of lamotrigine N2-glucuronidation and the lamotrigine-valproic acid interaction. *Drug Metab Dispos* 34(6): 1055-1062.

Rowland A, Gaganis P, Elliot DJ, Mackenzie PI, Knights KM, and Miners JO (2007). Binding of inhibitory fatty acids is responsible for the enhancement of UDP-glucuronosyltransferase 2B7 activity by albumin: implications for in vitro-in vivo extrapolation. *J Pharmacol Exp Ther* 321(1): 137-147.

Rowland A, Knights KM, Mackenzie PI, and Miners JO (2008b). The "albumin effect" and drug glucuronidation: bovine serum albumin and fatty acid-free human serum albumin enhance the glucuronidation of UDP-glucuronosyltransferase (UGT) 1A9 substrates but not UGT1A1 and UGT1A6 activities. *Drug Metab Dispos* 36(6): 1056-1062.

Rowland M, and Matin SB (1973). Kinetics of drug-drug interactions *J Pharmacokinet Pharmacodyn* 1(6): 553–567.

Sahai J, Gallicano K, Pakuts A, and Cameron DW (1994). Effect of fluconazole on zidovudine pharmacokinetics in patients infected with human immunodeficiency virus. *J Infect Dis* 169(5): 1103-1107.

Sakaguchi K, Green M, Stock N, Reger TS, Zunic J, and King C (2004). Glucuronidation of carboxylic acid containing compounds by UDP-glucuronosyltransferase isoforms. *Arch Biochem Biophys* 424(2): 219-225.

Segel IH. Enzyme kinetics: behavior and analysis of rapid equilibrium and steady-state enzyme systems. New York: John Wiley & Sons, Inc.; 1993.

Senafi SB, Clarke DJ, and Burchell B (1994). Investigation of the substrate specificity of a cloned expressed human bilirubin UDP-glucuronosyltransferase: UDP-sugar specificity and involvement in steroid and xenobiotic glucuronidation. *Biochem J* 303 (Pt 1): 233-240.

Shou M, Mei Q, Ettore MW, Jr., Dai R, Baillie TA, and Rushmore TH (1999). Sigmoidal kinetic model for two co-operative substrate-binding sites in a cytochrome P450 3A4 active site: an example of the metabolism of diazepam and its derivatives. *Biochem J* 340 (Pt 3): 845-853.

Sindrup SH and Brosen K (1995). The pharmacogenetics of codeine hypoalgesia. *Pharmacogenetics* 5(6): 335-346.

Smith PA, Sorich MJ, Low LS, McKinnon RA, and Miners JO (2004). Towards integrated ADME prediction: past, present and future directions for modelling metabolism by UDP-glucuronosyltransferases. *J Mol Graph Model* 22(6): 507-517.

Smith PA, Sorich MJ, McKinnon RA, and Miners JO (2003a). In silico insights: chemical and structural characteristics associated with uridine diphosphate-glucuronosyltransferase substrate selectivity. *Clin Exp Pharmacol Physiol* 30(11): 836-840.

Smith PA, Sorich MJ, McKinnon RA, and Miners JO (2003b). Pharmacophore and quantitative structure-activity relationship modeling: complementary approaches for the rationalization and prediction of UDP-glucuronosyltransferase 1A4 substrate selectivity. *J Med Chem* 46(9): 1617-1626.

Soars MG, Burchell B, and Riley RJ (2002). In vitro analysis of human drug glucuronidation and prediction of in vivo metabolic clearance. *J Pharmacol Exp Ther* 301(1): 382-390.

Soars MG, Petullo DM, Eckstein JA, Kasper SC, and Wrighton SA (2004). An assessment of udp-glucuronosyltransferase induction using primary human hepatocytes. *Drug Metab Dispos* 32(1): 140-148.

Soars MG, Riley RJ, Findlay KA, Coffey MJ, and Burchell B (2001). Evidence for significant differences in microsomal drug glucuronidation by canine and human liver and kidney. *Drug Metab Dispos* 29(2): 121-126.

Soars MG, Ring BJ, and Wrighton SA (2003). The effect of incubation conditions on the enzyme kinetics of udp-glucuronosyltransferases. *Drug Metab Dispos* 31(6): 762-767.

Somogyi AA, Barratt DT, and Coller JK (2007). Pharmacogenetics of opioids. *Clin Pharmacol Ther* 81(3): 429-444.

Sorich MJ, Smith PA, McKinnon RA, and Miners JO (2002). Pharmacophore and quantitative structure activity relationship modelling of UDP-glucuronosyltransferase 1A1 (UGT1A1) substrates. *Pharmacogenetics* 12(8): 635-645.

Sorich MJ, Smith PA, Miners JO, Mackenzie PI, and McKinnon RA (2008). Recent advances in the in silico modelling of UDP glucuronosyltransferase substrates. *Curr Drug Metab* 9(1): 60-69.

Srinivasan V, Wielbo D, and Tebbett IR (1997). Analgesic effects of codeine-6-glucuronide after intravenous administration. *Eur J Pain* 1(3): 185-190.

Stone AN, Mackenzie PI, Galetin A, Houston JB, and Miners JO (2003). Isoform selectivity and kinetics of morphine 3- and 6-glucuronidation by human udp-glucuronosyltransferases: evidence for atypical glucuronidation kinetics by UGT2B7. *Drug Metab Dispos* 31(9): 1086-1089.

Sugio S, Kashima A, Mochizuki S, Noda M, and Kobayashi K (1999). Crystal structure of human serum albumin at 2.5 A resolution. *Protein Eng* 12(6): 439-446.

Takeda S, Kitajima Y, Ishii Y, Nishimura Y, Mackenzie PI, Oguri K, and Yamada H (2006). Inhibition of UDP-glucuronosyltransferase 2b7-catalyzed morphine glucuronidation by ketoconazole: dual mechanisms involving a novel noncompetitive mode. *Drug Metab Dispos* 34(8): 1277-1282.

Tang C, Lin Y, Rodrigues AD, and Lin JH (2002). Effect of albumin on phenytoin and tolbutamide metabolism in human liver microsomes: an impact more than protein binding. *Drug Metab Dispos* 30(6): 648-654.

Thorn CF, Klein TE, and Altman RB (2009). Codeine and morphine pathway. *Pharmacogenet Genomics* 19(7): 556-558.

Trapnell CB, Klecker RW, Jamis-Dow C, and Collins JM (1998). Glucuronidation of 3'-azido-3'-deoxythymidine (zidovudine) by human liver microsomes: relevance to clinical

pharmacokinetic interactions with atovaquone, fluconazole, methadone, and valproic acid. *Antimicrob Agents Chemother* 42(7): 1592-1596.

Tsoutsikos P, Miners JO, Stapleton A, Thomas A, Sallustio BC, and Knights KM (2004). Evidence that unsaturated fatty acids are potent inhibitors of renal UDP-glucuronosyltransferases (UGT): kinetic studies using human kidney cortical microsomes and recombinant UGT1A9 and UGT2B7. *Biochem Pharmacol* 67(1): 191-199.

Tucker GT (1992). The rational selection of drug interaction studies: implications of recent advances in drug metabolism. *Int J Clin Pharmacol Ther Toxicol* 30(11): 550-553.

Tukey RH and Strassburg CP (2000). Human UDP-glucuronosyltransferases: metabolism, expression, and disease. *Annu Rev Pharmacol Toxicol* 40: 581-616.

Turgeon D, Carrier JS, Chouinard S, and Belanger A (2003). Glucuronidation activity of the UGT2B17 enzyme toward xenobiotics. *Drug Metab Dispos* 31(5): 670-676.

Uchaipichat V, Galetin A, Houston JB, Mackenzie PI, Williams JA, and Miners JO (2008). Kinetic modeling of the interactions between 4-methylumbelliferone, 1-naphthol, and zidovudine glucuronidation by udp-glucuronosyltransferase 2B7 (UGT2B7) provides evidence for multiple substrate binding and effector sites. *Mol Pharmacol* 74(4): 1152-1162.

Uchaipichat V, Mackenzie PI, Elliot DJ, and Miners JO (2006a). Selectivity of substrate (trifluoperazine) and inhibitor (amitriptyline, androsterone, canrenoic acid, hecogenin, phenylbutazone, quinidine, quinine, and sulfinpyrazone) "probes" for human udp-glucuronosyltransferases. *Drug Metab Dispos* 34(3): 449-456.

Uchaipichat V, Mackenzie PI, Guo XH, Gardner-Stephen D, Galetin A, Houston JB, and Miners JO (2004). Human udp-glucuronosyltransferases: isoform selectivity and kinetics of 4-methylumbelliferone and 1-naphthol glucuronidation, effects of organic solvents, and inhibition by diclofenac and probenecid. *Drug Metab Dispos* 32(4): 413-423.

Uchaipichat V, Winner LK, Mackenzie PI, Elliot DJ, Williams JA, and Miners JO (2006b). Quantitative prediction of in vivo inhibitory interactions involving glucuronidated drugs from in vitro data: the effect of fluconazole on zidovudine glucuronidation. *Br J Clin Pharmacol* 61(4): 427-439.

Ueng YF, Kuwabara T, Chun YJ, and Guengerich FP (1997). Cooperativity in oxidations catalyzed by cytochrome P450 3A4. *Biochemistry* 36(2): 370-381.

Urata K, Kawasaki S, Matsunami H, Hashikura Y, Ikegami T, Ishizone S, Momose Y, Komiyama A, and Makuuchi M (1995). Calculation of child and adult standard liver volume for liver transplantation. *Hepatology* 21(5): 1317-1321.

Vozeh S (1988). Therapeutic drug monitoring. *Clin Pharmacol Ther* 44(6): 713-714.

Vree TB, van Dongen RT, and Koopman-Kimenai PM (2000). Codeine analgesia is due to codeine-6-glucuronide, not morphine. *Int J Clin Pract* 54(6): 395-398.

Vree TB, and Verwey-van Wissen CP (1992). Pharmacokinetics and metabolism of codeine in humans. *Biopharm Drug Dispos* 13(6): 445-460.

Wallenstein SL, Houde RW, and Bellwille JW. Relative potency and effectiveness of codeine and morphine. Fed Proc; 1961; 1961. p. 311.

Wang JS, Wen X, Backman JT, and Neuvonen PJ (2002). Effect of albumin and cytosol on enzyme kinetics of tolbutamide hydroxylation and on inhibition of CYP2C9 by gemfibrozil in human liver microsomes. *J Pharmacol Exp Ther* 302(1): 43-49.

Wang RW, Newton DJ, Scheri TD, and Lu AY (1997). Human cytochrome P450 3A4-catalyzed testosterone 6 beta-hydroxylation and erythromycin N-demethylation. Competition during catalysis. *Drug Metab Dispos* 25(4): 502-507.

Watanabe Y, Nakajima M, Ohashi N, Kume T, and Yokoi T (2003). Glucuronidation of etoposide in human liver microsomes is specifically catalyzed by UDP-glucuronosyltransferase 1A1. *Drug Metab Dispos* 31(5): 589-595.

Wiggins CA and Munro S (1998). Activity of the yeast MNN1 alpha-1,3-mannosyltransferase requires a motif conserved in many other families of glycosyltransferases. *Proc Natl Acad Sci U S A* 95(14): 7945-7950.

William DG, Hatch DJ, and Howard RF (2001). Codeine phosphate in paediatric medicine. *Br J Anaesth* 86(3): 413-421.

Wong H, Tong V, Riggs KW, Rurak DW, Abbott FS, and Kumar S (2007). Kinetics of valproic acid glucuronidation: evidence for in vivo autoactivation. *Drug Metab Dispos* 35(8): 1380-1386.

Yue QY, Svensson JO, Alm C, Sjoqvist F, and Sawe J (1989). Interindividual and interethnic differences in the demethylation and glucuronidation of codeine. *Br J Clin Pharmacol* 28(6): 629-637.

Zhang JY, Wang Y, and Prakash C (2006). Xenobiotic-metabolizing enzymes in human lung. *Curr Drug Metab* 7(8): 939-948.

Zhou Q, Matsumoto S, Ding LR, Fischer NE, and Inaba T (2004). The comparative interaction of human and bovine serum albumins with CYP2C9 in human liver microsomes. *Life Sci* 75(18): 2145-2155.

Zhu B, Bush D, Doss GA, Vincent S, Franklin RB, and Xu S (2008). Characterization of 1'-hydroxymidazolam glucuronidation in human liver microsomes. *Drug Metab Dispos* 36(2): 331-338.

Zunszain PA, Ghuman J, Komatsu T, Tsuchida E, and Curry S (2003). Crystal structural analysis of human serum albumin complexed with hemin and fatty acid. *BMC Struct Biol* 3: 6.

APPENDIX

Raungrut P, Uchaipichat V, Elliot DJ, Janchawee B, Somogyi AA and Miners JO. In vitro – in vivo extrapolation predicts drug – drug interactions arising from inhibition of codeine glucuronidation by dextropropoxyphene, fluconazole, ketoconazole and methadone in humans. Journal of Pharmacology and Experimental Therapeutics 2010; 334(2): 609–618.

0090-9556/10/3803-609–615$20.00
THE JOURNAL OF PHARMACOLOGY AND EXPERIMENTAL THERAPEUTICS
Copyright © 2010 by The American Society for Pharmacology and Experimental Therapeutics
JPET 334:609–615, 2010

Vol. 334, No. 3
167316/3537759
Printed in U.S.A.

In Vitro–In Vivo Extrapolation Predicts Drug–Drug Interactions Arising from Inhibition of Codeine Glucuronidation by Dextropropoxyphene, Fluconazole, Ketoconazole, and Methadone in Humans[S]

Pritsana Raungrut, Verawan Uchaipichat, David J. Elliot, Benjamas Janchawee, Andrew A. Somogyi, and John O. Miners

Department of Clinical Pharmacology, Flinders University School of Medicine, Adelaide, Australia (P.R., V.U., D.J.E., J.O.M.); Department of Biomedical Sciences, Prince of Songkla University, Hat Yai, Thailand (P.R., B.J.); Faculty of Pharmaceutical Science, Khon Kaen University, Khon Kaen, Thailand (V.U.); and Discipline of Pharmacology, Faculty of Health Sciences, University of Adelaide, Adelaide, Australia (A.A.S.)

Received March 3, 2010; accepted May 17, 2010

ABSTRACT

Because codeine (COD) is eliminated primarily via glucuronidation, factors that alter COD glucuronide formation potentially affect the proportion of the dose converted to the pharmacologically active metabolite morphine. Thus, in vitro–in vivo extrapolation approaches were used to identify potential drug–drug interactions arising from inhibition of COD glucuronidation in humans. Initial studies characterized the kinetics of COD-6-glucuronide (C6G) formation by human liver microsomes (HLM) and demonstrated an 88% reduction in the Michaelis constant (K_m) (0.29 versus 2.32 mM) for incubations performed in the presence of 2% bovine serum albumin (BSA). Of 13 recombinant UDP-glucuronosyltransferase (UGT) enzymes screened for COD glucuronidation activity, only UGT2B4 and UGT2B7 exhibited activity. The respective S_{50} values (0.32 and 0.27 mM) generated in the presence of BSA were comparable with the mean K_m observed in HLM. Known inhibitors of UGT2B7 activity in vitro or in vivo and drugs marketed as compound formulations with COD were investigated for inhibition of C6G formation by HLM. Inhibition screening identified potential interactions with dextropropoxyphene, fluconazole, ketoconazole, and methadone. Inhibitor constant values generated for dextropropoxyphene (3.5 μM), fluconazole (202 μM), ketoconazole (0.66 μM), and methadone (0.32 μM) predicted 1.60- to 3.66-fold increases in the area under the drug plasma concentration–time curve ratio for COD in vivo. Whereas fluconazole and ketoconazole inhibited UGT2B4- and UGT2B7-catalyzed COD glucuronidation to a similar extent, inhibition by dextropropoxyphene and methadone resulted largely from an effect on UGT2B4. Interactions with dextropropoxyphene, fluconazole, ketoconazole, and methadone potentially affect the intensity and duration of COD analgesia.

The opioid codeine (COD) is one of the most widely used drugs worldwide. COD is used extensively in the treatment of mild to moderate pain, either alone or in combination with other analgesics. Furthermore, COD is used as an antitussive and for the treatment of diarrhea. It is generally accepted that COD analgesia arises from CYP2D6 catalyzed O-demethylation to form morphine (Somogyi et al., 2007). Approximately 4 to 10% of a COD dose is converted to morphine in CYP2D6-extensive metabolizers (Chen et al., 1991; Yue et al., 1991). Other elimination pathways include glucuronidation, N-demethylation, and renal clearance of unchanged drug. Of these, glucuronidation, to form COD-6-glucuronide (C6G), is the dominant metabolic pathway, accounting for 80 to 85% of the COD dose recovered in urine (Yue et al., 1991).

Accumulating evidence indicates that the relative formation of morphine plays a pivotal role in COD response. In

This study was supported by the National Health and Medical Research Council of Australia [Grant 486417]. V.U. was supported by an Australian Education International Endeavour Fellowship (Department of Education, Employment, and Workplace Relations, Australian Federal Government). P.R. was supported by a Prince of Songkla University Graduate Studies grant.

Article, publication date, and citation information can be found at http://jpet.aspetjournals.org.

doi:10.1124/jpet.110.167916.

[S] The online version of this article (available at http://jpet.aspetjournals.org) contains supplemental material.

ABBREVIATIONS: COD, codeine; AUC, area under the drug plasma concentration–time curve; BSA, bovine serum albumin; C6G, codeine-6-glucuronide; CL_H, hepatic clearance; DDI, inhibitory drug–drug interaction; HLM, human liver microsomes; IVIVE, in vitro–in vivo extrapolation; K_i, inhibitor constant; K_m, Michaelis constant; UGT, UDP-glucuronosyltransferase; V_{max}, maximal velocity; fu_{inc}, fraction unbound in incubations; CYP2D6, cytochrome P450 2D6; HPLC, high-performance liquid chromatography; UDPGA, UDP-glucuronic acid; HEK, human embryonic kidney.

particular, variability in COD O-demethylation caused by genetic polymorphism of CYP2D6 is known to influence both analgesia and the occurrence of morphine-related adverse effects (Gasche et al., 2004; Somogyi et al., 2007; Madadi et al., 2009). Because glucuronidation is the dominant route of COD metabolism, changes in C6G formation will potentially affect the proportion of the dose metabolized via the O-demethylation pathway and hence the intensity and duration of pharmacological response. However, factors that influence COD glucuronidation in humans are poorly understood.

It has been reported that COD 6-glucuronidation is catalyzed by UGT2B7, with a possible contribution of UGT2B4 (Court et al., 2003). UGT2B7 is arguably the most important drug-metabolizing UGT enzyme in humans (Miners et al., 2010). Apart from COD, UGT2B7 also glucuronidates other opioids (e.g., morphine, naloxone), many nonsteroidal anti-inflammatory agents, valproic acid, and zidovudine. A relatively common coding region polymorphism, UGT2B7*2 (H268Y), seems not to affect the glucuronidation of opioids, including COD (Bhasker et al., 2000; Court et al., 2003). Compelling evidence linking other *UGT2B7* variants and opioid disposition and response is similarly lacking (Thorn et al., 2009). In contrast, data from both in vitro and in vivo studies indicate that inhibition of UGT2B7 may potentially result in significant drug–drug interactions (DDIs), with reduced clearance via glucuronidation. For example, DDIs in vivo have been reported between fluconazole and zidovudine (Sahai et al., 1994) and methadone and zidovudine (McCance-Katz et al., 1998), whereas dextropropoxyphene, fluconazole, ketoconazole, methadone, and valproic acid have been shown to inhibit human liver microsomal morphine or zidovudine glucuronidation (Trapnell et al., 1998; Morrish et al., 2005; Takeda et al., 2006; Uchaipichat et al., 2006b).

Our recent studies have demonstrated that the magnitude of an in vivo inhibitory DDI with a UGT2B7 substrate as the object drug may be predicted accurately from an inhibitor constant (K_i) generated in vitro when incubations of human liver microsomes (HLM) are conducted in the presence of bovine serum albumin (BSA). Long-chain unsaturated fatty acids released from the microsomal membrane during the course of an incubation act as potent competitive inhibitors of UGT2B7 and UGT1A9, resulting in overestimation of the K_m and K_i values of substrates and inhibitors of these enzymes (Rowland et al., 2007, 2006b). BSA sequesters the inhibitory unsaturated long-chain fatty acids and, as a consequence, K_i (and K_m) values are reduced by approximately one order of magnitude compared with data generated in the absence of albumin (Miners et al., 2006, 2010). It is noteworthy that in vitro K_i values obtained in the presence of 2% BSA accurately predicted the magnitude of the fluconazole–zidovudine and valproic acid–lamotrigine interactions in vivo (Rowland et al., 2006; Uchaipichat et al., 2006b).

The primary aim of the present study was to use in vitro–in vivo extrapolation (IV-IVE) to identify potential DDIs resulting in inhibition of COD glucuronidation. In vitro inhibition data were generated by using HLM, with and without BSA, as the enzyme source. Drugs investigated included those previously identified from in vitro and in vivo inhibition studies with UGT2B7 substrates (namely, dextropropoxyphene, fluconazole, ketoconazole, methadone, and valproic acid), and acetaminophen, ibuprofen, and salicylic acid (the primary active metabolite of aspirin), which are marketed as compound formulations with COD for enhanced analgesia. The work additionally sought to confirm the involvement of both UGT2B7 and UGT2B4 in C6G formation and characterize the effect of BSA (2%) on the kinetics of COD glucuronidation in vitro and to assess the relative inhibition of these enzymes by inhibitors of human liver microsomal COD glucuronidation.

Materials and Methods

Materials. Acetaminophen, alamethicin (from *Trichoderma viride*), codeine, BSA, dextropropoxyphene hydrochloride, *R,S*-ibuprofen, salicylic acid, UDP-glucuronic acid (UDPGA; trisodium salt), and valproic acid were purchased from Sigma-Aldrich (Sydney, Australia); C6G was from Toronto Research Chemicals, Inc. (North York, ON, Canada); and Supersomes expressing UGT2B4, 2B7, and 2B15 were from BD Biosciences (San Jose, CA). Fluconazole was obtained from Pfizer Australia (Sydney, Australia); ketoconazole was from Janssen-Cilag Pty Ltd (Sydney, Australia); and *R,S*-methadone was from the National Institute on Drug Abuse (Rockville, MD). Solvents and other reagents were of analytical reagent grade.

Human Liver Microsomes and Expression of UGT Proteins. Human livers (HL 7, 10, 12, 13, and 40) were obtained from the human liver "bank" of the Department of Clinical Pharmacology, Flinders Medical Centre. Approval was obtained from the Flinders Medical Centre Research Ethics Committee for the use of human liver tissue in xenobiotic metabolism studies. HLM were prepared by differential centrifugation, as described by Bowalgaha et al. (2005). Before use in incubations, HLM were activated by the addition of the pore-forming peptide alamethicin (50 μg/mg protein) with preincubation on ice for 30 min (Bouse and Miners, 2002).

UGT1A1, 1A3, 1A4, 1A6, 1A7, 1A8, 1A9, 1A10, 2B10, 2B17, and 2B28 cDNAs were stably expressed in a human embryonic kidney cell line (HEK293), as described previously (Uchaipichat et al., 2004). After growth to at least 80% confluence, cells were harvested, washed with 0.1 M phosphate-buffered saline, pH 7.4, and lysed by sonication (Heat Systems Ultrasonics, Plainview, NY) using a microtip limit of four, with four 1-s "bursts," separated by 3 min with cooling on ice. Lysed samples were centrifuged at 12,000*g* for 1 min at 4°C, and the supernatant fraction was subsequently separated and stored at −80°C until use. Given the relatively low activity of UGT2B4, 2B7, and 2B15 expressed in HEK293 cells, Supersomes (BD Biosciences) expressing these enzymes were used in activity studies. The use of UGT2B enzymes from this source also allowed direct comparison of data from a previous study of codeine glucuronidation (Court et al., 2003).

Expression of each UGT was demonstrated by immunoblotting with an anti-UGT1A antibody (BD Biosciences), a nonselective UGT antibody (raised against purified mouse Ugt; see Uchaipichat et al., 2004), and an antibody that recognizes UGT2B7 and UGT2B10 (Kerdpin et al., 2009). In addition, activity measurements were performed with the recombinant proteins. Activities of recombinant UGT1A1, 1A3, 1A6, 1A7, 1A8, 1A9, 1A10, 2B4, 2B7, 2B15, 2B17, and 2B28 were confirmed by using the nonselective substrate 4-methylumbelliferone according to a previously published procedure (Rowland et al., 2007). UGT1A4 activity was demonstrated by using trifluoperazine as the substrate (Uchaipichat et al., 2006a), and UGT2B10 activity was confirmed by measurement of cotinine glucuronidation (Kerdpin et al., 2009).

C6G Glucuronidation Assay. Microsomal incubations, in a total volume of 100 μl (recombinant enzymes) or 200 μl (HLM), contained phosphate buffer (0.1 M, pH 7.4), $MgCl_2$ (4 mM), UDP-glucuronic acid (5 mM), COD (0.025–10 mM), and activated HLM (1 mg/ml) or recombinant UGT enzyme (1 mg/ml). After preincubation for 5 min, reactions were initiated by the addition of UDPGA (5 mM) and performed at 37°C in a shaking water bath for 60 min (HLM) or 120 min (UGT2B4 and UGT2B7). Reactions were terminated by the addition of $HClO_4$ (70% v/v; 2.5 μl) and cooling on ice for 20 min.

Samples were subsequently centrifuged at 9000*g* for 10 min at 10°C. A 120-μl aliquot of the supernatant fraction was transferred to a 1.5-ml Eppendorf tube containing 2 μl of KOH (4 M), and a 5-μl aliquot was injected directly into the HPLC column. For reactions performed in the presence of 2% (w/v) BSA, a lower range of COD concentrations (0.01–3 mM) was used as a consequence of the lower K_m in the presence of albumin (see *Results*). Conditions were as described for incubations performed in the absence of BSA except, because of the higher total protein content, reactions were terminated with 8 μl of $HClO_4$ and the supernatant fraction was treated with 6 μl of KOH. UGT enzyme (UGT1A1, 1A3, 1A4, 1A6, 1A7, 1A8, 1A9, 1A10, 2B4, 2B7, 2B10, 2B15, 2B17, and 2B28) activity screening studies were conducted at three COD concentrations (0.5, 2, and 10 mM), in the absence and presence of 2% BSA, using the incubation and assay conditions described above. C6G formation was not detected when UDPGA was incubated with lysate from untransfected HEK293 cells or control Supersomes. Likewise, there was no evidence for the formation of a glucoside conjugate when lysate from untransfected HEK293 cells or control Supersomes was incubated with UDPGA (which may contain UDP-glucose as an impurity).

Quantification of C6G Formation. HPLC was performed with an Agilent 1100 series instrument (Agilent Technologies, Sydney, Australia) fitted with a SecurityGuard C18 cartridge (4 × 2 mm; Phenomenex, Sydney, Australia) and a Synergi Hydro-RP C18 column (4 μm, 150 × 3 mm; Phenomenex). The mobile phase was a mixture of 2 mM triethylamine (pH adjusted to 2.7 with $HClO_4$) and 14% acetonitrile, delivered at a flow rate of 1 ml/min. Column eluant was monitored by UV absorbance at 205 nm. Retention times of C6G and COD were 2.08 and 2.76 min, respectively. C6G formation in incubation samples was quantified by comparison of peak areas to those of a standard curve prepared over the concentration range 1 to 40 μM. The formation of C6G was linear with incubation times to at least 100 min and microsomal protein concentrations to at least 1.5 mg/ml. Overall within-day assay reproducibility was assessed by measuring C6G formation in nine separate incubations of the same batch of pooled HLM. Coefficients of variation were 2.1 and 2.6% for COD concentrations of 0.5 and 10 mM, respectively.

COD and Inhibitor Binding to HLM and BSA. The binding of drugs (COD and inhibitors) to HLM and to BSA plus HLM was characterized by equilibrium dialysis according to the method of McLure et al. (2000). One side of the dialysis cell contained the drug in phosphate buffer (0.1 M, pH 7.4), whereas the other compartment contained a suspension of either pooled HLM (1 mg/ml) or a combination of 2% BSA and HLM (1 mg/ml) in phosphate buffer (0.1 M, pH 7.4). Drug binding was characterized at five or six concentrations over the ranges shown in Table 1: COD, 25 to 10,000 μM; dextropropoxyphene, 2.5 to 80 μM; ketoconazole, 2.5 to 250 μM; methadone, 0.25 to 12 μM; and valproic acid, 500 to 6000 μM. The dialysis cell assembly was immersed in a water bath maintained at 37°C and rotated at 12 rpm for 4 to 5 h. Control experiments were performed with phosphate buffer or HLM, or a combination of 2% BSA with HLM on both sides of the cell, at low and high drug concentrations, to ensure that equilibrium was attained. A 200-μl aliquot was collected from each cell and treated with 800 μl of ice-cold methanol containing 4% glacial acid or 800 μl of ice-cold acetonitrile (samples containing ketoconazole). Samples were chilled on ice for 20 min and subsequently centrifuged at 13,000*g* for 5 min at 4°C. An aliquot of the supernatant fraction was analyzed by HPLC.

The HPLC system used was as described previously for the measurement of C6G formation. Chromatography conditions for each analyte are detailed in Supplemental Table 1. Drug concentrations of dialysis samples recovered from each side of the cell were calculated by reference to peak areas of standard curves that spanned both the bound and unbound concentrations of each compound. Binding to incubation components, calculated as the drug concentration in the buffer compartment divided by the drug concentration in the protein compartment, is expressed as the fraction unbound in incubations (fu_{inc}). We have reported microsomal and BSA binding data for fluconazole previously (Uchaipichat et al., 2006b).

Inhibition of COD Glucuronidation. Inhibition experiments with pooled HLM, prepared by mixing equal protein amounts of microsomes from the five livers used in the C6G kinetic studies, were carried out in the absence and presence of 2% BSA. Initial inhibition screening studies were performed at COD concentrations corresponding to the K_m for C6G formation (with and without BSA) at four inhibitor concentrations. Subsequent experiments conducted to determine the K_i and inhibition mechanism included four inhibitor concentrations (see *Results*) at each of three COD concentrations: 1, 2, and 4 mM in the absence of BSA, and 0.15, 0.3, and 0.6 mM in the presence of 2% BSA. Inhibitors were added as aqueous solutions, except for ketoconazole and valproic acid, which were dissolved in methanol such that the final concentration of solvent in incubations was 1% v/v. This concentration of methanol has a negligible effect on UGT enzyme activity (Uchaipichat et al., 2004). Experiments that characterized the relative inhibition of recombinant UGT2B4 and UGT2B7 by dextropropoxyphene, fluconazole, ketoconazole, and methadone included 2% BSA. The COD concentration corresponded to the approximate S_{50} for C6G formation by these enzymes (0.3 mM), whereas the inhibitor concentrations corresponded to the K_i value corrected for binding to incubation components.

Data Analysis. Data points represent the mean of duplicate estimates (<10% variance). The Michaelis-Menten, substrate inhibition, and Hill equations (see Uchaipichat et al., 2004 for expressions) were fit to kinetic data for C6G formation by using EnzFitter (Biosoft, Cambridge, UK). CL_{int} was calculated as V_{max}/K_m. K_i values for inhibition of COD glucuronidation were determined by fitting the expressions for competitive, uncompetitive, noncompetitive, and mixed inhibition to experimental data by using EnzFitter. Goodness of fit was assessed from comparison of the *F* statistic, r^2 values, parameter standard error estimates, and 95% confidence intervals.

IV-IVE. The extent of inhibition of COD hepatic clearance (determined as the ratio of the areas under the plasma COD concentration–time curves with and without inhibitor coadministration) was predicted by using the equation for oral administration of a hepatically cleared drug (Miners et al., 2010):

$$\frac{AUC_i}{AUC} = \frac{1}{\dfrac{f_m}{1 + [I]/K_i} + (1 - f_m)} \quad (1)$$

where [I] is the inhibitor concentration; f_m is the fraction of COD hepatic clearance via glucuronidation (taken here as 80%; Yue et al., 1991); and K_i is the inhibition constant generated in vitro. The inhibitor concentration ([I]) was taken as the maximum hepatic maximum inlet concentration of the drug in vivo (Miners et al., 2010):

$$[I_{max,u}] = [I_{max}] + \frac{k_a \times F_a \times Dose}{Q_H} \quad (2)$$

where $[I_{max}]$, k_a, F_a, and Q_H are the maximum total drug concentration in the systemic circulation associated with a given dose

TABLE 1
Binding of codeine and inhibitors to human liver microsomes (1 mg/ml) in the absence and presence of bovine serum albumin (2% w/v)
Results are presented as fraction unbound in the incubation mixture (fu_{inc}) ± S.D.

	HLM	HLM Plus 2% BSA
Codeine	0.98 ± 0.013	0.96 ± 0.007
Dextropropoxyphene	0.89 ± 0.029	0.29–0.51[a]
Fluconazole[b]	1.04 ± 0.020	0.92 ± 0.027
Ketoconazole	0.27 ± 0.005	0.09 ± 0.003
Methadone	0.72 ± 0.039	0.56 ± 0.018
Valproic acid	0.99 ± 0.007	0.29–0.77[c]

[a] fu_{inc} concentration dependent in the range 2.5 to 20 μM.
[b] Data taken from Uchaipichat et al., 2006b.
[c] fu_{inc} concentration dependent in the range 0.5 to 6 mM.

(see Table 6), absorption rate constant, fraction absorbed from the gastrointestinal tract, and liver blood flow (taken as 90 liter/h), respectively. The hepatic maximum unbound inlet concentration was calculated as the product of $[I_{total,max}]$ and fraction unbound in blood. Maximum hepatic inlet concentrations (total and unbound) were calculated from published pharmacokinetic data for dextropropoxyphene (Welling et al., 1976; Giacomini et al., 1978; Gran et al., 1979; Inturrisi et al., 1982), fluconazole (Suhal et al., 1994; Uchaipichat et al., 2006b), and methadone (Inturrisi et al., 1987; Foster et al., 2004). It was not possible to calculate $I_{total,max}$ for ketoconazole because reliable estimates of k_a and F_a are not available. Thus, IV-IVE was based on the reported maximum concentration of ketoconazole in plasma (total and unbound; Badcock et al., 1987; Daneshmend and Warnock, 1988).

Results

Binding of COD and Inhibitors to HLM and BSA. Nonspecific binding to HLM and binding to HLM plus BSA was characterized here for COD and the putative inhibitors dextropropoxyphene, ketoconazole, methadone, and valproic acid (Table 1). Our previous studies demonstrated that fluconazole does not bind nonspecifically to HLM, and binding of fluconazole to HLM plus 2% BSA is minor (Uchaipichat et al., 2006b). The binding of COD and valproic acid to HLM alone was negligible across the concentration ranges investigated. The binding of COD to the mixture of HLM and BSA (2%) was also minor. Dextropoxypoxyphene and methadone bound modestly to both HLM and HLM plus BSA. The binding of dextropropoxyphene to the HLM/BSA mixture was concentration-dependent over the range investigated (2.5–20 μM). Ketoconazole bound extensively to both HLM and HLM plus BSA, with mean $f_{u,inc}$ values of 0.27 ± 0.01 and 0.09 ± 0.01, respectively. Consistent with a previous report (Rowland et al., 2006), the binding of valproic acid to the HLM/BSA mixture was concentration-dependent; $f_{u,inc}$ values ranged from 0.29 at the lowest valproic acid concentration (0.5 mM) to 0.77 at the highest concentration (6 mM). Where observed, binding of inhibitors to HLM and to HLM plus BSA was accounted for in the calculation of IC_{50} and K_i values (i.e., parameters are based on the unbound concentration in the incubation mixture).

C6G Glucuronidation by HLM. Representative kinetic plots for C6G formation by HLM in the absence and presence of 2% BSA are shown in Fig. 1, and derived kinetic constants are given in Table 2. C6G formation by HLM in the absence of BSA was well described by the Michaelis-Menten equation, whereas weak substrate inhibition (K_{si} approximately 40 times higher than K_m) was apparent for kinetic studies performed in the presence of BSA (2%). A transition from Michaelis-Menten to weak substrate inhibition kinetics in the presence of BSA has been observed previously for the glucuronidation of zidovudine (Uchaipichat et al., 2006b), another UGT2B7 substrate. The addition of BSA to incubations resulted in an 88% reduction in mean K_m, from 2.32 to 0.29 mM, without an effect on V_{max} (Table 2). Microsomal CL_{int} increased in proportion to the change in K_m. Kinetic constants for COD glucuronidation by pooled HLM, prepared by mixing equal protein amounts of microsomes from the five separate livers, were similar to

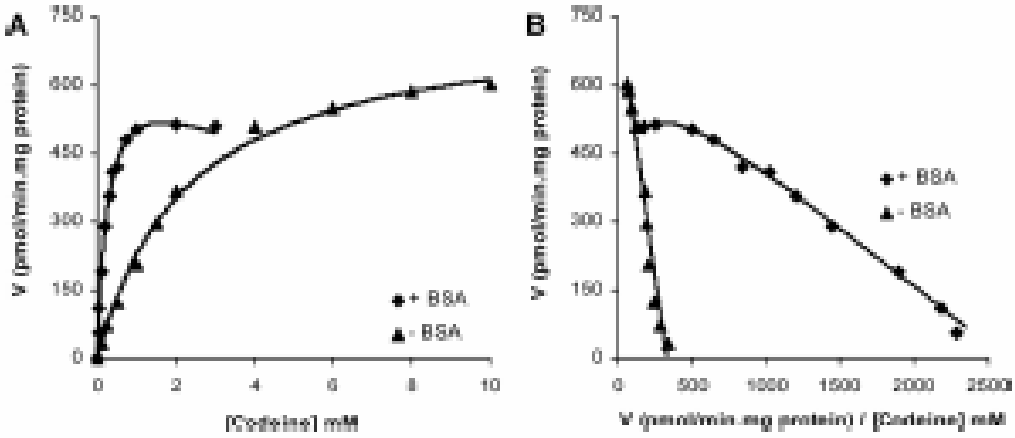

Fig. 1. Kinetic plots for codeine 6-glucuronidation by microsomes from a representative human liver (HL13) generated in the presence and absence of BSA (2% w/v). A, plot of the rate of product (C6G) formation versus substrate concentration. B, Eadie-Hofstee plot. Points are experimentally derived values, and curves are from model fitting.

TABLE 2
Derived kinetic parameters for codeine glucuronidation by human liver microsomes determined in the absence and presence of 2% (w/v) bovine serum albumin.

	Without BSA[a,b]			With 2% BSA[a,c]			
	K_m	V_{max}	CL_{int}[d]	K_m	V_{max}	K_{si}	CL_{int}[d]
	mM	pmol/min.mg	μl/min.mg	mM	pmol/min.mg	mM	μl/min.mg
H7	2.35 ± 0.01	440 ± 1.2	0.19	0.32 ± 0.01	430 ± 9.7	8.20 ± 1.04	1.34
H10	2.63 ± 0.02	312 ± 0.9	0.12	0.34 ± 0.01	302 ± 6.2	9.49 ± 1.19	0.89
H12	3.13 ± 0.18	920 ± 20.8	0.29	0.26 ± 0.02	848 ± 23.8	14.42 ± 2.78	3.03
H13	2.29 ± 0.12	754 ± 13.2	0.33	0.26 ± 0.001	880 ± 0.7	10.63 ± 0.12	2.62
H40	1.16 ± 0.01	4.16 ± 0.6	0.38	0.24 ± 0.01	447 ± 6.6	14.46 ± 1.80	1.86
Mean ± S.D.	2.32 ± 0.73	673 ± 253	0.28 ± 0.11	0.29 ± 0.04	841 ± 218	11.44 ± 2.87	1.96 ± 0.88
Pooled HLM	2.15 ± 0.13	884 ± 18	0.27	0.23 ± 0.01	436 ± 12	8.18 ± 1.08	1.90

[a] Data presented as mean ± standard error of parameter fit.
[b] Kinetic constants derived from fitting with the Michaelis-Menten equation.
[c] Kinetic constants derived from fitting with the substrate inhibition equation.
[d] CL_{int} calculated as V_{max}/K_m for both Michaelis-Menten and substrate inhibition kinetics.

the mean data obtained for the separate livers (Table 2). Although COD kinetic parameters were calculated based on the unbound concentration present in incubations, binding of COD to HLM plus BSA was minor (Table 1) and corrected and uncorrected K_m values differed minimally.

COD Glucuronidation by Recombinant UGT Enzymes. UGT1A1, 1A3, 1A4, 1A6, 1A7, 1A8, 1A9, 1A10, 2B4, 2B7, 2B10, 2B15, 2B17, and 2B28 were screened for C6G formation at three COD concentrations (0.5, 2, and 10 mM), both in the absence and presence of BSA (2%). As noted in *Materials and Methods*, all UGT enzymes except UGT 2B4, 2B7, and 2B15 were expressed in HEK293 cells. Given the relatively low expression of these enzymes in HEK293 cells, Supersomes were used as the recombinant enzyme source. The use of UGT 2B4 and 2B7 from this source further allowed direct comparison of data to a previously published study (Court et al., 2000). Although expression of all UGT enzymes was demonstrated by immunoblotting and activity measurements (data not shown), only UGT2B4 and UGT2B7 catalyzed the 6-glucuronidation of COD. Rates of C6G formation by UGT2B4 for COD concentrations of 0.5, 2, and 10 mM were 6, 24, and 59 pmol/min-mg in the absence of BSA, and 23, 37, and 39 pmol/min-mg in the presence of BSA. For UGT2B7, rates of C6G formation at COD concentrations of 0.5, 2, and 10 mM were 13, 33, and 39 pmol/min-mg in the absence of BSA, and 36, 46, and 48 pmol/min-mg in the presence of BSA. Although it is acknowledged that UGT expression may differ from enzyme to enzyme and between expression systems, the use of positive controls precluded absent activity as a reason for the inability of UGTs other than 2B4 and 2B7 to form C6G.

In contrast to HLM, COD glucuronidation by recombinant UGT2B4 and UGT2B7 exhibited sigmoidal kinetics (Fig. 2), which was modeled by using the Hill equation. Addition of BSA to incubations resulted in approximate 8- and 4-fold reductions in the respective S_{50} values for UGT2B4 and UGT2B7 (Table 3). The respective S_{50} values (0.32 and 0.27 mM) generated in the presence of BSA were comparable with the mean K_m observed in HLM. Although the addition of BSA had no effect on the V_{max} and Hill coefficients for UGT2B7-

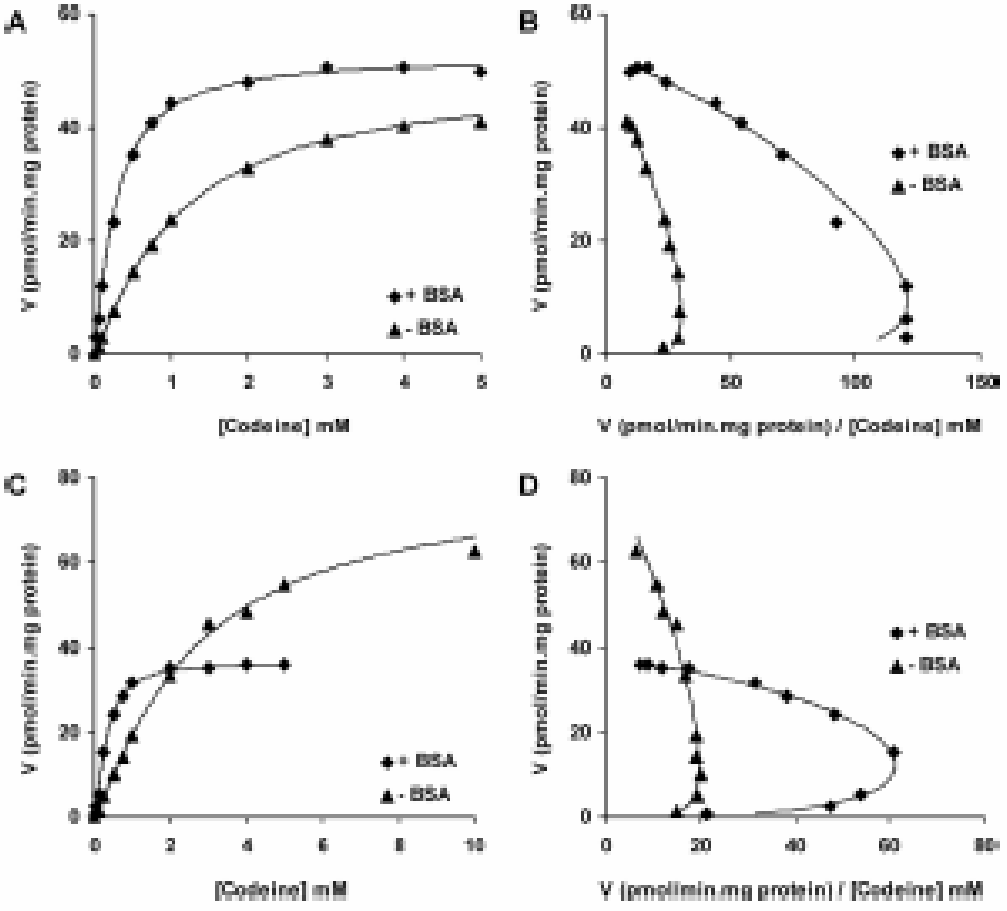

Fig. 2. Kinetic plots for codeine 6-glucuronidation by recombinant UGT2B4 and UGT2B7 generated in the presence and absence of BSA (2% w/v). A and C, plots of the rate of product (C6G) formation versus substrate concentration for UGT2B7 (A) and UGT2B4 (C). B and D, Eadie-Hofstee plots for UGT2B7 (B) and UGT2B4 (D). Points are experimentally derived values, and curves are from model fitting.

TABLE 3

Derived kinetic parameters for codeine glucuronidation by recombinant UGT2B4 and UGT2B7 determined in the absence and presence of 2% (w/v) bovine serum albumin

Data are cited as mean ± standard error of parameter fit. Kinetic constants were derived from fitting with the Hill equation.

	Without BSA				With 2% BSA			
	S_{50}	V_{max}	n	Cl_{max}[a]	S_{50}	V_{max}	n	Cl_{max}[a]
	mM	*pmol/min-mg*		*µl/min-mg*	*mM*	*pmol/min-mg*		*µl/min-mg*
UGT2B4	2.61 ± 0.001	79 ± 0.02	1.19 ± 0.001	0.02	0.32 ± 0.004	37 ± 0.16	1.50 ± 0.03	0.06
UGT2B7	1.07 ± 0.03	49 ± 0.23	1.17 ± 0.02	0.03	0.27 ± 0.01	53 ± 0.44	1.22 ± 0.03	0.12

[a] Cl_{max} calculated as $V_{max}/S_{50} \times (n-1/n)(n-1)^{1/n}$.

catalyzed COD glucuronidation, the V_{max} and Hill coefficient obtained for UGT2B4 in the presence of BSA were decreased and increased, respectively, compared with experiments performed in the absence of albumin (Table 2). It should be noted that, in contrast to the known effects of alamethicin on human liver microsomal UGT activities (Boase and Miners, 2002), preliminary experiments showed that preincubation of Supersomes expressing UGT2B4 and UGT2B7 with alamethicin (50 μg/mg protein) had no effect on the rate of COD glucuronidation (data not shown). Thus, alamethicin preincubation of Supersomes expressing UGT enzymes was not routinely performed.

Inhibition of Human Liver Microsomal COD Glucuronidation. Experiments conducted to calculate IC_{50} and K_i values used pooled HLM as the enzyme source, with and without 2% BSA. The effects of four concentrations of each putative inhibitor were assessed initially at the COD concentrations corresponding to the approximate mean K_m values for C6G formation in the absence (2 mM) and presence (0.3 mM) of 2% BSA (Table 4). Inhibitor binding to HLM and BSA was accounted for in the calculation of inhibition parameters (IC_{50} and K_i). Acetaminophen, fluconazole, ibuprofen, salicylic acid, and valproic acid were weak to moderate inhibitors of COD glucuronidation, with estimated IC_{50} values >2 mM in the absence of BSA (Table 4). Potent inhibition was observed for detroproproxyphene, ketoconazole, and methadone, with IC_{50} values ranging from 4.5 to 25 μM. Addition of BSA (2%) to incubations typically resulted in an 6- to 12-fold reduction in the IC_{50} (Table 4). It is noteworthy that IC_{50} values for detroproproxyphene, ketoconazole, and methadone ranged from 0.7 to 2.9 μM. It should be noted that the high binding of ibuprofen and salicylic acid to BSA precluded inhibition studies in the presence of albumin.

Based on data from the inhibition screening studies, kinetic experiments were performed to determine K_i values for detroproproxyphene, fluconazole, ketoconazole, and methadone. Results are shown in Fig. 3 as Dixon plots. Inhibition data for fluconazole, ketoconazole, and methadone were well modeled by using the expression for competitive inhibition, whereas the equation for noncompetitive inhibition provided the best fit for dextropropoxyphene inhibition of human liver microsomal COD glucuronidation. Consistent with the IC_{50} data, K_i values generated in the presence of BSA were lower (approximately 7- to 15-fold) compared with K_is obtained in the absence of albumin. Potent inhibition of C6G formation was observed for detropropoxyphene, ketoconazole, and methadone (Table 5).

Inhibition of UGT2B4- and UGT2B7-Catalyzed COD Glucuronidation. Effects of detropropoxyphene, fluconazole, ketoconazole, and methadone on UGT2B4- and UGT2B7-catalyzed C6G formation were determined to assess whether these compounds selectively inhibited the two enzymes involved in COD glucuronidation. Effects of inhibitors were measured in the presence of BSA (2% w/v) at the COD concentration corresponding to the approximate S_{50} value observed for C6G formation by recombinant UGT2B4 and UGT2B7 (namely, 0.3 mM; see Table 2). The concentration of each inhibitor added to incubations corresponded to the K_i value (Table 5) corrected for the binding of the compound to HLM plus BSA (i.e., K_i/fu_{inc}; see Fig. 4 legend). Although it is acknowledged that binding to HLM and Supersomes may not be identical because of differences in membrane composition, similarities in the predicted and observed inhibition pattern (see below) suggest comparable drug binding between HLM plus BSA and Supersomes plus BSA. Whereas fluconazole and ketoconazole inhibited COD glucuronidation by each enzyme to a similar extent, the inhibition by dextropropoxyphene and methadone arose predominantly via an effect on UGT2B4. By reference to the equations for competitive and noncompetitive inhibition (Segel, 1993) when the substrate and inhibitor concentrations correspond to K_m and K_i, respectively, it can be shown that 33% inhibition is expected for a competitive inhibitor whereas 50% inhibition is expected for a noncompetitive inhibitor. The data shown in Fig. 4 are broadly consistent with the degree of inhibition predicted for the competitive (fluconazole, ketoconazole, and methadone) and noncompetitive (dextropropoxyphene) inhibitors of UGT2B4- or UGT2B7-catalyzed C6G formation under the experimental conditions used.

IV-IVE for DDI Potential. Predicted changes in the AUC for COD when coadministered with dextroproxyphene, fluconazole, ketoconazole, or methadone are given in Table 6. Based on total inhibitor concentration in blood for the doses indicated in Table 6, a 60% or more increase in AUC was predicted for the four interactions; increases in the AUC ratio ranged from 1.60- to 3.66-fold. When considered in terms of unbound inhibitor concentration in blood, the magnitude of the predicted interactions with methadone and dextropropoxyphene decreased by approximately 70%, whereas no interaction was predicted with ketoconazole. The predicted change in the AUC ratio based on unbound fluconazole concentration did not change appreciably given the minor plasma protein binding of this compound.

TABLE 4

IC_{50} values for inhibition of human liver microsomal codeine glucuronidation determined in the absence and presence of 2% (w/v) bovine serum albumin

Data are given as IC_{50} ± S.E. of parameter fit. Concentration range of each inhibitor shown in parentheses.

Inhibitor	IC_{50}	
	Without BSA	With 2%BSA
	μM	
Dextropropoxyphene	24.6 ± 0.4[a] (0.39–500 μM)[b]	2.9 ± 0.2[a] (0.29–500 μM)[b]
Fluconazole	2970 ± 18 (50–2500 μM)	371 ± 0.8[a] (46–2300 μM)[b]
Ibuprofen	2280 ± 23 (1–5 mM)	N.D.[c]
Ketoconazole	17.2 ± 0.11[a] (4.8–270 μM)[b]	2.0 ± 0.02[a] (1.8–90 μM)[b]
Methadone	3.9 ± 0.03[a] (0.72–100 μM)[b]	0.7 ± 0.01[a] (0.28–88 μM)[b]
Acetaminophen	> 10 mM (2–30 mM)	8772 ± 22 (2–30 mM)
Salicylic acid	> 20 mM (2–20 mM)	N.D.[c]
Valproic acid	4604 ± 509 (1–20 mM)	880 ± 1.78[a] (0.18–8.6 mM)[b]

[a] IC_{50} value is the unbound concentration in the incubation medium (i.e. corrected for binding to HLM and BSA).

[b] Not determined because of extensive binding to BSA.

Discussion

Initial studies aimed to characterize the effect of BSA on COD glucuronidation by HLM and confirm the contributions of UGT2B4 and UGT2B7 to C6G formation. Kinetic param-

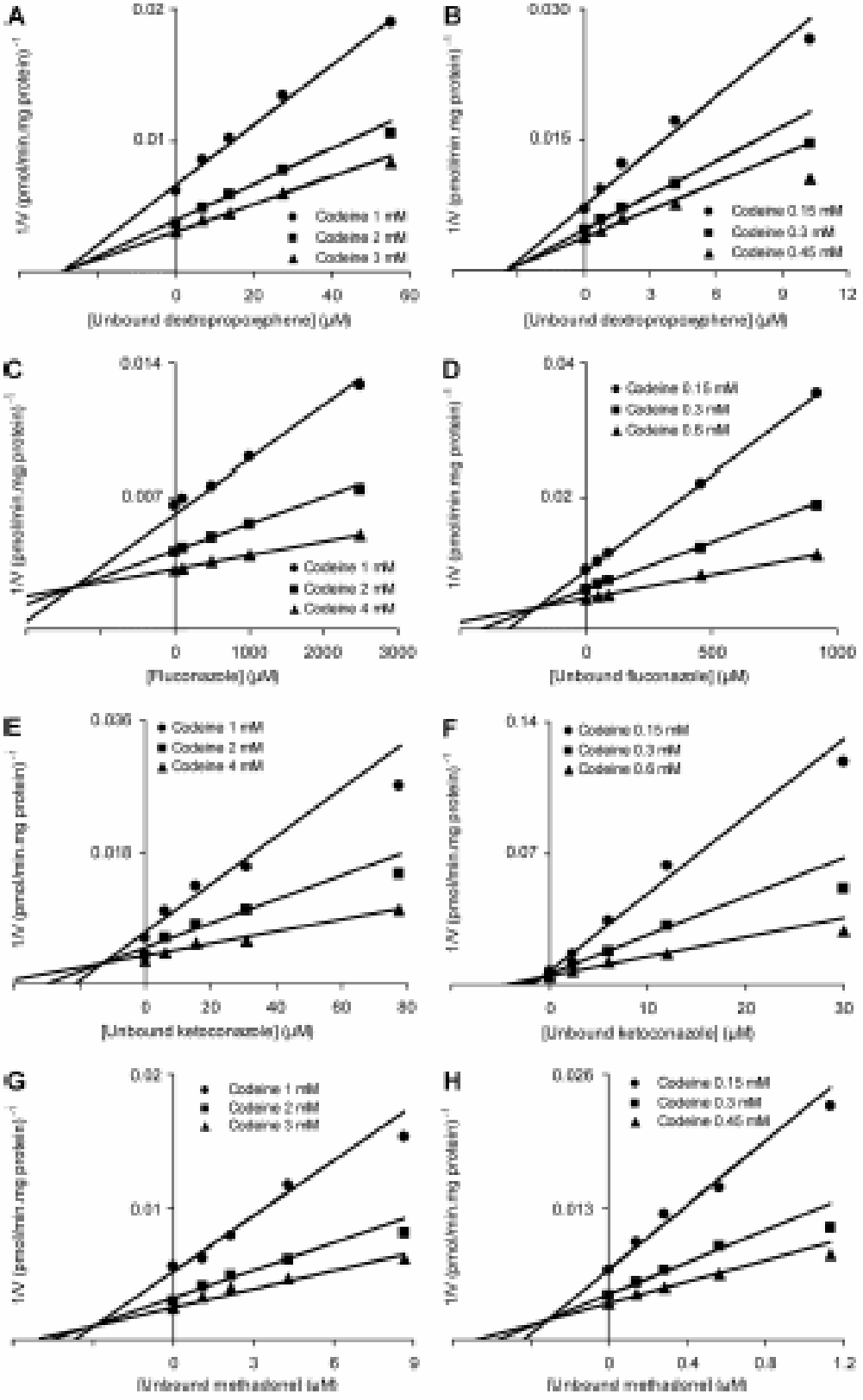

Fig. 8. Dixon plots for dextropropoxyphene, fluconazole, ketoconazole, and methadone inhibition of codeine 6-glucuronidation by pooled human liver microsomes generated in the absence (A, C, E, and G) and presence (B, D, F, and H) of BSA (2% w/v). Inhibitor concentrations are corrected for binding to human liver microsomes and BSA (i.e., unbound concentration in the incubation medium).

ters for C6G formation in HLM in the absence of BSA were similar to those reported previously by Court et al. (2003). Addition of BSA (2%) to incubations resulted in an 88% reduction in K_m without an effect on V_{max}. A similar effect has been reported for the glucuronidation of several other UGT2B7 substrates by HLM (Rowland et al., 2007; Kilford et al., 2009), confirming that K_m or microsomal intrinsic clearance values for UGT2B7 substrates are overestimated and underestimated, respectively, by approximately an order of magnitude when HLM are used as the enzyme source in the absence of albumin supplementation.

Also consistent with previous published data (Court et al., 2003), the screening of 13 recombinant enzymes demonstrated that only UGT2B4 and UGT2B7 glucuronidated

TABLE 5

K_i values for the inhibition of human liver microsomal codeine glucuronidation determined in the absence and presence of 2% (w/v) bovine serum albumin

K_i ± S.E. of parameter fit is shown. Data were best fitted with the expression for competitive inhibition, except for inhibition by dextropropoxyphene (noncompetitive inhibition).

Inhibitor	K_i	
	Without BSA	With 2% BSA
	μM	
Dextropropoxyphene	22.1 ± 1.2[a]	3.33 ± 0.2[a]
Fluconazole	1341 ± 0.04	202 ± 0.001[a]
Ketoconazole	11.1 ± 1.8[a]	0.62 ± 0.01[a]
Methadone	2.96 ± 0.06[a]	0.32 ± 0.03[a]

[a] K_i value based on the unbound concentration in the incubation medium (i.e. corrected for binding to HLM and BSA.

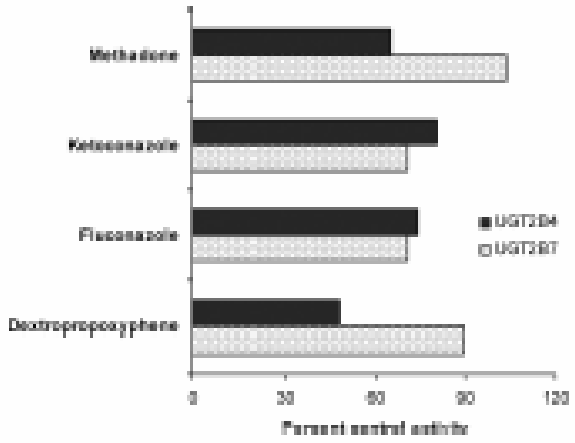

Fig. 4. Dextropropoxyphene, fluconazole, ketoconazole, and methadone inhibition of codeine 6-glucuronidation by recombinant UGT2B4 and UGT2B7. Incubations included 2% BSA. The codeine concentration was 0.2 mM, and the added inhibitor concentrations corresponded to the K_i values shown in Table 5 corrected for the predicted binding to incubation constituents (i.e., K_i/fu_{inc}): dextropropoxyphene, 12 μM; fluconazole, 220 μM; ketoconazole, 7.5 μM; and methadone, 0.6 μM.

TABLE 6

Predicted increase in the area under the codeine plasma concentration-time from coadministration of dextropropoxyphene, fluconazole, ketoconazole, or methadone

Drug (In Vivo Dose)[a]	Predicted Fold Increase in AUC Ratio Based On:	
	Total Inhibitor Concentration[b]	Unbound Inhibitor Concentration[b]
Dextropropoxyphene (117 mg 8-hourly[c])	1.33	1.26
Fluconazole (400 mg once daily[d])	1.60	1.34
Ketoconazole (200 mg once daily[e])	2.97	1.94
Methadone (74 mg once daily[f])	3.66	1.72

[a] Dose calculated as free base where drug was administered as a salt.
[b] Hepatic maximum input concentration, except for ketoconazole (maximum plasma concentration; see Materials and Methods).
[c] Interrist et al., 1982.
[d] Zuhal et al., 1994.
[e] Backman et al., 1997.
[f] Foster et al., 2004.

COD. In contrast to the Michaelis-Menten (or weak substrate inhibition) kinetics observed for C6G formation by HLM, COD glucuronidation by UGT2B4 and UGT2B7 exhibited sigmoidal kinetics. Differences in kinetic behavior between HLM and recombinant UGTs have been observed in other studies (e.g., Bowalgaha et al., 2005). Reasons for the inter-system differences remain unknown, but may reflect membrane effects on protein function (Miners et al., 2006). The difference in the kinetic model (sigmoidal versus hyperbolic) between present and previously (Court et al., 2003) reported data for UGT2B7 may arise from our use of more points at lower substrate concentrations, which favors detection of sigmoidal kinetics. S_{50} values for COD glucuronidation by both UGT2B4 and UGT2B7 were reduced by BSA, and S_{50} values generated in the presence of BSA were close in value. However, in contrast to HLM and UGT2B7, the V_{max} for UGT2B4 was also reduced by BSA. Although it is not possible to determine the relative contribution of UGT enzymes to a metabolic pathway in the absence of relative protein expression data, it is noteworthy that UGT2B4 mRNA expression in human liver exceeds that of UGT2B7 9-fold (Ohno and Nakajin, 2009). Collectively, these data suggest a significant, perhaps major, contribution of UGT2B4 to human liver microsomal COD glucuronidation. UGT2B4 and UGT2B7 seem to exhibit overlapping substrate selectivities (Jin et al., 1997; Court et al., 2003), although activities toward most aglycones are usually higher with UGT2B7.

Drugs previously identified as potential UGT2B7 inhibitors in either in vitro or in vivo studies (namely, dextropropoxyphene, fluconazole, ketoconazole, methadone, and valproic acid) along with acetaminophen, ibuprofen, and salicylic acid (the primary active metabolite of aspirin), which are marketed as compound formulations with COD for enhanced analgesia, were screened for inhibition of human liver microsomal COD glucuronidation. Acetaminophen, ibuprofen, and salicylic acid inhibited C6G formation to a minor extent only, indicating that inhibition of COD glucuronidation by drugs present in compound formulations is unlikely. In contrast, IC_{50} values generated for dextropropoxyphene, fluconazole, ketoconazole, and methadone in the presence of BSA were in the ranges of plasma concentrations observed for therapeutic doses in vivo. Thus, K_i values were determined for these compounds. As with the IC_{50}s, K_i values generated from incubations supplemented with BSA (and corrected for binding to HLM and albumin) were 6.5- to 17-fold lower than the corresponding parameters determined in the absence of BSA. A similar effect of BSA was observed in studies of the fluconazole–zidovudine and valproic acid–lamotrigine interactions in vitro (Rowland et al., 2006; Uchaipichat et al., 2006b) and confirm that, like the K_m, K_i values for UGT2B7 inhibitors are overestimated when BSA is not present in incubations of HLM. It has been reported recently that fluconazole and ketoconazole are glucuronidated by hepatic UGTs (Bourcier et al., 2010), although a contribution of glucuronidation to dextropropoxyphene and methadone elimination seems not to have been shown to date.

It is noteworthy that dextropropoxyphene, fluconazole, ketoconazole, and methadone differentially inhibited UGT2B4- and UGT2B7-catalyzed C6G formation. Whereas fluconazole and ketoconazole inhibited each enzyme to a similar extent, dextropropoxyphene and methadone selectively inhibited UGT2B4-catalyzed COD glucuronidation (Fig. 4). These observations suggest that dextropropoxyphene and methadone may cause lesser inhibition of drugs that are selectively glucuronidated by UGT2B7. Indeed, K_i values obtained here for fluconazole (from incubations with and without BSA) of human liver microsomal COD glucuronidation were approximately 20% higher than the corresponding K_is we previously reported for inhibition of zidovudine glucuronidation (Uchaipichat et al., 2006b). K_i values determined here for metha-

done and ketoconazole inhibition of COD glucuronidation also differ from inhibition studies with the predominantly UGT2B7 substrate morphine, which reported less potent inhibition (Morrish et al., 2005; Takeda et al., 2006). While this may be caused in part by the differing contributions of UGT2B4 and UGT2B7 to COD and morphine (3- and 6-) glucuronidation and the differential inhibition of each enzyme by methadone, binding to HLM was not accounted for in the morphine inhibition studies and effects of BSA were not investigated.

Based on total inhibitor concentration in blood, extrapolation of the K_i values for dextropropoxyphene, fluconazole, ketoconazole, and methadone predicted 1.60- to 3.66-fold increases in the AUC ratio for COD when coadministered with each inhibitor at the doses shown in Table 6. When considered in terms of unbound inhibitor concentration in blood, the inhibition potential of fluconazole was unaltered and a lesser interaction (1.72-fold increase in AUC) was predicted with methadone, whereas predicted inhibitory effects of dextropropoxyphene were minor or negligible. Although there is no consensus whether DDI potential should be predicted based on total or unbound concentration of the perpetrator drug in plasma, optimum prediction of the magnitude of inhibitory interactions involving both cytochrome P450 and UGT substrates is achieved when total maximum hepatic input concentration is used in eq. 2 (Ito et al., 2004; Brown et al., 2005; Rowland et al., 2006; Uchaipichat et al., 2006b; Miners et al., 2010). On this basis, significant DDIs involving inhibition of COD glucuronidation by dextropropoxyphene, fluconazole, ketoconazole, and methadone would be predicted in vivo. Consistent with these predictions, it has been reported in abstract form that plasma COD concentrations were 3-fold higher in subjects receiving methadone compared with those on buprenorphine (Somogyi et al., 2009). Furthermore, the urinary metabolic ratio (COD/C6G) for COD glucuronidation was substantially higher in the methadone-treated subjects. It is noteworthy that the 3-fold increase in COD plasma concentration observed in vivo is close to the 3.6-fold increase in the AUC ratio predicted here (Table 6). In addition to effects on UGT2B7-catalyzed drug glucuronidation, recent in vitro data suggest ketoconazole may inhibit the elimination of drugs cleared by UGT1A1 and UGT1A9 (Yong et al., 2005).

Like the prediction of DDI potential, IV-IVE may be used to determine in vivo hepatic clearance (CL_H) and extraction ratio from the experimentally measured microsomal intrinsic clearance, calculated as $CL_{int} = V_{max}/K_m$ (see Miners et al., 2006, 2010 for approach). Estimates of CL_H for COD clearance via hepatic glucuronidation were derived with the equation for the well stirred model of hepatic clearance using scaling factors given in Rowland et al. (2006a), 0.93 as the fraction of COD unbound in blood, and the mean K_m and V_{max} values generated here for human liver microsomal COD glucuronidation (Table 2). Predicted hepatic clearances were 0.8 and 6 liter/h for kinetic constants obtained in the absence and presence of BSA, respectively. The approximate 10-fold increase in predicted CL_H from in vitro CL_{int} values determined from incubations supplemented with BSA is consistent with previous studies kinetic studies of UGT1A9, UGT2B7, and cytochrome P450 2C9 substrates conducted in this and other laboratories (Rowland et al., 2007, 2006a,b; Kilford et al., 2009). Despite this, the extrapolated CL_H from experiments performed in the presence of BSA still underpredicts the known in vivo CL_H for COD via glucuronidation [approximately 36 liter/h; assuming a systemic clearance of 45 liter/h (Soars et al., 2002) and $f_m = 0.8$; see *Materials and Methods*]. The data are consistent with the 2- to 5- fold underprediction observed for the predicted in vivo clearances of UGT2B7 substrates from in vitro data obtained in the presence of BSA (Rowland et al., 2007; Kilford et al., 2009), but contrasts to the near-exact prediction of in vivo CL_H for the UGT1A9 substrate propofol and the cytochrome P450 2C9 substrate phenytoin when in vitro kinetic data generated in the presence of BSA are used for IV-IVE (Rowland et al., 2006a). Because it is believed that the Michaelis constant obtained from experiments with HLM supplemented with BSA reflects "true" hepatocellular K_m (Rowland et al., 2007), other factors such as underprediction of V_{max}, extrahepatic glucuronidation or uptake barriers presumably contribute to the accuracy of in vivo clearance prediction for moderately polar UGT2B7 substrates.

In summary, IV-IVE predicts significant DDIs arising from inhibition of COD metabolic clearance via glucuronidation by coadministered dextropropoxyphene, fluconazole, ketoconazole, and methadone. Available evidence is generally consistent with superior pain relief from COD in CYP2D6-extensive metabolizers, and absent or minor COD analgesia in poor metabolizers (Somogyi et al., 2007). Conversely, the relative conversion of COD to morphine is approximately 2- to 3-fold higher in CYP2D6 ultra-rapid metabolizers compared with extensive metabolizer and this may result in an exaggerated response, including sedation and respiratory depression. Thus, it may be speculated that inhibition of COD glucuronidation by coadministered dextropropoxyphene, fluconazole, ketoconazole, and methadone will potentially result in enhanced and prolonged analgesia caused by increased formation of morphine. Furthermore, marked inhibition of the glucuronidation of high-dose COD could conceivably result in morphine toxicity.

References

Bodenham NR, Bartholomeusz FD, Prewitt DR, Sansom LN, and Reid JG (1987) The pharmacokinetics of ketoconazole after chronic administration in adults. *Eur J Clin Pharmacol* **33**:531–534.

Bhasker CR, McKinnon W, Stone A, Lo AC, Kubota T, Ishizaki T, and Miners JO (2000) Genetic polymorphism of UDP-glucuronosyltransferase 2B7 (UGT2B7) at amino acid 268: ethnic diversity of alleles and potential clinical significance. *Pharmacogenetics* **10**:379–386.

Boase S and Miners JO (2002) In vitro–in vivo correlations for drugs eliminated by glucuronidation: investigations with the model substrate zidovudine. *Br J Clin Pharmacol* **54**:493–503.

Bourcier K, Rylance R, Kempshall S, Jones R, Maximilien J, Irvine N and Jones B (2010) Investigation into UDP-glucuronosyltransferase enzyme kinetics of imidazole and triazole containing antifungal drugs in human liver microsomes and recombinant UGT enzymes. *Drug Metab Dispos* **38**:822–828.

Bowalgaha K, Elliot DJ, Mackenzie PI, Knight KM, Swedmark S, and Miners JO (2005) S-Naproxen and desmethylnaproxen glucuronidation by human liver microsomes and recombinant human UDP-glucuronosyltransferases (UGT): role of UGT2B7 in the elimination of naproxen. *Br J Clin Pharmacol* **60**:423–432.

Brown HS, Ito K, Galetin A, and Houston JB (2005) Prediction of in vivo drug–drug interactions from in vitro data: impact of incorporating parallel pathways of drug elimination and inhibitor absorption rate constant. *Br J Clin Pharmacol* **60**:508–518.

Chen ZR, Somogyi AA, Reynolds G, and Bochner F (1991) Disposition and metabolism of codeine after single and chronic dose in one poor and seven extensive metabolizers. *Br J Clin Pharmacol* **31**:381–391.

Court MH, Krishnaswamy S, Hao Q, Duan SX, Patten CJ, Von Moltke LL, and Greenblatt DJ (2003) Evaluation of 3′-azido-3′-deoxythymidine, morphine, and codeine as probe substrates for UDP-glucuronosyltransferase 2B7 (UGT2B7) in human liver microsomes: specificity and influence of the UGT2B7*2 polymorphism. *Drug Metab Dispos* **31**:1125–1133.

Dansirikul TK and Warnock DW (1988) Clinical pharmacokinetics of ketoconazole. *Clin Pharmacokinet* **14**:13–34.

Foster DJ, Somogyi AA, White JM, and Bochner F (2004) Population pharmacokinetics of (*R*)-, (*S*)-, and racemethadone in methadone maintenance patients. *Br J Clin Pharmacol* **57**:742–755.

Gasche Y, Daali Y, Fathi M, Chiappe A, Cottini S, Dayer P, and Desmeules J (2004) Codeine intoxication associated with ultrarapid CYP2D6 metabolism. *N Engl J Med* 351:2827–2831.

Giacomini KM, Gibson TP, and Levy G (1978) Plasma protein binding of n-propoxyphene in normal and anephric patients. *J Clin Pharmacol* 18:106–109.

Gram LF, Schou J, Way WL, Hellberg J, and Rodin NO (1979) n-Propoxyphene kinetics after single and oral intravenous dose in man. *Clin Pharmacol Ther* 26:473–482.

Inturrisi CE, Colburn WA, Kaiko RF, Houde RW, and Foley KM (1987) Pharmacokinetics and pharmacodynamics of methadone in patients with chronic pain. *Clin Pharmacol Ther* 41:392–401.

Inturrisi CE, Colburn WA, Vanbury K, Barton HE, Woody GE, and O'Brien CP (1982) Propoxyphene and norpropoxyphene kinetics after single and repeated doses of propoxyphene. *Clin Pharmacol Ther* 31:127–137.

Ito K, Brown HS, and Houston JB (2004) Database analyses for the prediction of in vivo drug–drug interactions from in vitro data. *Br J Clin Pharmacol* 57:473–486.

Jin CJ, Mackenzie PI, and Miners JO (1997) The regio- and stereo-selectivity of C19 and C21 hydroxysteroid glucuronidation by UGT2B7 and UGT2B11. *Arch Biochem Biophys* 341:287–294.

Kerdpin O, Mackenzie PI, Bowalgaha K, Finel M, and Miners JO (2009) Influence of N-terminal domain histidine and proline residues on the substrate selectivities of human UDP-glucuronosyltransferase 1A1, 1A6, 1A9, 2B7, and 2B10. *Drug Metab Dispos* 37:1948–1955.

Kilford PJ, Stringer R, Sohal B, Houston JB, and Galetin A (2009) Prediction of drug clearance by glucuronidation from in vitro data: use of combined cytochrome P450 and UDP-glucuronosyltransferase cofactors in alamethicin-activated human liver microsomes. *Drug Metab Dispos* 37:82–89.

Madadi P, Ross CJ, Hayden MR, Carleton BC, Gaedigk A, Leeder JS, and Koren G (2009) Pharmacogenetics of neonatal opioid toxicity following maternal use of codeine during breastfeeding: a case-control study. *Clin Pharmacol Ther* 85:31–35.

McCance-Katz EF, Rainey PM, Jatlow P, and Friedland G (1998) Methadone effects on zidovudine disposition (AIDS Clinical Trials Group 262). *J Acquir Immune Defic Syndr Hum Retrovirol* 18:425–443.

McLure JA, Miners JO, and Birkett DJ (2000) Nonspecific binding of drugs to human liver microsomes. *Br J Clin Pharmacol* 49:453–461.

Miners JO, Knights KM, Houston JB, and Mackenzie PI (2006) In vitro–in vivo correlation for drugs and other compounds eliminated by glucuronidation in humans: pitfalls and promises. *Biochem Pharmacol* 71:1531–1539.

Miners JO, Mackenzie PI, and Knights KM (2010) The prediction of drug glucuronidation parameters in humans: UDP-glucuronosyltransferase enzyme-selective substrate and inhibitor probe for reaction phenotyping and in vitro–in vivo extrapolation of drug clearance and drug–drug interaction potential. *Drug Metab Rev* 42:196–201.

Morrish GA, Fisher DJ, and Somogyi AA (2005) Differential in vitro inhibition of M3G and M6G formation from morphine by (R)- and (S)-methadone and structurally related opioids. *Br J Clin Pharmacol* 61:226–235.

Ohno S and Nakajin S (2009) Determination of mRNA expression of human UDP-glucuronosyltransferases and application for localization in various human tissues by real-time reverse transcriptase-polymerase chain reaction. *Drug Metab Dispos* 37:32–40.

Rowland A, Elliot DJ, Knights KM, Mackenzie PI, and Miners JO (2008a) The albumin effect and in vitro–in vivo extrapolation: sequestration of long-chain unsaturated fatty acids enhances phenytoin hydroxylation by human liver microsomal and recombinant cytochrome P450 2C9. *Drug Metab Dispos* 36:870–877.

Rowland A, Elliot DJ, Williams JA, Mackenzie PI, Dickinson RG, and Miners JO (2006) In vitro characterization of lamotrigine N2-glucuronidation and the lamotrigine–valproic acid interaction. *Drug Metab Dispos* 34:1055–1062.

Rowland A, Gaganis P, Elliot DJ, Mackenzie PI, Knights KM, and Miners JO (2007) Binding of inhibitory fatty acids is responsible for the enhancement of UDP-glucuronosyltransferase 2B7 activity by albumin: implications for in vitro–in vivo extrapolation. *J Pharmacol Exp Ther* 321:137–147.

Rowland A, Knights KM, Mackenzie PI, and Miners JO (2008b) The "albumin effect" and drug glucuronidation: bovine serum albumin and fatty acid-free human serum albumin enhance the glucuronidation of UDP-glucuronosyltransferase (UGT) 1A3 substrates but not UGT1A1 and UGT1A6 activities. *Drug Metab Dispos* 36:1056–1062.

Sohal J, Gallicano K, Pakuts A, and Cameron DW (2004) Effect of fluconazole on zidovudine pharmacokinetics in patients infected with human immunodeficiency virus. *J Infect Dis* 189:1103–1107.

Segel IH (1993) *Enzyme Kinetics: Behavior and Analysis of Rapid Equilibrium and Steady-State Enzyme Systems*, pp 104 and 128, J. Wiley and Sons, New York.

Soars MG, Burchell B, and Riley RJ (2002) In vitro analysis of human drug glucuronidation and prediction of in vivo metabolic clearance. *J Pharmacol Exp Ther* 301:382–390.

Somogyi AA, Barratt DT, and Coller JK (2007) Pharmacogenetics of opioids. *Clin Pharmacol Ther* 81:429–444.

Somogyi AA, Gebski R, Coller JK, White JM, and Schmidt H (2009) Methadone inhibits CYP2D6 and UGT2B7 in vivo: a study using codeine as the substrate. *Drug Metab Rev* 41(Suppl 1):45–46.

Takeda S, Kitajima Y, Ishii Y, Nishimura Y, Mackenzie PI, Oguri K, and Yamada H (2005) Inhibition of UDP-glucuronosyltransferase 2B7-catalyzed morphine glucuronidation by beloxamide: dual mechanisms involving a novel noncompetitive mode. *Drug Metab Dispos* 34:1277–1282.

Thorn CF, Klein TE, and Altman RB (2009) Codeine and morphine pathway. *Pharmacogenet Genomics* 19:556–558.

Trapnell CB, Klecker RW, Jarvis-Dow C, and Collins JM (1996) Glucuronidation of 3′-azido-3′-deoxythymidine (zidovudine) by human liver microsomes: relevance to clinical pharmacokinetic interactions with atovaquone, fluconazole, methadone, and valproic acid. *Antimicrob Agents Chemother* 40:1552–1558.

Uchaipichat V, Mackenzie PI, Elliot DJ, and Miners JO (2006a) Selectivity of substrate (trifluoperazine) and inhibitor (amitriptyline, androsterone, canrenoic acid, hecogenin, phenylbutazone, quinidine, quinine, and sulfinpyrazone) "probes" for human UDP-glucuronosyltransferases. *Drug Metab Dispos* 34:449–456.

Uchaipichat V, Mackenzie PI, Guo XH, Gardner-Stephen D, Galetin A, Houston JB, and Miners JO (2004) Human UDP-glucuronosyltransferases: isoform selectivity and kinetics of 4-methylumbelliferone and 1-naphthol glucuronidation, effects of organic solvents, and inhibition by diclofenac and probenecid. *Drug Metab Dispos* 32:413–423.

Uchaipichat V, Winner LK, Mackenzie PI, Elliot DJ, Williams JA, and Miners JO (2006b) Quantitative prediction of in vivo inhibitory interactions involving glucuronidated drugs from in vitro data: the effect of fluconazole on zidovudine glucuronidation. *Br J Clin Pharmacol* 61:427–439.

Welling PG, Lyons LL, Tse FL, and Craig WA (1976) Propoxyphene and norpropoxyphene: influence of diet and acid fluid on plasma levels. *Clin Pharmacol Ther* 19:553–565.

Yong WP, Ramirez J, Innocenti F, and Ratain MJ (2005) Effects of beloxamide on glucuronidation by UDP-glucuronosyltransferase enzymes. *Clin Cancer Res* 11:6699–6704.

Yue QY, Hasselström J, Svensson JO, and Sawe J (1991) Pharmacokinetics of codeine and its metabolites in Caucasian healthy volunteers: comparisons between extensive and poor hydroxylators of debrisoquine. *Br J Clin Pharmacol* 31:625–642.

Address correspondence to: Professor John O. Miners, Department of Clinical Pharmacology, Flinders University School of Medicine, Flinders Medical Centre, Bedford Park, SA 5042, Australia. E-mail: john.miners@flinders.edu.au

VITAE

Name Miss Pritsana Raungrut

Student ID 4910031001

Educational Attainment

Degree	Name of Institution	Year of Graduation
B.Sc.(Biology)	Prince of Songkla University	2001
M.Sc.(Pharmacology)	Prince of Songkla University	2005

Scholarship Awards during Enrolment

Prince of Songkla University Graduate Studies grant

Work position and Address

Lecturer Department of Biomedical Sciences, Faculty of Medicine, Prince of Songkla University, Hat-Yai, Songkla, 90110, Thailand

List of Publication and Proceedings

Raungrut P, Uchaipichat V, Elliot DJ, Janchawee B, Somogyi AA and Miners JO. In vitro – in vivo extrapolation predicts drug – drug interactions arising from inhibition of codeine glucuronidation by dextropropoxyphene, fluconazole, ketoconazole and methadone in humans. Journal of Pharmacology and Experimental Therapeutics 2010; 334(2): 609–618.

Raungrut P, Janchawee, Uchaipichat V, Elliot DJ and Miners JO. Effect of albumin on in vitro codeine glucuronidation. In abstract: 3rd Asian Pacific Regional Meeting of the International Society for the Study of Xenobiotics (ISSX) 2009, Bangkok, Thailand.

Raungrut P, Janchawee B, Uchaipichat V, Elliot DJ and Miners JO. The effect of valproic acid on codeine glucuronidation of multiple UDP-glucuronosyltransferase 2B7 (UGT2B7) substrate binding sites. In abstract: the 35th Congress on Science and Technology of Thailand (STT35) 2009, Chonburi, Thailand.